NASA CR-175209

POTENTIAL IMPACT OF REMOTE SENSING DATA ON SEA-STATE ANALYSIS AND PREDICTION

Vincent J. Cardone
Oceanweather Inc.
5 River Road
Cos Cob, Conn. 06807

December, 1983
Final Report

Prepared for
GODDARD SPACE FLIGHT CENTER
Greenbelt, Maryland 20771

(E84-10083) POTENTIAL IMPACT OF REMOTE SENSING DATA ON SEA-STATE ANALYSIS AND PREDICTION Final Report, 1 Mar. 1982 - 31 Dec. 1983 (Ocean Weather, Inc.) 105 p HC A06/MF A01 CSCL 08C G3/43

N84-19954

Unclas 00083

TECHNICAL REPORT STANDARD TITLE PAGE

1. Report No.	2. Government Accession No.	3. Recipient's Catalog No.
	blank	

4. Title and Subtitle	5. Report Date
POTENTIAL IMPACT OF REMOTE SENSING DATA ON SEA-STATE ANALYSIS AND PREDICTION	DECEMBER 1983
	6. Performing Organization Code: blank
7. Author(s): Vincent J. Cardone	8. Performing Organization Report No.
9. Performing Organization Name and Address: OCEANWEATHER INC. SUITE 1 5 RIVER ROAD COS COB, CT 06807	10. Work Unit No.: blank
	11. Contract or Grant No.: NAS5-26890
12. Sponsoring Agency Name and Address: Goddard Space Flight Center Greenbelt Road Greenbelt, MD 20771	13. Type of Report and Period Covered: FINAL REPORT 1 MAR 82 - 31 DEC 83
	14. Sponsoring Agency Code: blank

15. Supplementary Notes

16. Abstract

A case study of the severe North Atlantic storm of September 9-11, 1978 which damaged the ocean liner Queen Elizabeth 2 (QE2) is performed to assess the impact of remotely sensed marine surface wind data obtained by Seasat-A, on sea state specifications and forecasts. Alternate representations of the surface wind field in the QE2 storm were produced from the Seasat enhanced data base, and from operational analyses based upon conventional data. The wind fields were used to drive a high resolution spectral ocean surface wave prediction model.

It is demonstrated that sea-state analyses would have been vastly improved during the period of storm formation and explosive development had remote sensing wind data been available in real time. It is also shown in this study that a modest improvement in operational 12-24 hour wave forecasts would have followed automatically from the improved initial state specification made possible by the remote sensing data in both numerical and sea state prediction models, but that significantly improved 24-48 hour wave forecasts will require in addition to remote sensing data, refinement in the numerical and physical aspects of weather prediction models.

17. Key Words (Selected by Author(s))	18. Distribution Statement
Ocean surface wave prediction Seasat-A marine wind explosive cyclogenesis	blank

19. Security Classif. (of this report)	20. Security Classif. (of this page)	21. No. of Pages	22. Price*
		105	

*For sale by the Clearinghouse for Federal Scientific and Technical Information, Springfield, Virginia 22151.

Figure 2. Technical Report Standard Title Page

PREFACE

The primary objective of this study is to demonstrate that remotely sensed marine surface wind and wave data can improve the operational analysis and prediction of surface winds and waves in intense marine extratropical cyclones. This objective was achieved through a case study of the severe North Atlantic storm of September 9-11, 1978 which damaged the ocean liner Queen Elizabeth 2 (QE2), and in which remotely sensed marine surface wind data were obtained by Seasat-A.

Alternate representations of the surface wind field in the QE2 storm were produced in order to compare the specifications possible from the Seasat enhanced data base with wind fields derived from operational analyses based upon conventional data. The operational analyses were found to be very poor in the QE2 storm despite the fact that the storm formed and moved through the active North Atlantic shipping lanes.

Detailed man-machine mix techniques were applied to provide the most accurate surface wind fields possible from combined conventional and Seasat data. The wind fields were used to drive a high resolution spectral ocean surface wave prediction model. The model derived wave hindcasts provided a basis for quantifying the errors in operationally produced wave analyses and forecasts in the storm. It is demonstrated that sea-state analyses would have been vastly improved during the period of storm formation and explosive development had the remote sensing data been available in real time. It is also shown in this study that a modest improvement in operational 12-24 hour wave forecasts would have followed automatically from the improved initial state specification made possible by the remote sensing data in both numerical and sea state prediction models, but that significantly improved 24-48 hour wave forecasts will require in addition to remote sensing data, refinement in the numerical and physical aspects of weather prediction models.

This study also included an evaluation of the wave model used against directional wave measurements made by an experimental airborne scanning radar altimeter in a separate intense North Atlantic cyclone. The model validation confirmed the high accuracy of wave height specifications shown

previously for the wave model but also revealed deficiencies in the treatment of directional processes. The high resolution directional wave measurements made by the scanning radar altimeter provide a basis for development of improved empirically based treatments of directional wave processes and should guide the development of improved theory. On an operational satellite the system would provide data which could directly update the sea state directional spectrum representation carried in operational wave prediction models. Improvements in the initial state alone could lead to significant increases in skill of 12-24 hour sea state forecasts, and probably to improved prediction at longer forecast ranges in wave regimes dominated by swell.

Table of Contents

LIST OF FIGURES

List of Tables

1. Introduction

SEASAT-A was launched on 26 June 1978 and stopped transmitting after acquiring global data from each instrument over a 99 day period. After a period of extensive evaluation of limited data sets and tuning of algorithms which retrieve geophysical data from the sensor data, global data sets for each instrument except the synthetic aperature radar (SAR) had been produced for the entire experimental period. The success of the scatterometer (SASS) experiment in demonstrating the ability to remotely sense surface marine winds has by now been well documented. In a recent review, Pierson (1983) cites r.m.s. differences between the SASS winds and meteorological winds of 1.2 m/s in speed and 17° in direction with negligable bias.

A number of planning studies conducted prior to the launch of SEASAT showed that tremendous economic and human benefits would accrue to the marine community from improved short (12-48 hours) and medium range (3-5 days) operational wind and sea state forecasts. It is widely believed that the global availability of remotely sensed marine winds on future operational satellites shall have great effects on weather and sea state forecasts but to date only very limited research based on actual SEASAT-A data has been reported to support this view.

Simulation studies using numerical weather prediction models (Cane et al., 1981) suggest that improvements in the initial state provided by SASS type data improve analyses and forecasts of surface pressure and low and midtropospheric wind fields over both land and sea. To date these results have not been confirmed in experiments involving real SASS data but such experimental programs are underway at a number of centers, including the NASA Goddard Space Flight Center and NOAA's National Meteorological Center.

In this study, we attempt to document through a case study, the potential impact of remote sensing wind data on the specification and forecasting of sea states in a particularly dangerous class of meteorological phenomenon: the explosively deepening marine extratropical cyclones or more simply "bombs" (Sanders and Gyakum, 1980). Such storms have become the focus of intense interest in recent years for several reasons.

First "bombs" are clearly a hazard to shipping and other offshore interests and seem to be largely responsible for weather related loss of life and shipping in the high seas, even in well travelled shipping lanes. Two examples are the storm of August, 1979 in the eastern North Atlantic which occurred during the Fastnet yacht race, sinking 24 boats and killing 17 sailors, and the storm off the Grand Banks of Newfoundland of February, 1981, in which the drilling rig Ocean Ranger sank killing 84 crewmen. The storm used for this case study occurred in early September, 1978 in the western N. Atlantic, and was responsible for the loss of a fishing trawler with all hands off Georges Bank and extensive damage to the oceanliner Queen Elizabeth II along with injury to 20 of its passengers. This QE2 storm has been studied extensively by Gyakum (1983) and Anthes et al, (1983).

Bombs are interesting also because the physical mechanisms responsible for their explosive development are not well understood. There is increasing evidence that an important source of energy is convective heating; bombs therefore bear some similarity energetically to tropical cyclones.

Finally, as pointed out by Leary (1971) and Sanders and Gyakum (1980), operational numerical weather prediction models often fail to predict explosive cyclogenesis over the oceans. Bombs therefore have not participated in the very significant improvements in skill in numerical weather forecasting exhibited over the past two decades. Also, since bombs usually form as very small scale but intense circulations, detection is more difficult and storms may not be resolved in analyses produced objectively to initialize numerical weather prediction models.

For this study, we have assembled a comprehensive data set for the QE2 storm consisting of conventional surface ship reports, recently reprocessed SASS data, and surface pressure and sea state analyses and forecasts prepared in real time by the NOAA National Meteorological Center (NMC) and the U.S. Navy Fleet Numerical Oceanography Center (FNOC).

The data sets were used to develop alternate representations of the surface wind over the western North Atlantic Ocean for the period of the formation and intensification of the QE2 storm. As expected, the wind fields developed from conventional data available in real time were found to be quite deficient despite the fact that the storm formed and moved

through a major shipping lane. On the other hand, the surface wind fields developed from a combination of conventional ship reports and SASS wind data documented the rapid formation of gale force winds about the incipient storm and the evolution of the scale and intensity of the surface wind field over the 48-hour period between the formation of the storm and the development of peak sea states in the storm at about the time of the encounter of the QE2 with the storm.

Since remote wave measurements were not made in the QE2 storm, a hindcast was made using a calibrated spectral wave model and the SASS based surface wind fields. This hindcast provided a base case wave specification against which operationally produced wave analyses and forecasts in this storm could be evaluated. Errors in conventional analyses and forecasts were extremely large, with peak sea states underestimated by as much as a factor of four. Hindcasts made with the calibrated wave model but driven by wind fields derived from conventional real time data showed little improvement over NMC or FNOC analyses, supporting the view that errors in operational wave analyses and forecasts are mainly caused by wind errors rather than wave model errors.

A series of three experiments were performed with the wave model to assess the impact of the SASS data on sea state forecasts. In one experiment, we performed a simulated 24-hour wave forecast for the period of explosive development, for which forecast wind fields were derived from a numerical weather prediction for the QE2 storm reported by Anthes et al (1983). Their forecast was based upon an improved initial state specification derived from SASS data and a high resolution numerical weather prediction model. The numerical weather prediction captured only about 50% of the explosive deepening, in terms of minimum surface pressure, and contained errors in the shape of the pressure field and in the location of the strongest winds. Those errors translated into significant wave height errors relative to the base case, though wave forecasts were much improved overall.

The second and third forecast experiments covered the 24-hour period prior to the QE2 encounter with the storm, a period in which the storm had stopped deepening explosively but during which peak sea state growth continued. Forecast wind fields for both experiments were derived from

operational NMC surface pressure forecasts. The experiments differed in the initial state specification. In one experiment, initial sea states were specified from the base case hindcast; in the other, initial sea states were derived from hindcasts made from conventional wind data alone.

These experiments showed that the improved initial state specifications resulted in improved forecasts at 12 hours, but that by 24 hours, errors in forecast winds had largely eliminated the differences between the two forecast runs. The tentative implication is that significant improvements in sea state forecasts beyond 24 hours will follow principally from increases in skill in numerical weather prediction with the exception of forecasts of swell which would benefit from improved remote wind and wave sensing systems even with numerical weather forecasts with current levels of skill.

A new remote sensing instrument, the real-aperature scanning beam Radar Ocean Wave Spectrometer (ROWS)(Jackson et al. 1983) has been shown recently to be capable of obtaining global satellite measurements of ocean wave directional spectra. Such data could be used in the specification of the initial state for wave forecasting systems, much like the way atmospheric observations are used to initialize numerical weather prediction models. The forecast experiments just summarized above estimate the impact on forecasts of such improved initial states for one storm type.

Wave prediction models are not perfect, and ROWS type data may also provide the wave data necessary to validate and further refine such models. In this study, the wave model used for the QE2 storm hindcasts, and an alternate model, were used to hindcast a separate intense N. Atlantic storm in which an airborne ROWS obtained directional wave spectra. The comparison of hindcast and measured wave heights and directional spectra beneath the flight path confirmed the skill on wave height specifications shown for the adopted wave model in prior studies but revealed certain deficiencies in the treatment of directional processes in the model theory.

2. Contemporary Wave Forecast Systems

In recent years there has been a shift at many forecast centers (e.g. those of the U.K., Japan, Norway, France) to the use of numerical spectral wave specification models to make operational wave height analyses and forecasts. The models are run in hindcast/forecast cycle, usually twice daily, from 0000 GMT and 1200 GMT initial states. The models are driven exclusively by input wind fields; in wave forecasting, unlike numerical weather prediction, the initial wave conditions for a forecast are not specified from wave measurements but are calculated by the wave model run in a hindcast mode using wind fields derived from measurements. The accuracy of wave forecasts therefore may be limited by errors in the initial state due to poor marine wind analysis, errors in forecast wind fields derived from numerical weather forecast models, and possibly errors in the wave models themselves, though the latter effect may be minimized through careful model development and calibration.

Contemporary wave prediction models were reviewed by Cardone and Ross (1979). The models are based upon the spectral energy balance equation, usually applied in its simplest form, that is, to surface gravity waves assumed to propagate through water of infinite depth that is otherwise at rest. In this form, the equation is written

$$\frac{\partial}{\partial t} E(f,\theta,\vec{x},t) + \vec{C}g(f,\theta) \cdot \nabla E(f,\theta,\vec{x},t) = S(f,\theta,\vec{x},t) \qquad 2.1$$

where E is the energy density of the wave field described as a function of frequency, f, direction of propagation θ, position $\vec{x}$, and time t; C_g is the deep water group velocity vector, and S, the source function represents all physical processes that transfer energy to or from the spectrum. Discrete type wave models represent the spectrum E in terms of a number of spectral components (bands) of finite width, and successively simulate wave propagation (the homogeneous part of 2.1) and local energy transfers (the r.h.s. of 2.1) in a series of discrete time steps on a grid representing the ocean basin of interest.

In this country, the only operational spectral wave forecast model is the SOWM model of the U.S. Navy FNOC. The SOWM resolves the wave spectrum into 180 spectral components representing 15 frequency and 12

direction bands. The SOWM is run operationally twice daily on a grid which represents all major northern hemisphere basins. The SOWM forecasts extend to 72 hours. Initial conditions, $E(f,\theta,\vec{x},t_0)$ are taken from a continuous hindcast history made with the same wave model driven by 6-hourly wind fields produced at FNOC routinely by objective analyses of ship reports of wind and sea-level pressure. In this report we will refer to numerical surface pressure field forecasts and SOWM wave analyses and forecasts for the North Atlantic Ocean in the QE2 storm.

In this study we have basically simulated the operational wave forecast system used at FNOC, in order to assess the potential impact of remote sensing data for a case of explosive cyclogenesis. However, our system differs from the FNOC system, in that: (1) analysis winds were produced in a "man-machine" mix procedure rather than through strictly computer-based analyses; (2) the wave model used here for the QE2 storm hindcasts is a newer version of the SOWM with improved calibration and higher spectral and spatial resolution.

3. Validation of ODGP/SAIL Models against ROWS Data

3.1 Introduction

In this section we present an evaluation of the wave model (ODGP) used for the QE2 storm case study, in storm conditions against directional wave measurements made by an aircraft mounted radar. The measurements were obtained with the Goddard ROWS in the Norwegian Sea in a severe storm which formed in late October, 1978. Conventional wave measurements were also made in the same storm from a waverider buoy, deployed in the area of the experiment. There were a total of 5 flights over a 7 day period during the experiment. The hindcast covered a 12 day period to encompass all periods of data collection. The radar data have been thoroughly analyzed however only for one of the flights, which sampled the most severe sea states in the experiment. Since the high resolution directional wave measurements of the ROWS provide a rare opportunity to evaluate the directional aspects of spectral wave model predictions, a model with an alternate source term treatment (SAIL) was also used and evaluated.

3.2 ODGP and SAIL Model Attributes

The ODGP (Ocean Data Gathering Program) model, developed by Cardone, Pierson and Ward (1976) is a part of the family of PTB discrete type spectral models described by Pierson, Tick and Baer, (1966). Current versions of the ODGP model use the propagation scheme proposed by Greenwood and Cardone (1977). Their scheme uses downstream interpolation to propagate waves along great circle paths in an energy conserving manner. The scheme is basically first order and therefore dispersive, a trait intended to simulate the natural lateral and longitudinal spreading of finite bandwidth spectral components. The properties of the scheme are described in more detail in the report of the wave model intercomparison panel to the IUCRM Symposium on Wave Dynamics and Radio Probing of the Sea Surface, Miami, Florida, May 1981 (SWAMP, 1983).

While the ODGP spectral growth/dissipation algorithm is of the PTB type, significant differences between it and the U.S. Navy SOWM model (also a PTB type) evolved in the application and verification of the ODGP model against measured wave spectra in hurricanes. An important difference is in the calculation of the wave growth as a function of the angle between the wave direction and wind direction. In the SOWM, the energy in

a given frequency component summed within ±90° of the local wind is the quantity subjected to growth. The incremental growth is then spread out over the same components. In the ODGP model each downwind spectral component is grown separately and after computation of growth for all components within ±90° of the local wind direction, energy is redistributed over angles. This algorithm leads to slower growth of wave height with time in a turning wind than in a wind of constant direction.

Recently, workers have attempted to investigate the response of the wave spectrum to a turning wind from pitch/roll buoy data by studying the response of the mean wave direction in individual frequency bands. Clearly, not enough detail is present in such data to observe the directional response in complicated wind fields, and considering the scant field evidence, it is not surprising that the SWAMP group found large differences in the directional relaxation rates between the ten spectral wave hindcast models compared.

The modelling of directional processes in the ODGP model is apparently sufficient to provide reasonably skilled simulation of the integrated properties of the directional spectrum of peak sea states in storms characterized by stationary or moving circular wind fields. In over 60 individual comparisons in 19 different storms, Reece and Cardone (1982) found that the model exhibited negligible bias and rms errors of less than 1 m in significant wave height and 1 second in peak spectral period. Comparisons of hindcast and measured directional wave properties are more limited. Forristall et al. (1978, 1980) shows comparisons in two Gulf of Mexico tropical cyclones. The directional spectrum was estimated from surface elevation and orbital velocity measurements. Directional properties were expressed in terms of the mean direction and spread as a function of frequency. Good agreement was found in both storms.

The directional wave measurements obtained in this study provide the first opportunity to check in great detail the predictions of the directional spectral shape. To accomplish this, the ODGP model was adapted on a high resolution grid of 100 km spacing covering the eastern two-thirds of the North Atlantic Ocean. The 100 km spacing dictates a time step of 3 hours for the spectral range modelled. For this hindcast, the frequency

banding of the 15 bands of the SOWM was adopted. However, a 15° directional banding, rather than the SOWM's 30° banding was used.

The SAIL model is based upon a completely different spectral growth algorithm from the ODGP model, but uses the same spectral resolution propagation scheme and grid system. The basic formulation of the SAIL model is described by Greenwood et al. (1983); its participation in the wave model intercomparison program is described in the SWAMP (1983) report.

The SAIL model has undergone much more limited validation than the ODGP. The model is tuned basically through the adopted implied fetch-wise energy growth law. For one particular tuning (SAIL II) the model was found to nearly match the skill of the ODGP model in specification of peak sea states in several hurricanes (Oceanweather, 1983).

A hindcast with the SAIL model is included here basically to check whether the rather different treatment of directional processes from that of the ODGP model leads to any discernible difference in the specification of the full 2-d spectrum.

3.3 Wind Field Preparation

Cardone et al. (1980) describe and compare alternate marine wind field analysis methods with particular emphasis on the impact of wind field errors on wave specification. For typical mid and high latitude storm scenarios, specification of surface winds from conventional surface pressure analyses produced in real time at operational forecast centers generally was found to lead to wave hindcasts (with the ODGP model) containing both large rms errors and systematic underestimation of peak sea states, compared to errors (e.g. Reece and Cardone, 1982) found in hindcasts when wind fields were specified through reanlaysis of surface pressure and wind fields using enhanced ship report data files, and kinematic analysis techniques.

For this study, surface wind fields were specified at 6-hourly intervals over the period 0000 GMT 10/25/78-1800 GMT 11/07/78, over the domain 40°N-80°N, 50°W-30°E. For model spinup and periods in-between flights, winds were derived from the pressure analyses shown on the 6-hourly Northern Hemisphere Surface Analyses produced in real-time at

the NOAA National Meteorological Center. The procedure was to grid the sea level pressures manually on a 2.5° latitude-longitude grid and then objectively derive 19.5 meter level winds using the marine planetary boundary layer model of Cardone (1969). In that procedure, pressure gradients are derived by centered differencing, resulting in a highly smoothed wind field. For the critical periods, a complete reanalysis of the surface pressure and wind field was performed. First, ship reports not available in real time were added from a file of punched ship log reports produced at the NOAA National Climatic Center and replotted by machine. An example of replotted charts with reanalyzed isobaric and frontal analyses is shown in Figure 3.1. The number of ship reports shown overall in the maps exceeds by at least a factor of 2, the number available in real time. The number of reports from transient merchant ships decrease sharply north of about 60°N. The reanalysed pressure fields and the kinematic analyses were digitized at a 2.5° spacing since the data density hardly justified a finer spacing.

The map shown, depicts the synoptic situation leading up to the flight of interest on November 3. At 1800 GMT, November 2, a deep (958 mb) cyclone center is just north of the North Cape of Norway. That storm formed near 40°N, 50°W on 30 October and moved eastward at first. On 1 November, the storm turned northeastward, accelerated to a forward speed of 50 knots and deepened rapidly, the center passing just east of Iceland between 1200 and 1800 GMT 1 November. The center turned eastward and slowed to about 25 knots before passing north of the north coast of Norway early on 3 November. Maximum surface winds of 50-55 knots were measured by several ships in the right semi-circle of the storm of November 2nd and 3rd.

3.4 ROWS Data

Flight 9, the flight of interest, was conducted between 0800 GMT and 1000 GMT on 3 November, generally in the area between the storm just described, and a weaker frontal wave approaching from the west. A weak ridge of high pressure separated the two systems. The measured flight level winds along the flight line showed a complicated fine structure in the wind field near the ridge line. It is important to note that the

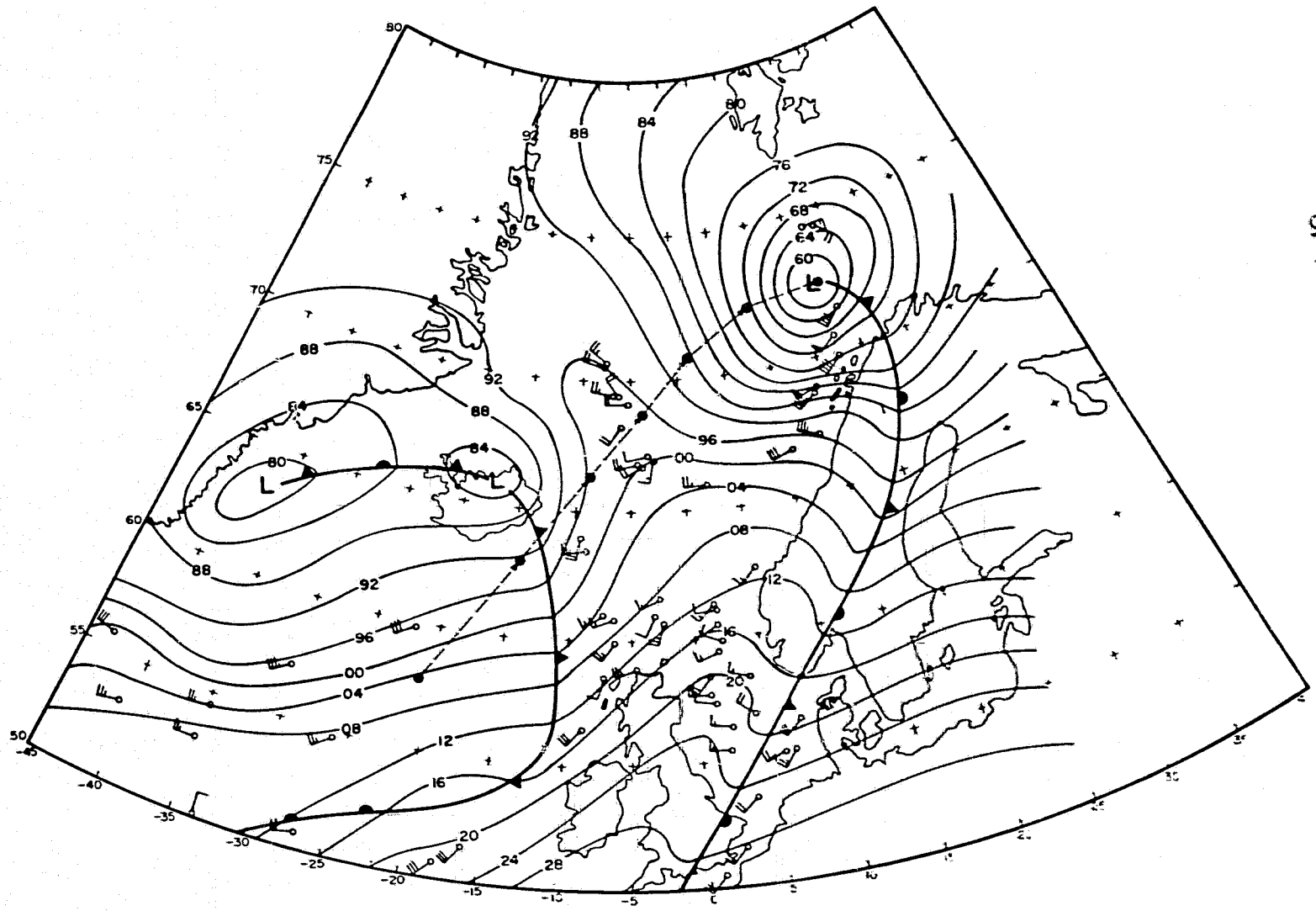

Figure 3.1 Surface weather map for 1800 GMT November 2, 1978 of northeastern N. Atlantic, showing track of storm (6-hour positions shown).

6-hourly 2.5° synoptic scale winds will not in general resolve such fine structure, and that therefore even a "perfect" wave model will be unable to resolve the details of the wave patterns along parts of the flight line.

Figure 3.2 shows 700 km by 150 km box pattern flown by the NASA CU990 in the area between the two extratropical cyclones. The figure also shows the wave model grid point locations in the vicinity of the box, the ROWS data files denoted by letters, and the location of the weather ship station Tromsoflakket near file A. The weather ship made 3-hourly surface wind measurements, and 3-hourly frequency spectra were estimated from measurements made by a wave rider buoy moored near the ship. The ROWS used was the NASA Goddard airborne 13.9 Ghz pulse-compression radar. The radar was equipped with a 6 rpm rotary antenna boresighted to 16° incidence providing a conical scanning bean of about .5 km lateral extent. A stable estimate of the directional spectrum is built up from data acquired over about 10 successive antenna rotations.

A full theoretical treatment of the principle of ROWS is given by Jackson (1981). The directional selectivity results basically from the radar ocean wave phase front matching across the lateral extent of the beam spot. The reflectivity mechanism is basically geometrical for the near vertical specular scatter regimes in which ROWS operates.

The details of the data reduction for the fall 1978 mission are given by Jackson et al. (1982). That mission included not only the Norwegian Sea flights, but flights over several North Pacific storms. During the mission, ten spectrometer files were coincident with surface wave measurements from buoys, including one comparison against a directional spectrum estimated from a NOAA pitch/roll buoy. The agreement in the frequency spectrum was found to be excellent, and overall significant wave height estimates derived from the volume under the 2-d spectrum were found to be unbiased with an rms error of 0.16m. For the directional comparison, the mean wave direction and spread as a function of frequency agreed to within a few degrees.

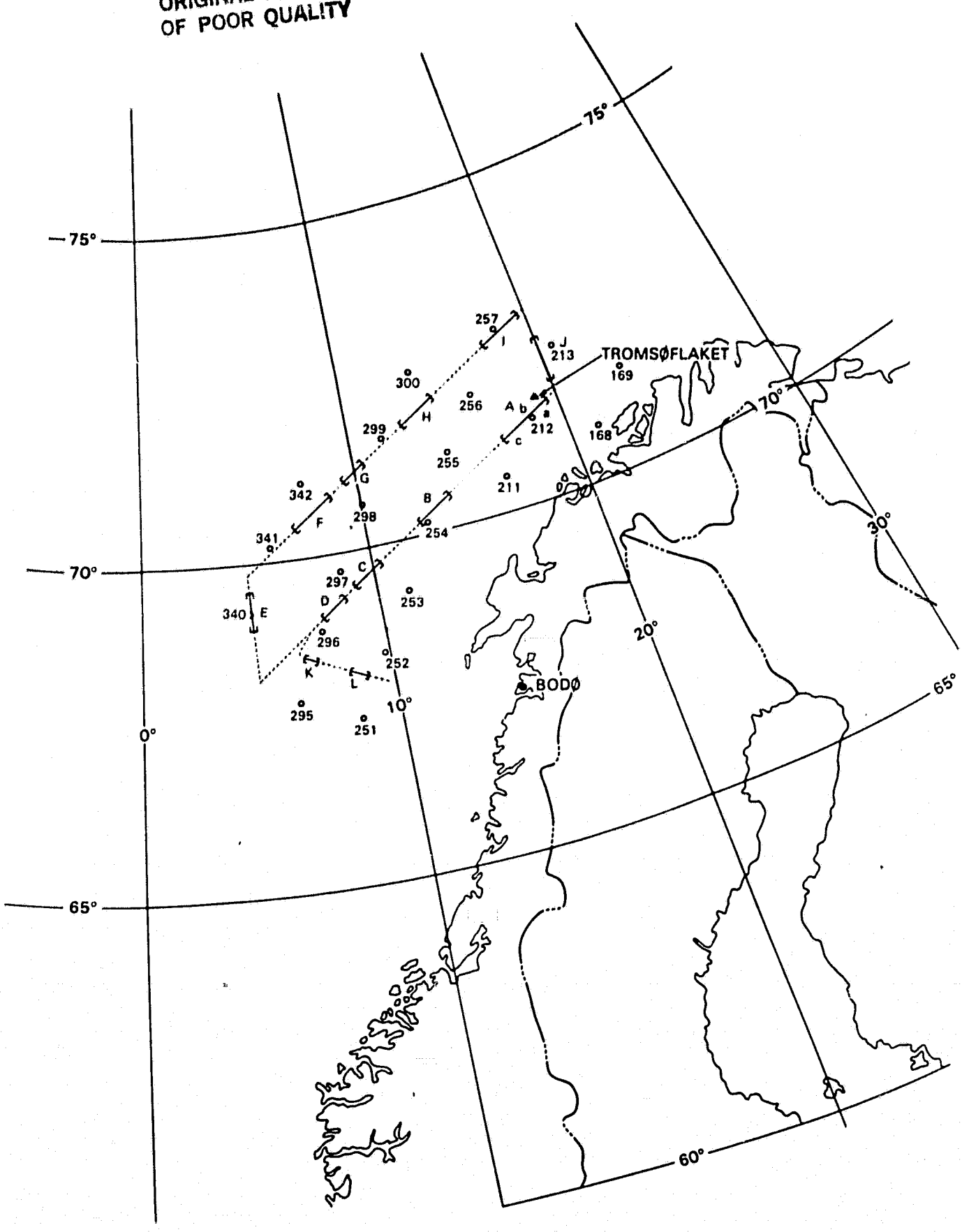

Figure 3.2 Flight path of C-990 during Flight 9, 0800-1000 GMT November 3, 1978, showing flight legs corresponding to ROWS data files A through C, and locations of wave hindcast model grid points near the flight path.

3.5 Hindcast Validation Against In-Situ Tromsoflakket Data

Figure 3.3 compares the specified surface winds at grid points near Tromsoflakket position and the measured winds. The periods for which kinematic analyses were produced are indicated. Measured winds are not available before October 30 because the station was not manned. The sequence of measured winds shows the rapid wind shifts and wind speed changes accompanying the several lows and frontal troughs which passed the station in the period modelled. The storm of 1-3 November was clearly the strongest system in the period studied, and flight 9 is sampling the trailing part of the storm which is shown in the measured time history as a rapidly decaying and shifting wind pattern.

The measured and hindcast significant wave height time histories are compared in Figure 3.4 In this and following figures, the ODGP model hindcast is referred to as hindcast I, and the SAIL model hindcast as hindcast II. The decaying sea states between 29 October and 1 November generally are well simulated by both models. Both hindcasts lead the buildup of seas at the onset of the major storm on 1 November but this may be related to the positive 5-7 knot bias in the analyzed wind speeds seen in the Tromsoflakket wind comparisons during the same period. The significant wave height at the model grid point nearest Tromsoflakket peaks at 2100 GMT 3 November at 10m in the ODGP model and 8m in the SAIL model hindcasts. The wave heights estimated from the buoy data fluctuate rapidly near the storm peak between 8.5 and 11.5 meters. This could be attributable to sampling variability, which for the 17 min 4 sec sampling period introduces an uncertainty in significant wave height of about 10-15%, at the 90% confidence level. The rest of the time series is generally well simulated by both models except for the period between 0000-1200 GMT on 6 November, when the ODGP model responds to the strong southeast winds which were measured early on the 6th, but which apparently did not lead to wave growth at the buoy location. The SAIL model produces a better match here but the comparison is made difficult by the poor resolution, even on the model grid spacing of 100 km, of the fetch at the buoy location and the complicated shoreline geometry upwind for this particular wind direction (about 140°). In summary, both model hindcasts,

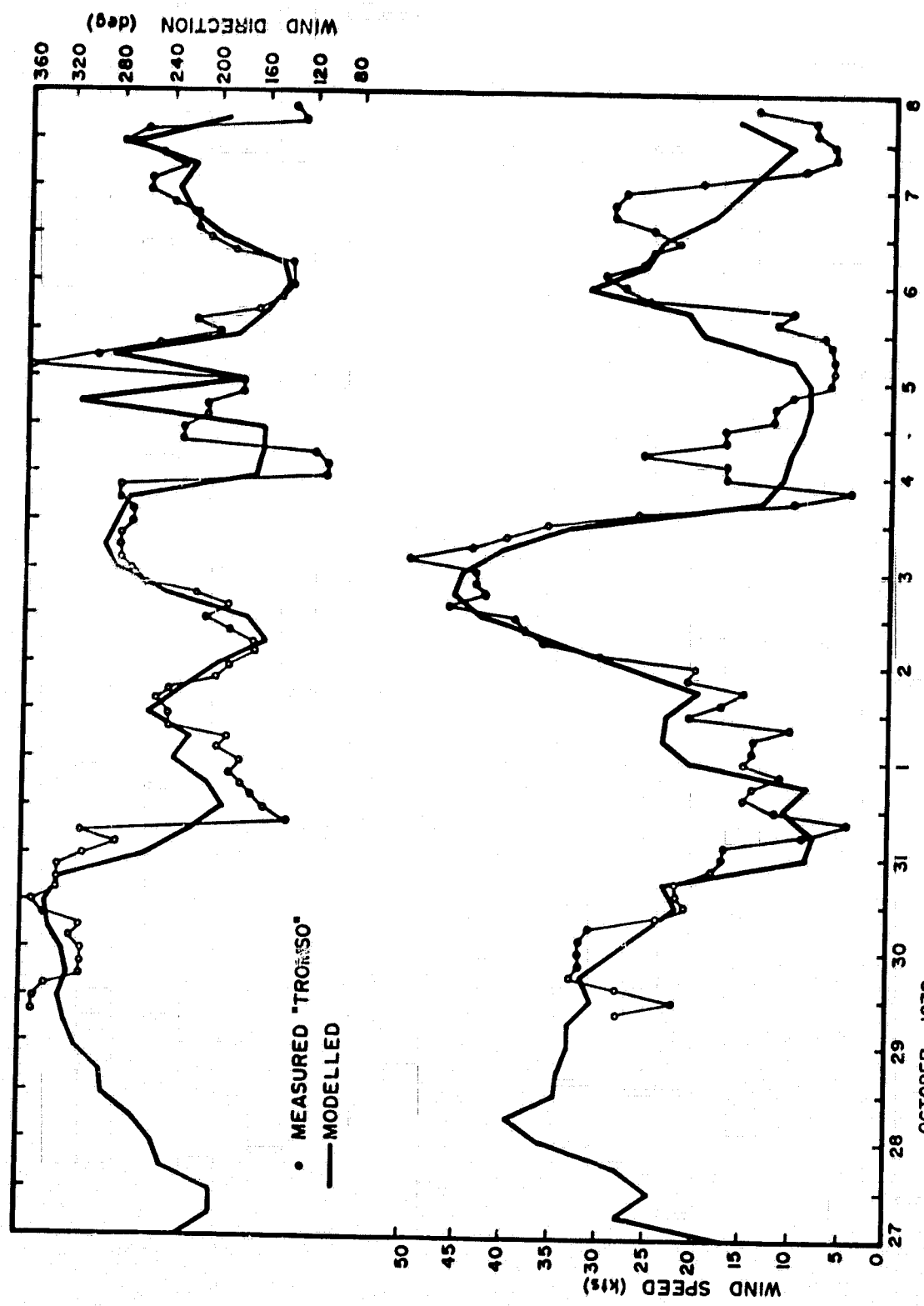

Figure 3.3 Comparison of measured and modelled surface winds at Tromsoflakket location during period of C 0990 Norwegian Sea experiment.

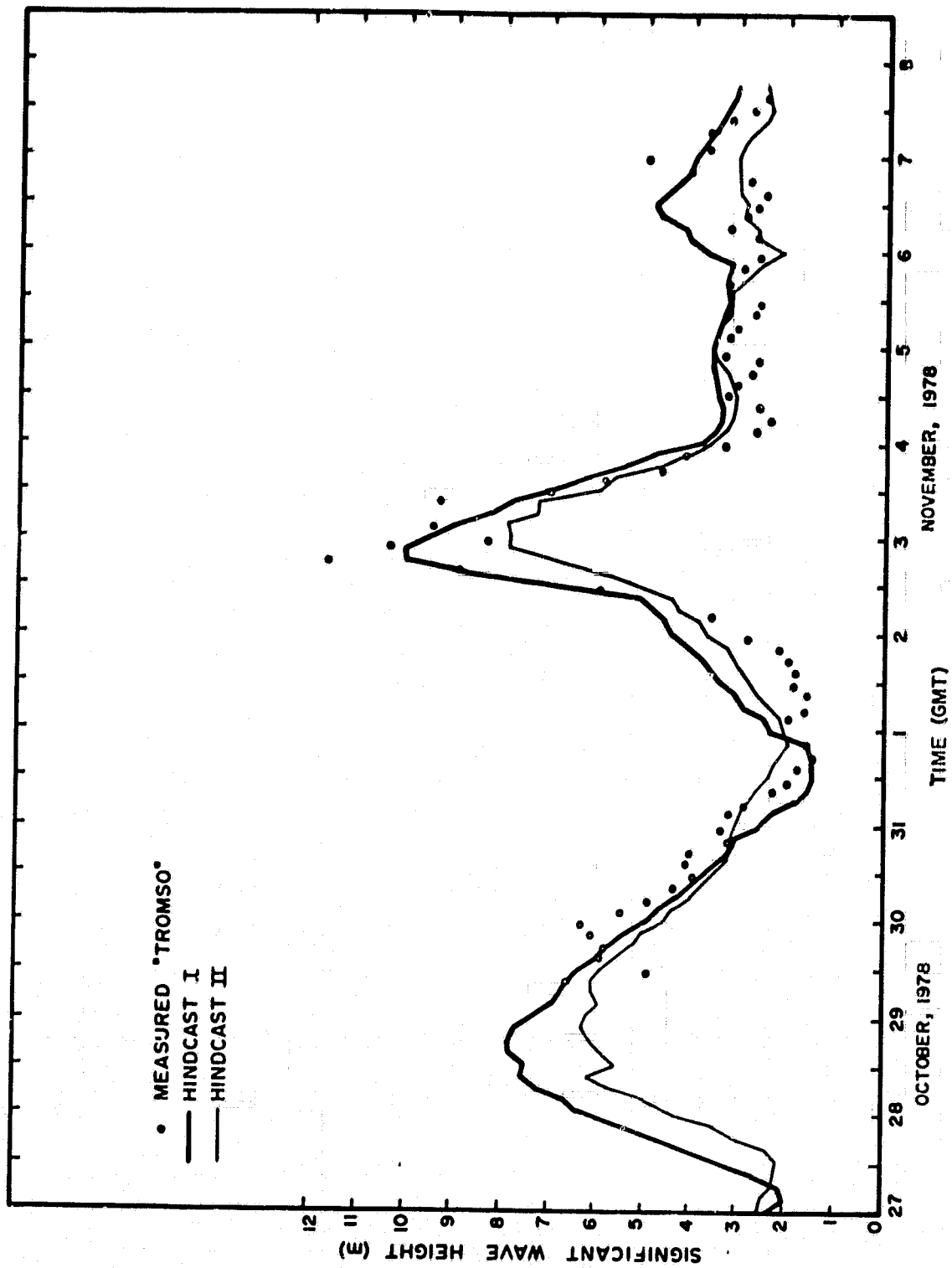

Figure 3.4 Comparison of measured and hindcast (grid point 212) time history of significant wave height at Tromsoflakket.

as validated at Tromsoflakket, display about the same level of skill in hindcasting the significant wave height as shown in previous studies, except that the SAIL model is lower than the ODGP model by about 20% in specification of the peak significant wave height on 3 November.

Figures 3.5 through 3.9 show a number of comparisons of estimated and hindcast frequency spectra at Tromsoflakket. Comparisons are shown for a time near each flight during the experimental period and near the storm peak on 3 November. The spectral comparisons are in a sense selected to produce favorable matches in significant wave height; that is, for a given comparison, the grid point and time step adjacent to the measured location and time respectively, giving the best agreement in $H_{1/3}$, was selected. The matches therefore are intended mainly to reveal errors in spectral shape. The approximate 90% confidence limits on the estimated spectra are 0.6 and 1.9 times the estimated value. The errors in hindcast spectral shape are evidently small. The spectral comparisons show also that the differences between the models at the storm peak (figure 3.9) is in the forward (low-frequency) face of the spectrum, with the ODGP apparently more correctly specifying the spectral peak frequency. It should be noted however, that the SAIL model growth law could be adjusted to produce better agreement though no specific tuning for this storm was performed.

3.6 Comparison of Hindcast and ROWS Wave Data

Jackson et al. (1982) have reduced the radar data collected in Flight 9 in a number of formats. One format, prepared specifically for comparison of the ROWS data with the hindcasts, involved the partitioning of estimated spectral variance over the same frequency and directional bands used in the hindcast model. The 2-d variance spectrum so produced may then be summed over frequency to compare the distribution of total energy over direction, or summed over direction to compare frequency spectra.

The estimated and hindcast frequency spectra for the ten processed ROWS files are compared in Figures 3.10 through 3.19. There is evidently a deficiency of low-frequency energy in the hindcast spectra at all sites, with the SAIL hindcasts more deficient in this regard than the ODGP hind-

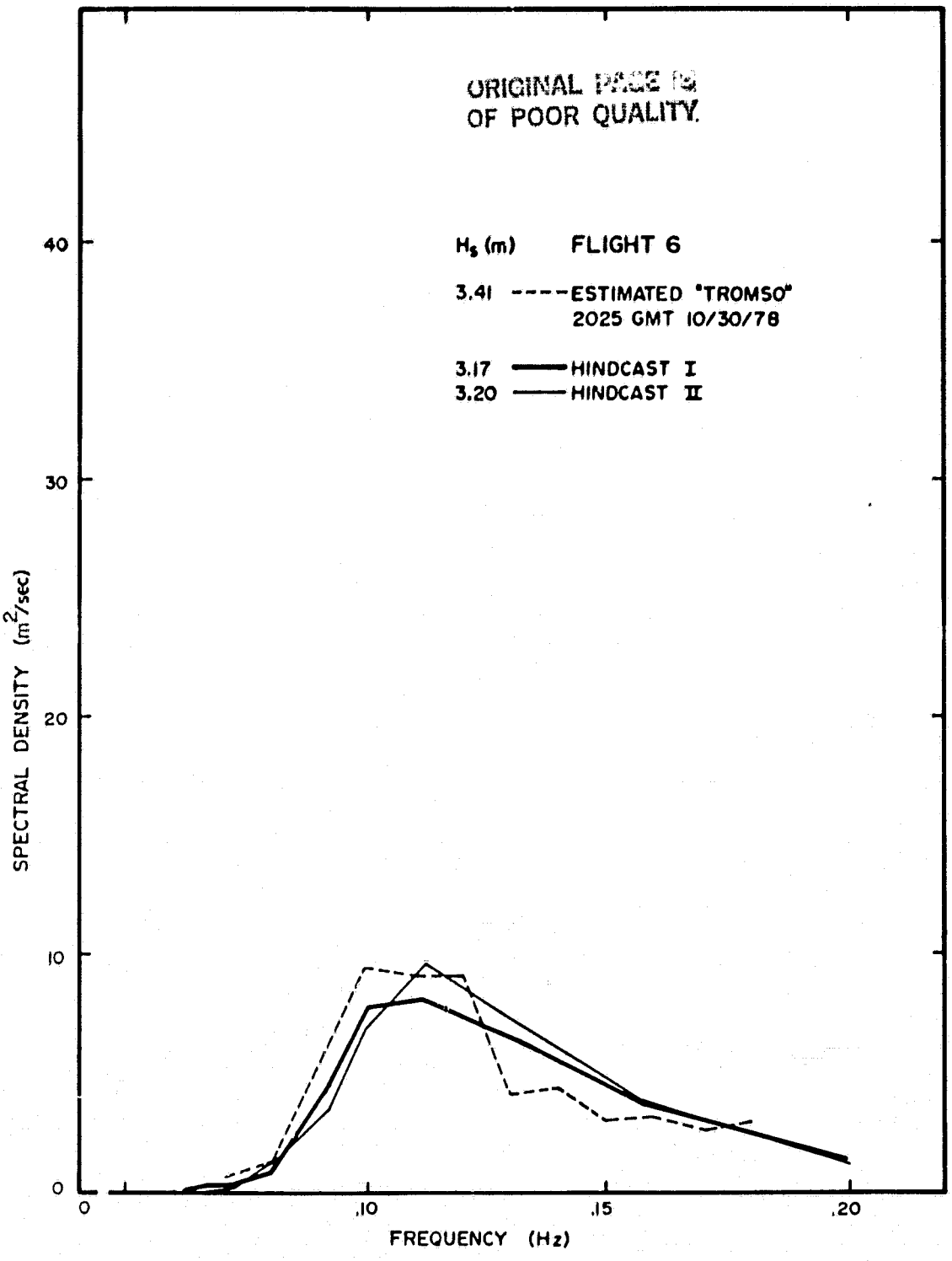

Figure 3.5 Comparison of hindcast and estimated frequency spectrum (from wave rider data) at Tromsoflakket for Flight 6.

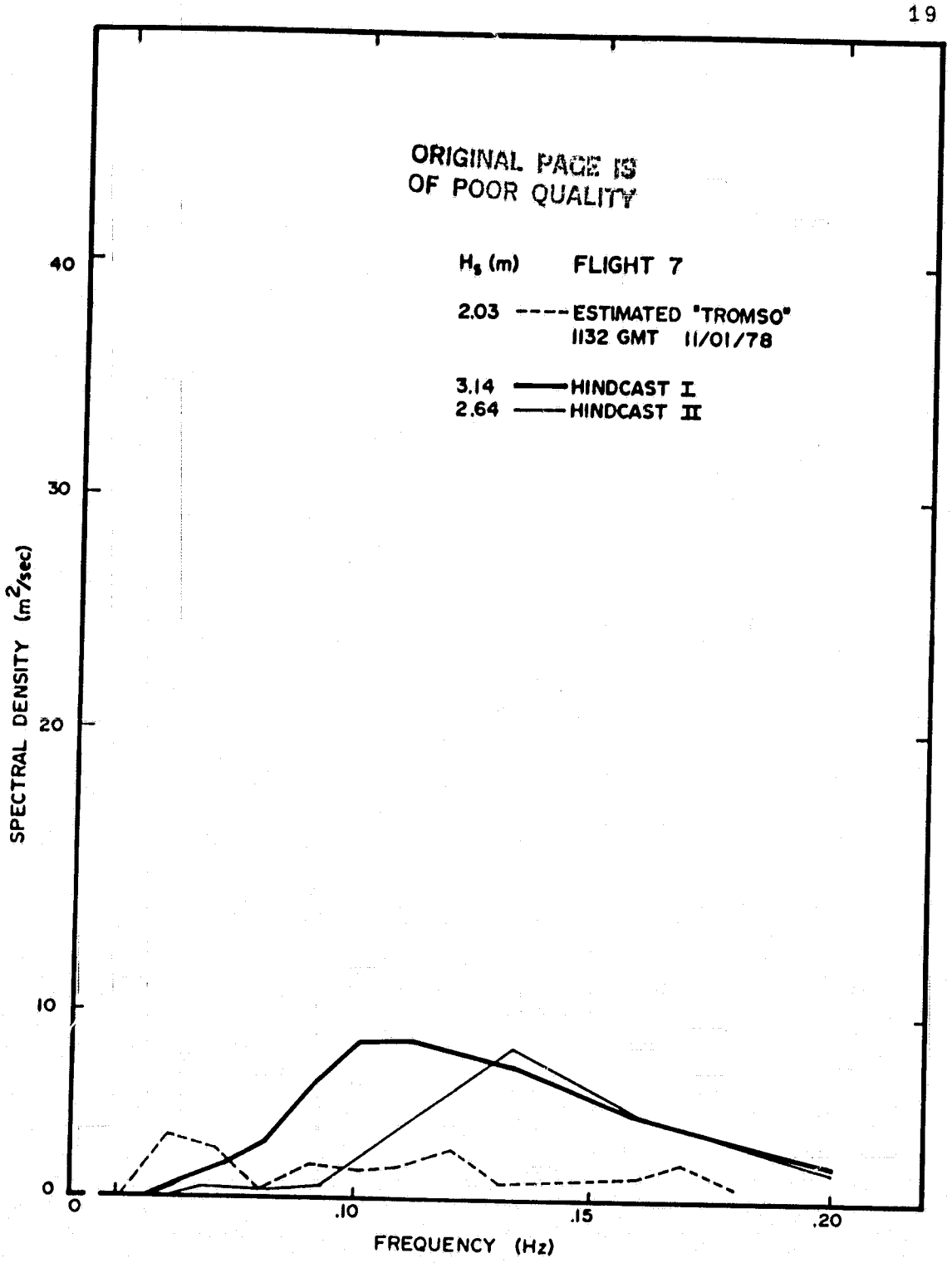

Figure 3.6 Same as Figure 3.5, except near time of Flight 7.

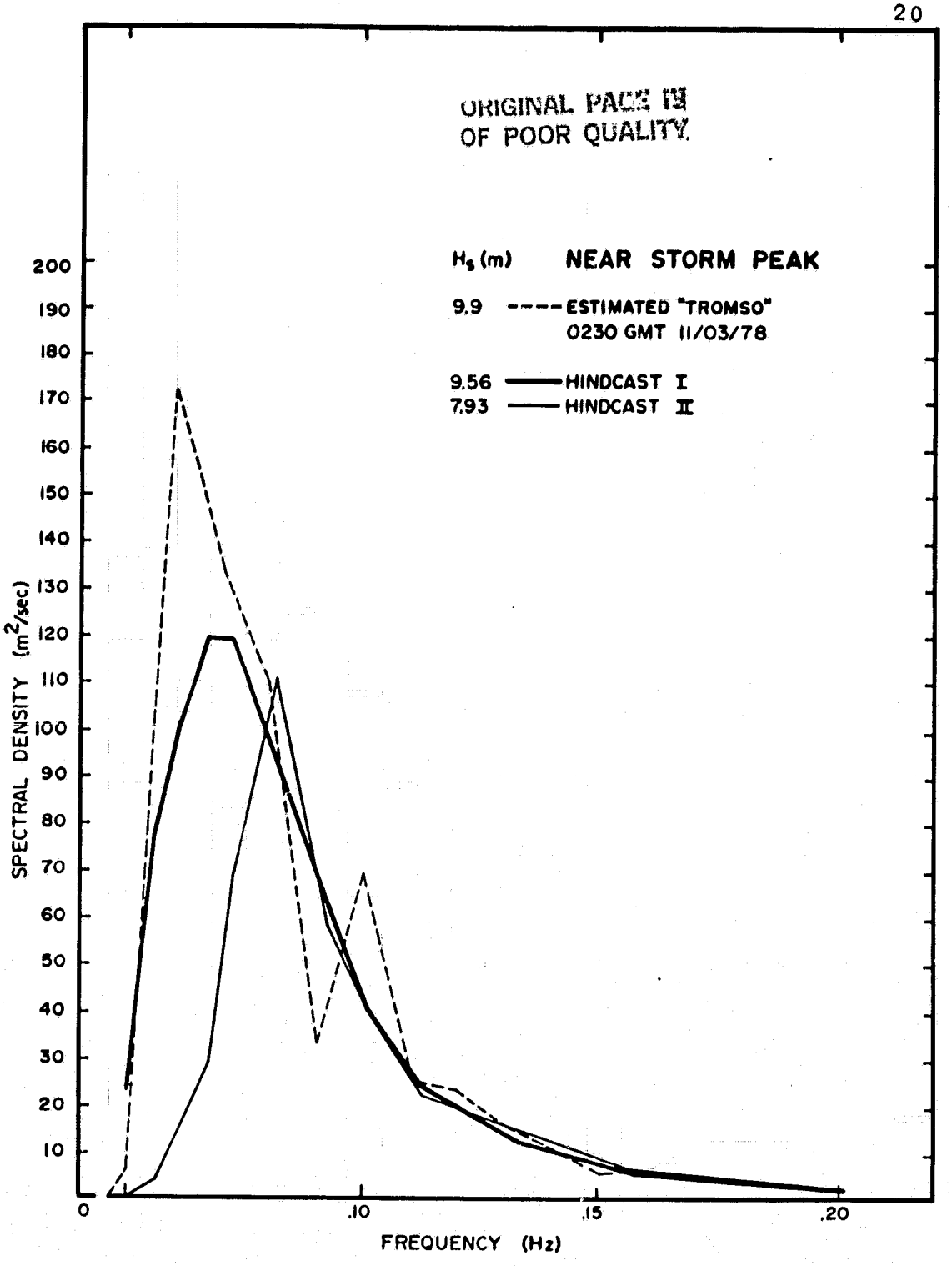

Figure 3.7 Same as Figure 3.5, except storm peak at Tromsoflakket.

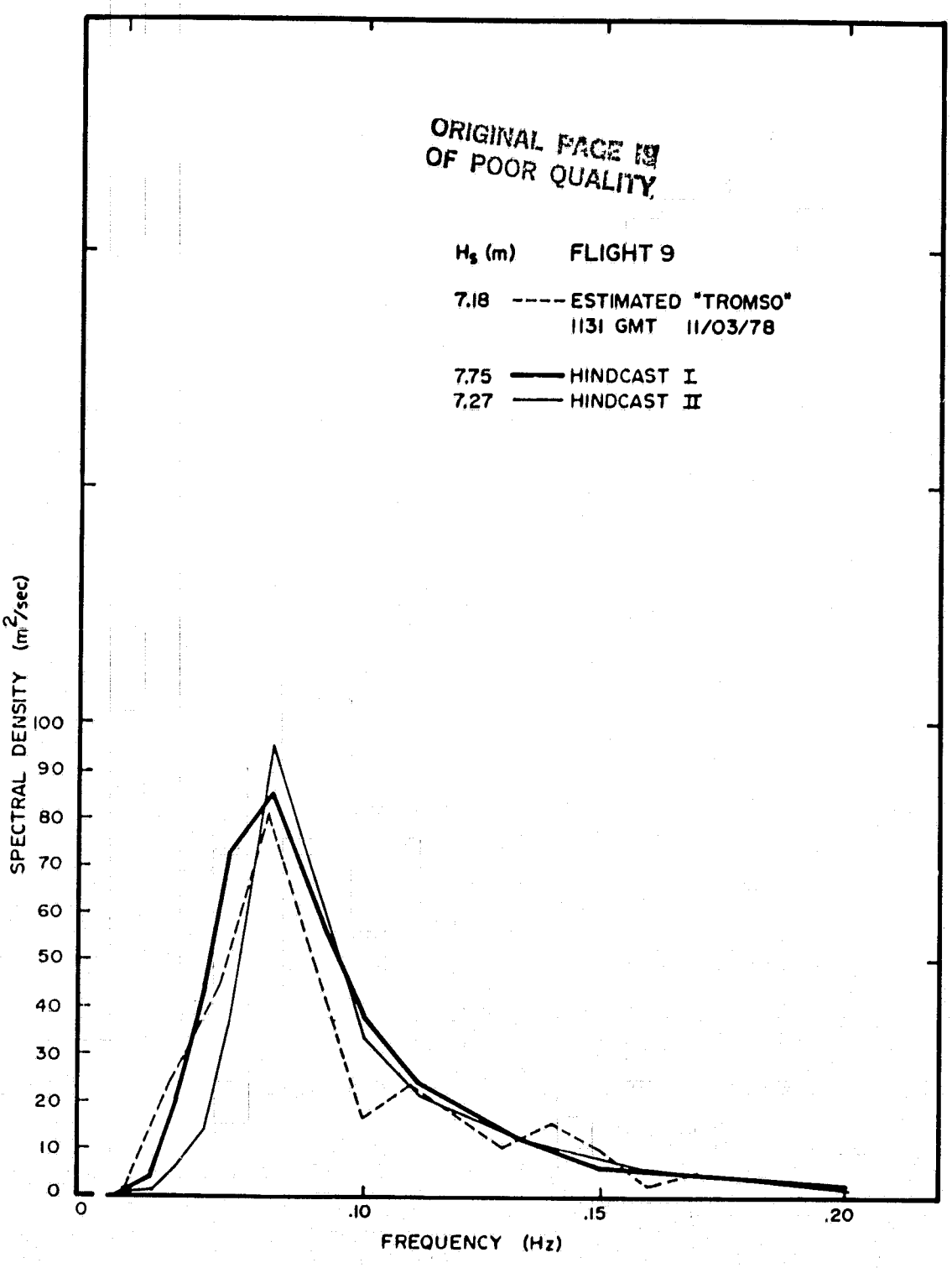

Figure 3.8 Same as Figure 3.5, except near time of Flight 9.

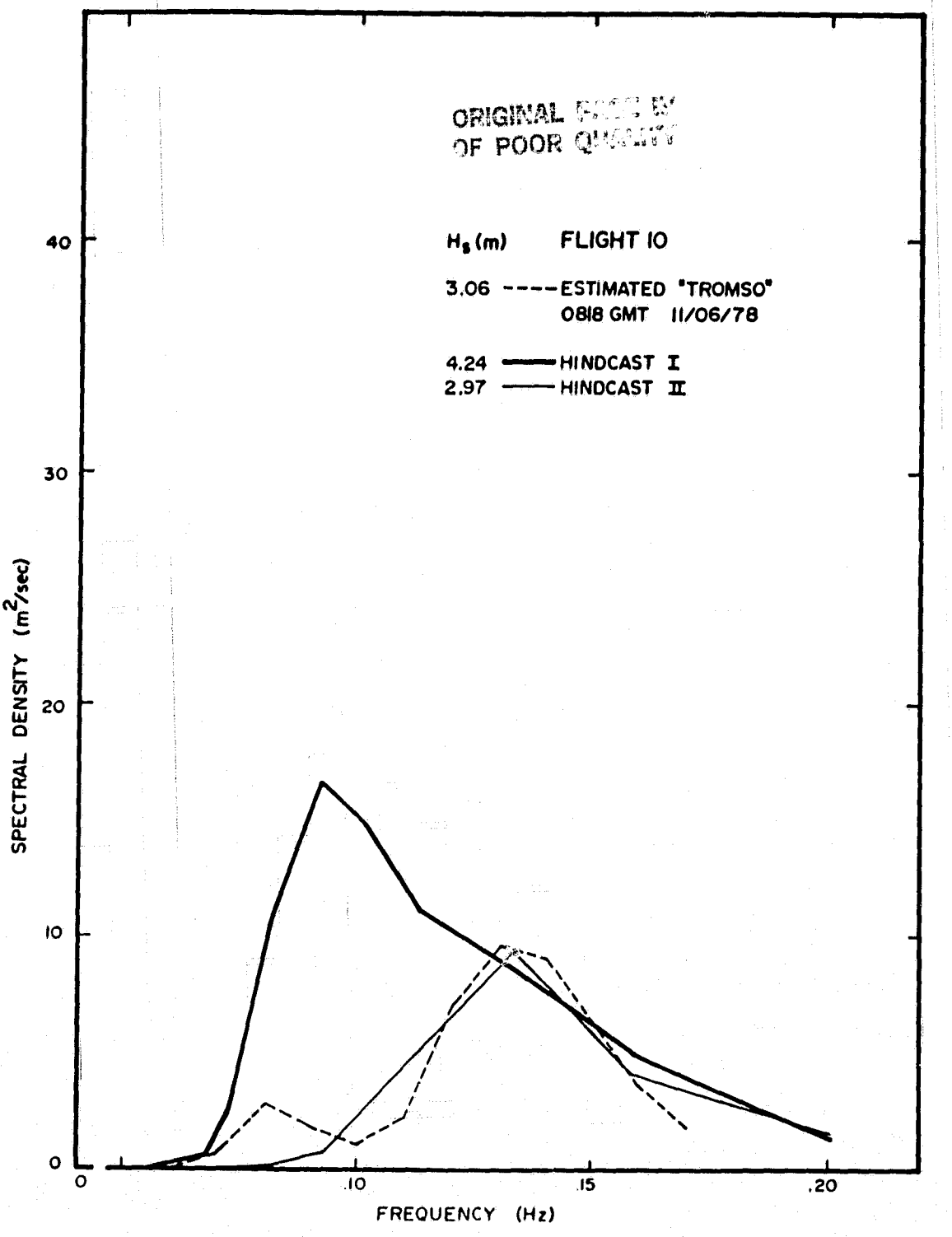

Figure 3.9 Same as Figure 3.5, except near time of Flight 10.

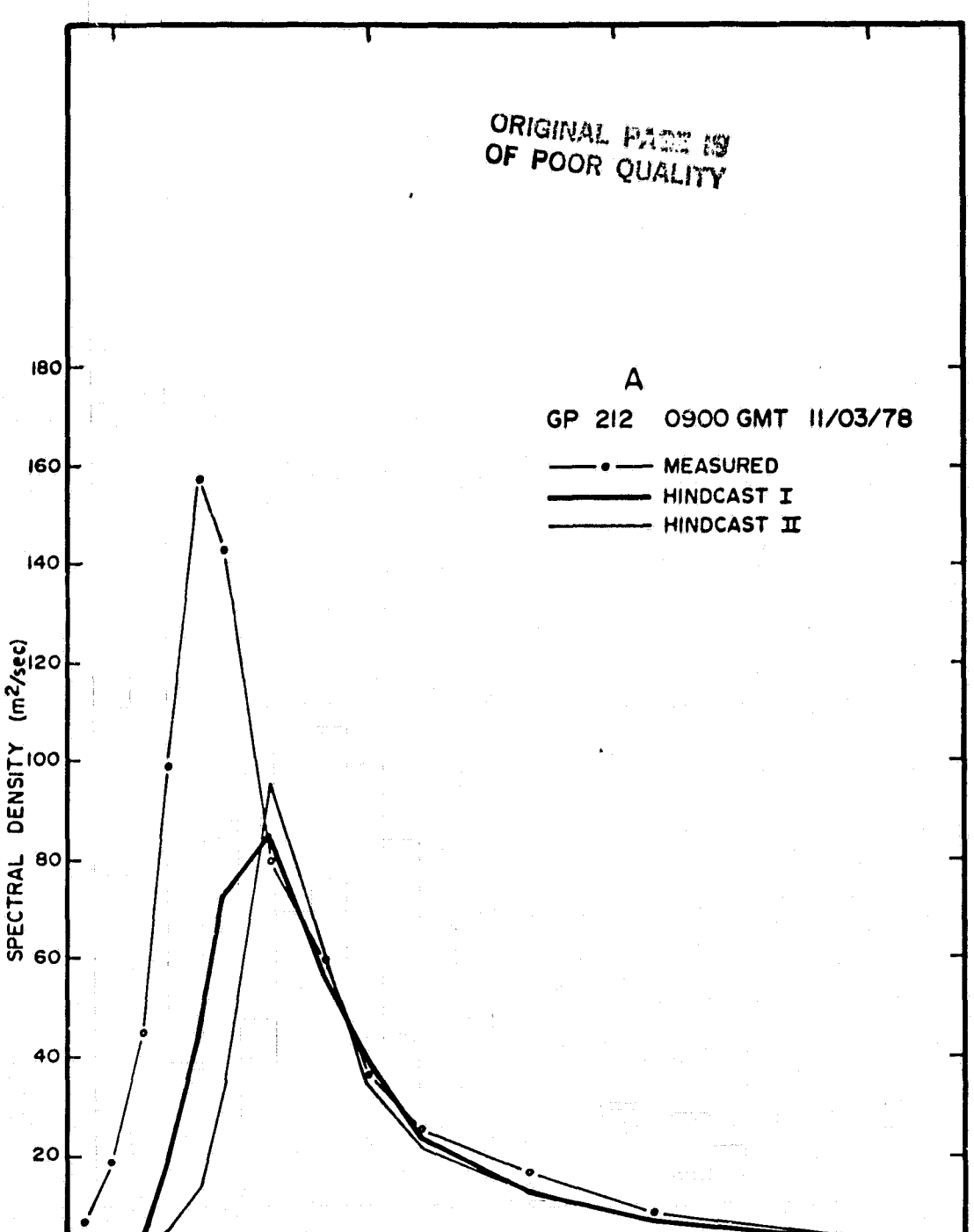

Figure 3.10 Comparison of hindcast and estimated (from ROWS data file A) frequency spectra in Flight 9.

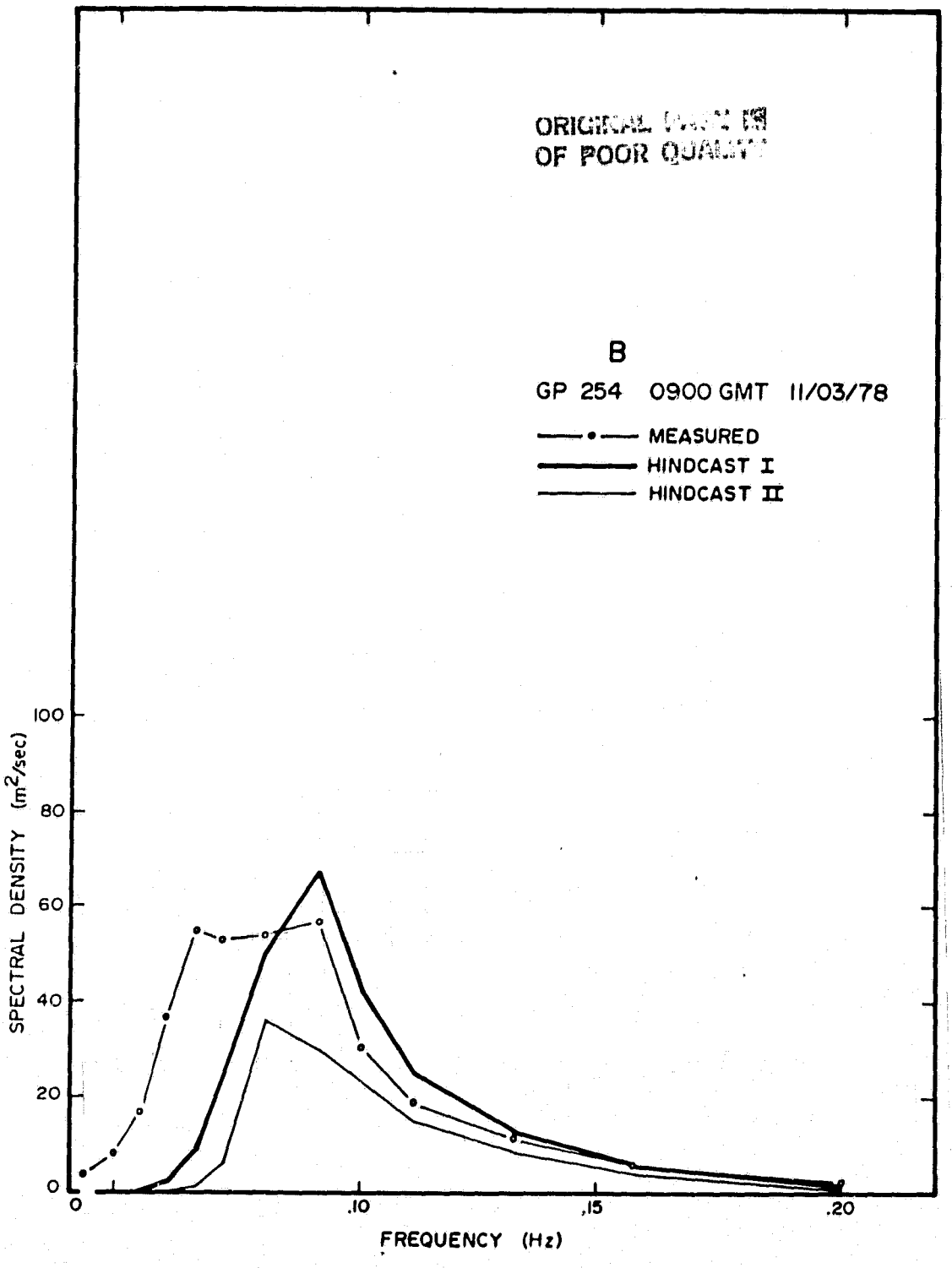

Figure 3.11 Same as Figure 3.10, except for ROWS data file B.

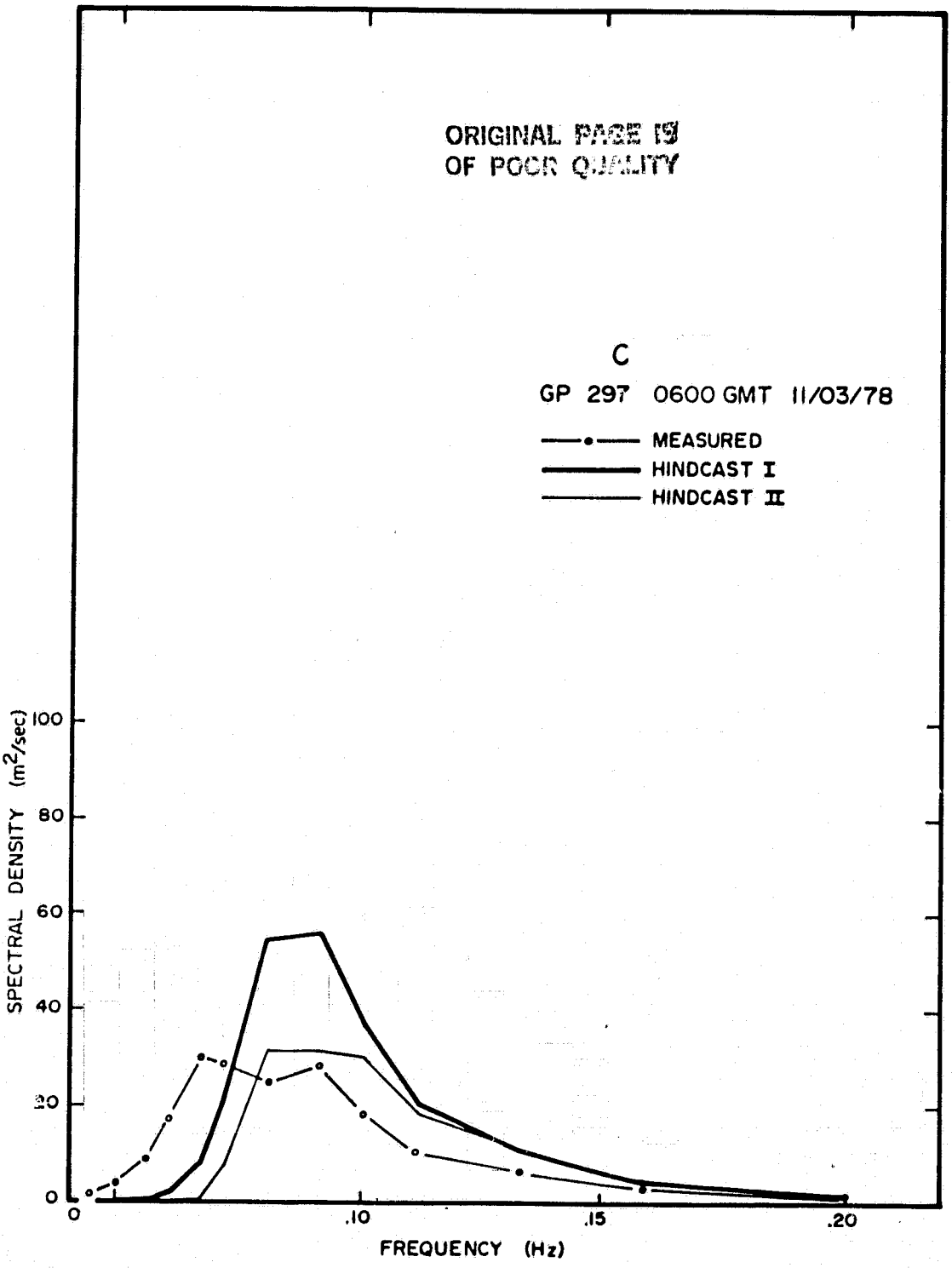

Figure 3.12 Same as Figure 3.10, except for ROWS data file C.

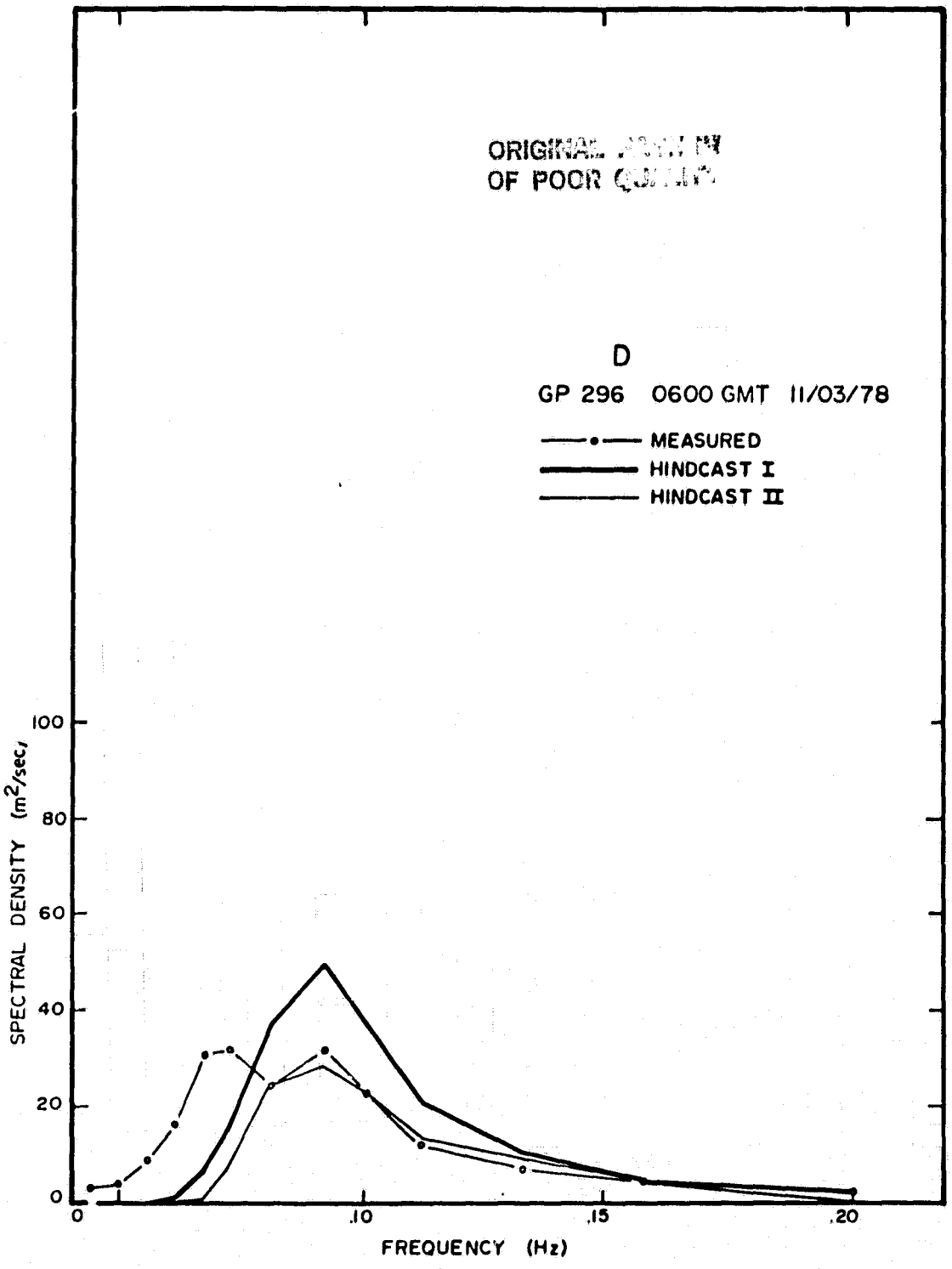

Figure 3.13 Same as Figure 3.10, except for ROWS data file D.

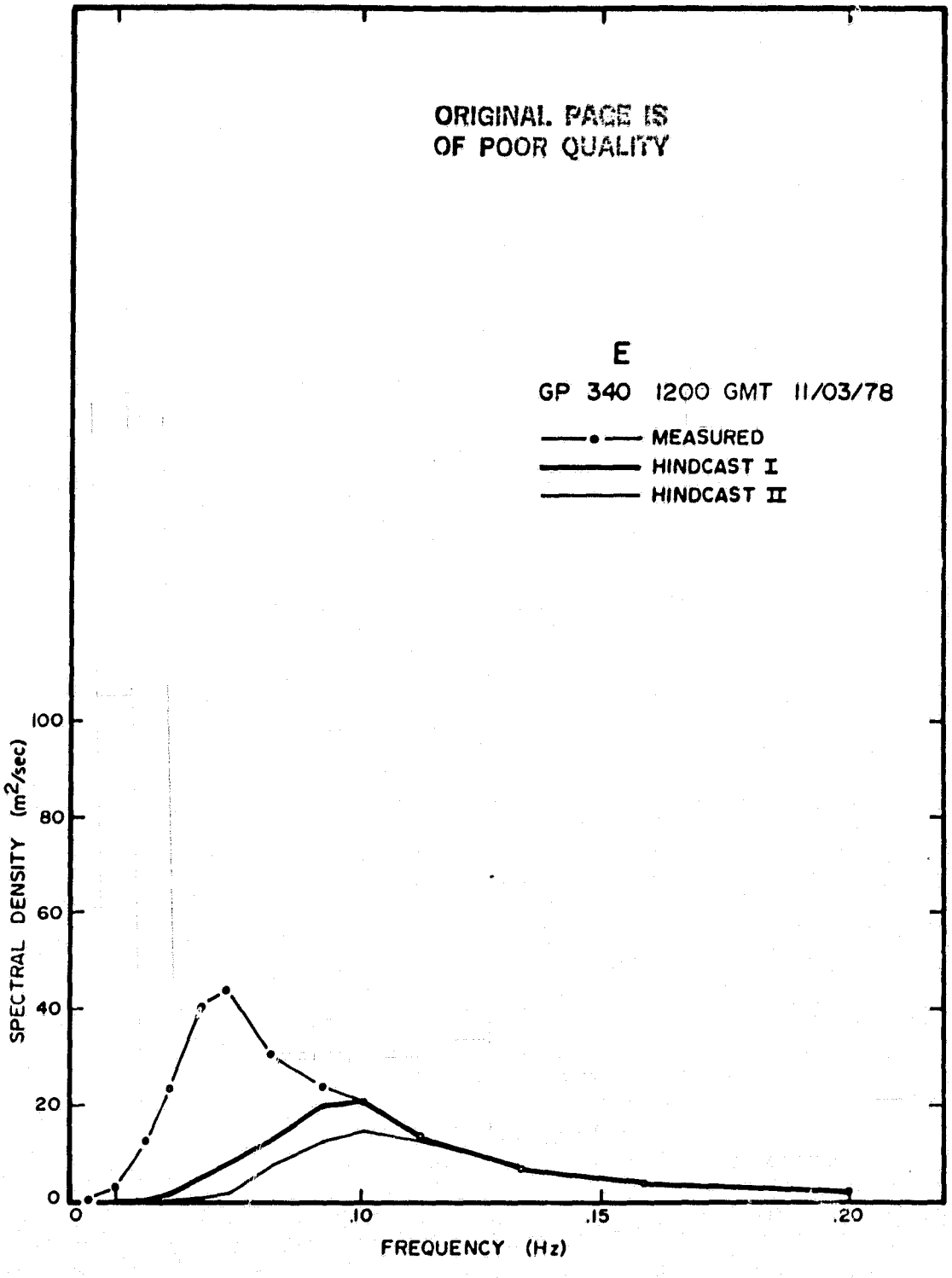

Figure 3.14 Same as Figure 3.10, except for ROWS data file E.

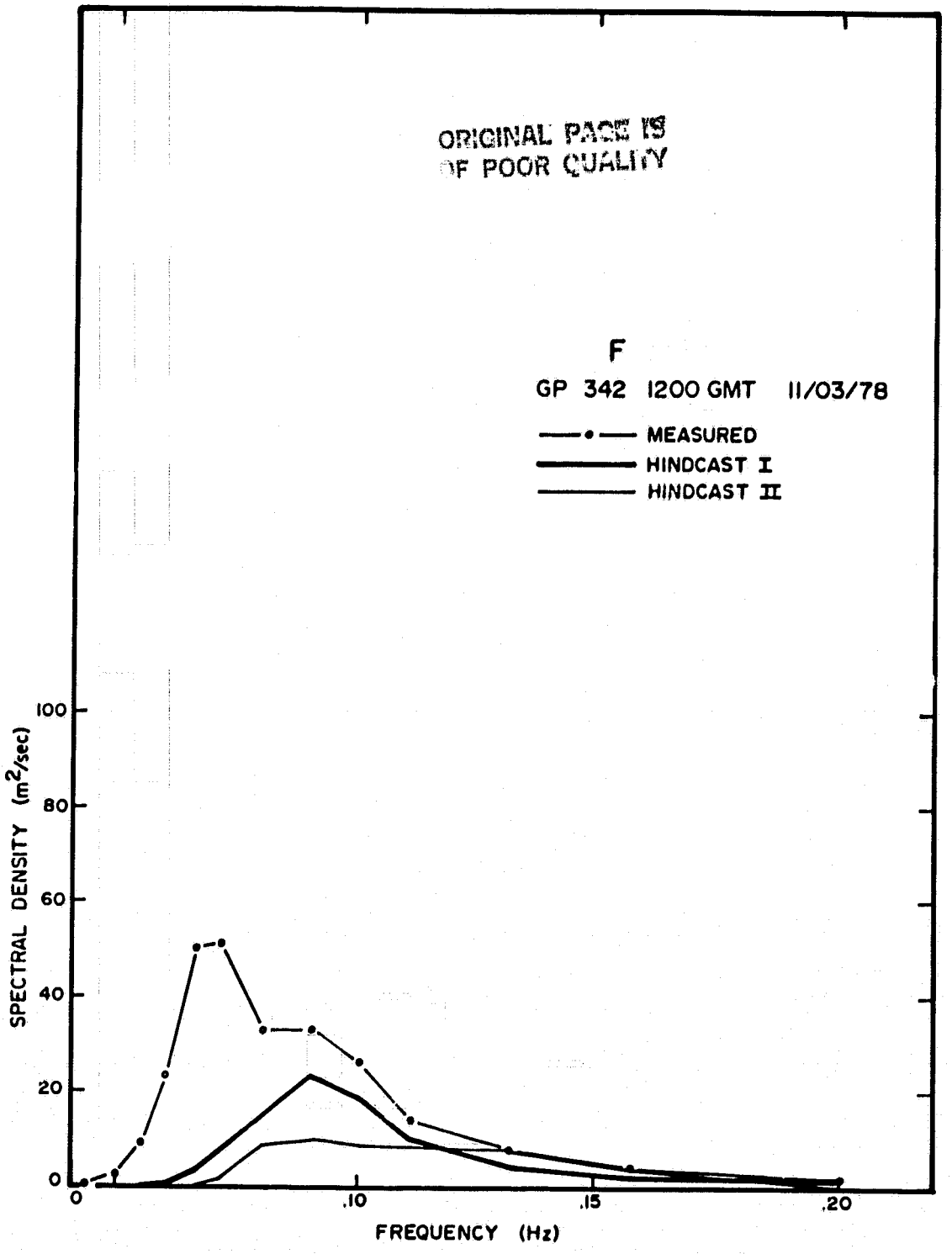

Figure 3.15 Same as Figure 3.10, except for ROWS data file F.

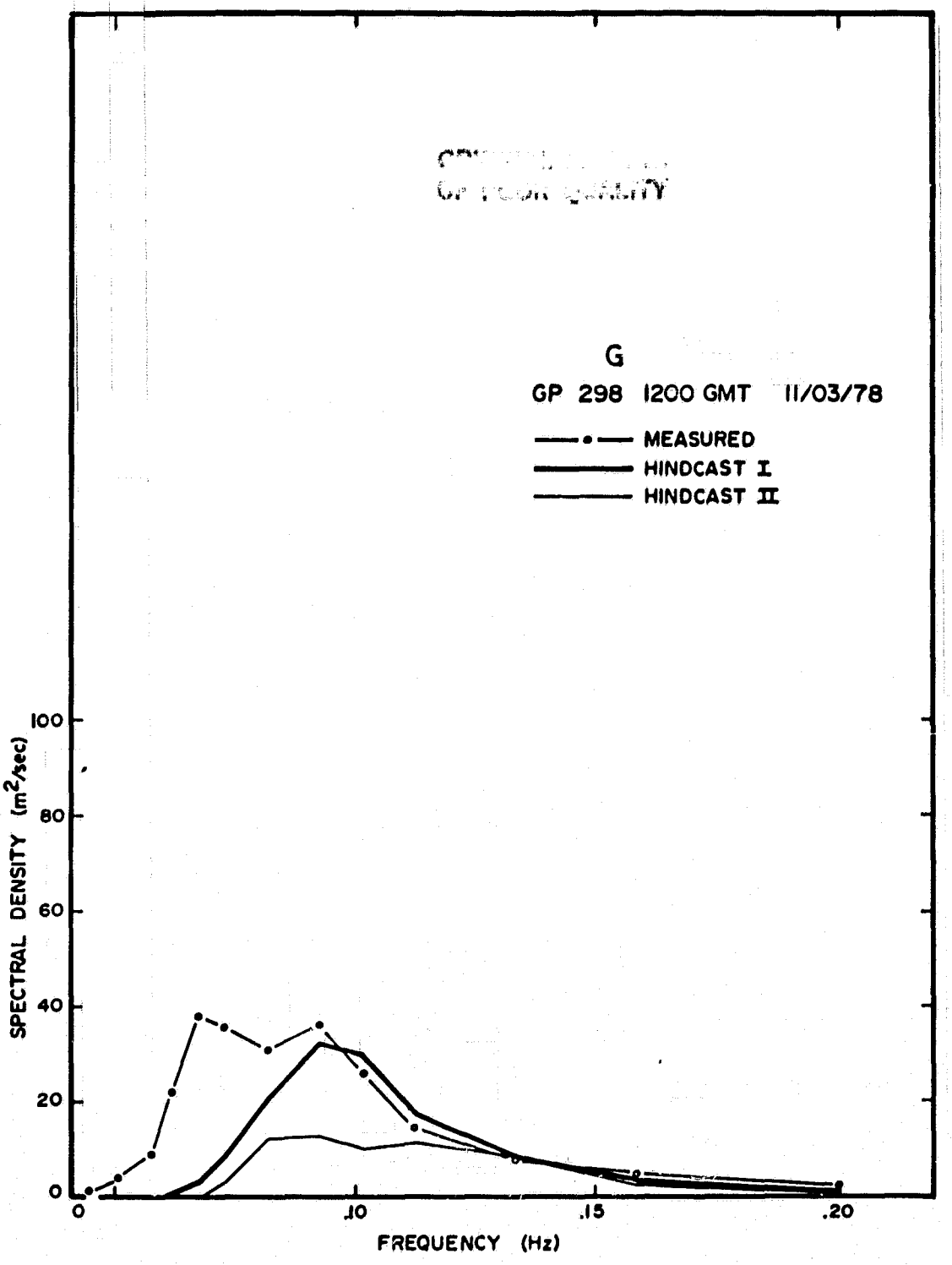

Figure 3.16 Same as Figure 3.10, escept for ROWS data file G.

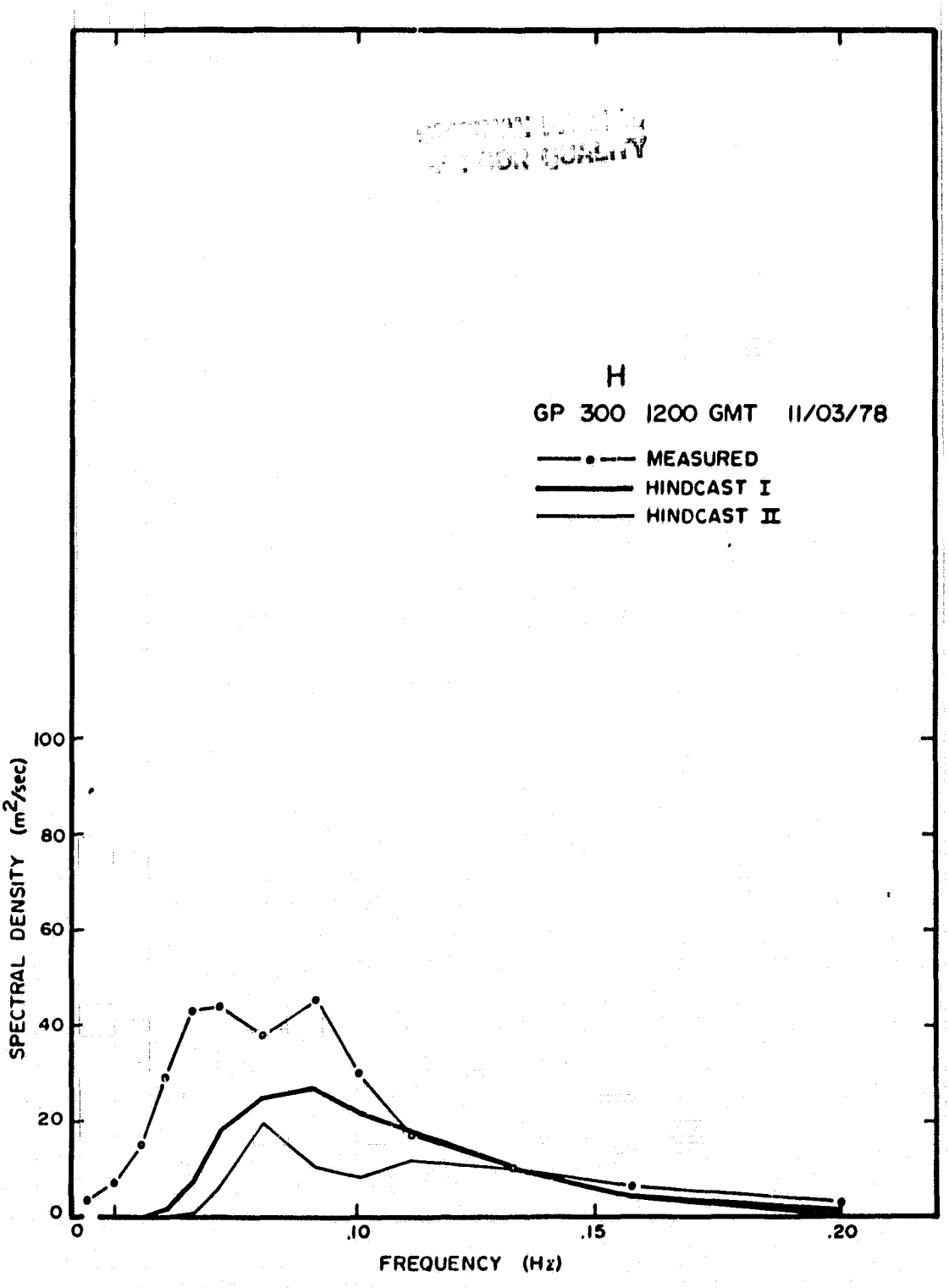

Figure 3.17 Same as Figure 3.10, except for ROWS data file H.

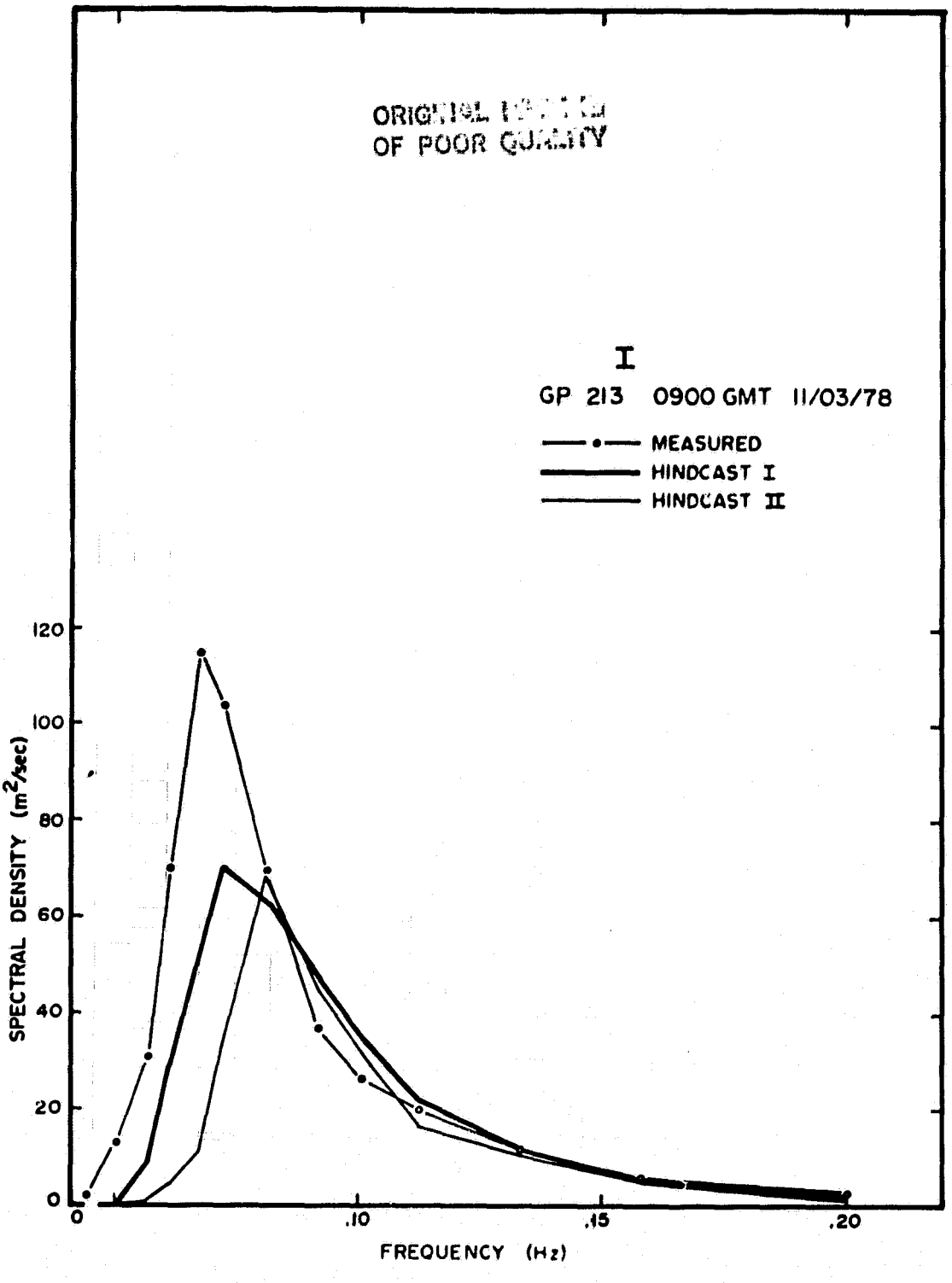

Figure 3.18 Same as Figure 3.10, except for ROWS data file I.

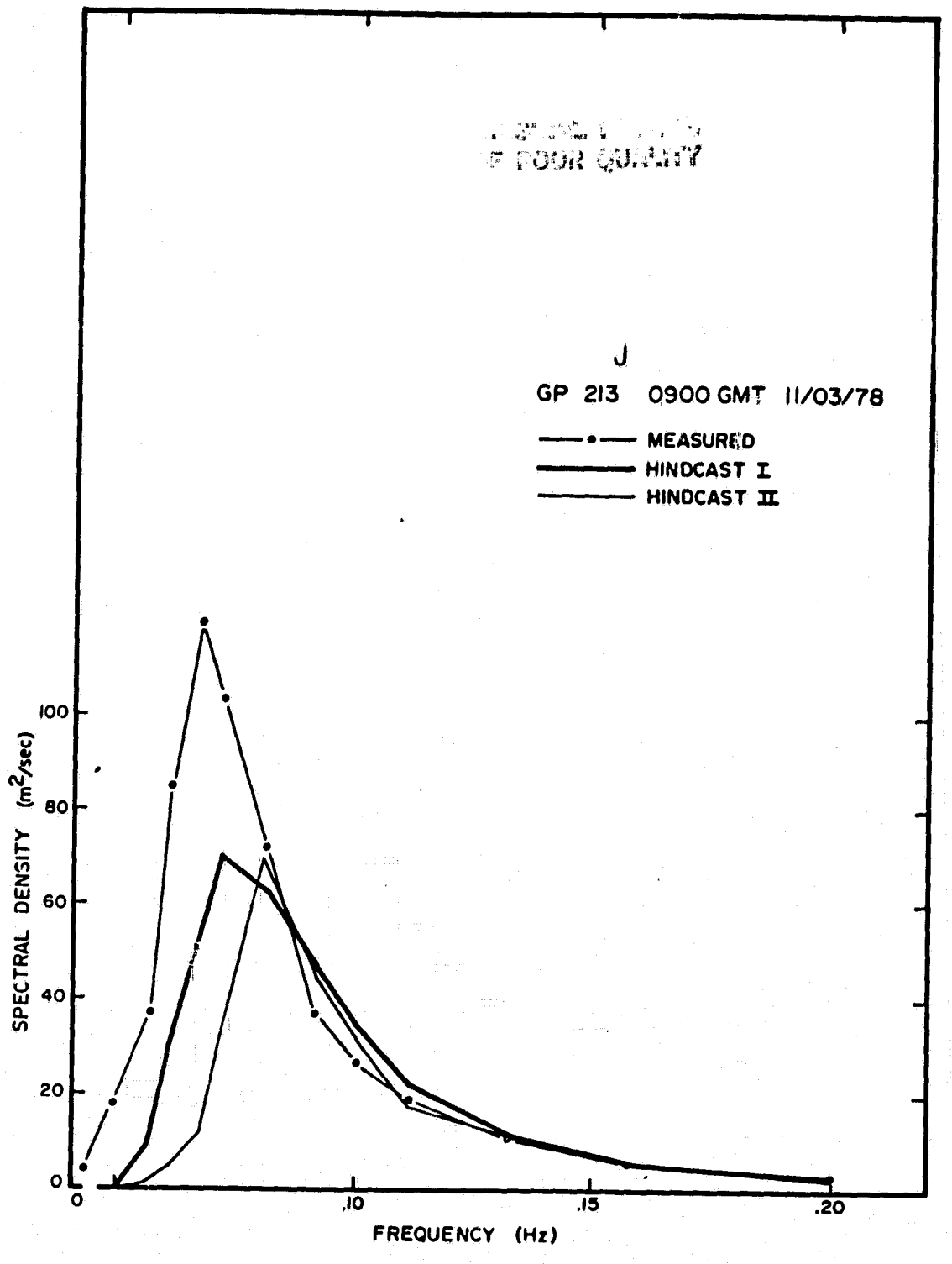

Figure 3.19 Same as Figure 3.10. except for ROWS data file J.

casts. This type of difference was evident also in the wave rider comparison near the storm peak as well (Figure 3.2). Since the ROWS file A frequency spectrum is in very close agreement with the corresponding measured wave rider spectrum (Figure 3.20, Jackson, 1983) the deficiency of low frequency energy in the flight 3 box at the time of the flight is most likely an error in the hindcasts. The hindcast error could have been caused by errors in the wind fields near the storm center earlier in its history or possibly by deficiencies in the formulation or tuning of the spectral growth algorithm.

The directional wave spectra provided by the ten ROWS files have been displayed as contour plots laid out on a map of the Norwegian Sea by Jackson (1983), as shown in Figure 3.21. The contour levels of each plot represent energy levels relative to the peak values, with the estimated zero moment significant wave height values given numerically (meters) beside each plot. This figure provides an unprecedented view of the spatial distribution of the directional wave properties in the rear quadrant of a fast-moving extratropical cyclone. Basically only two nearly orthogonal wave trains are detected. In the northeastern corner of the box, the ROWS file A sampled the 9.5m sea states southwest of the area of peak storm generated seas in the right rear quadrant of the storm. That is the area in which the highest sea states should be expected for a fast moving circular wind field. It is interesting that at A, the surface wind had shifted from southwest[1] to northwesterly about 12 hours earlier but very little energy has been excited in the new wind direction. ROWS files I and J also show only the northeasterly directed wave energy generated in the long fetch of southwesterly winds on the right side, relative to the track, of the cyclone.

- -

[1] wind directions are referred to as "from which", wave directions are referred to as "to which".

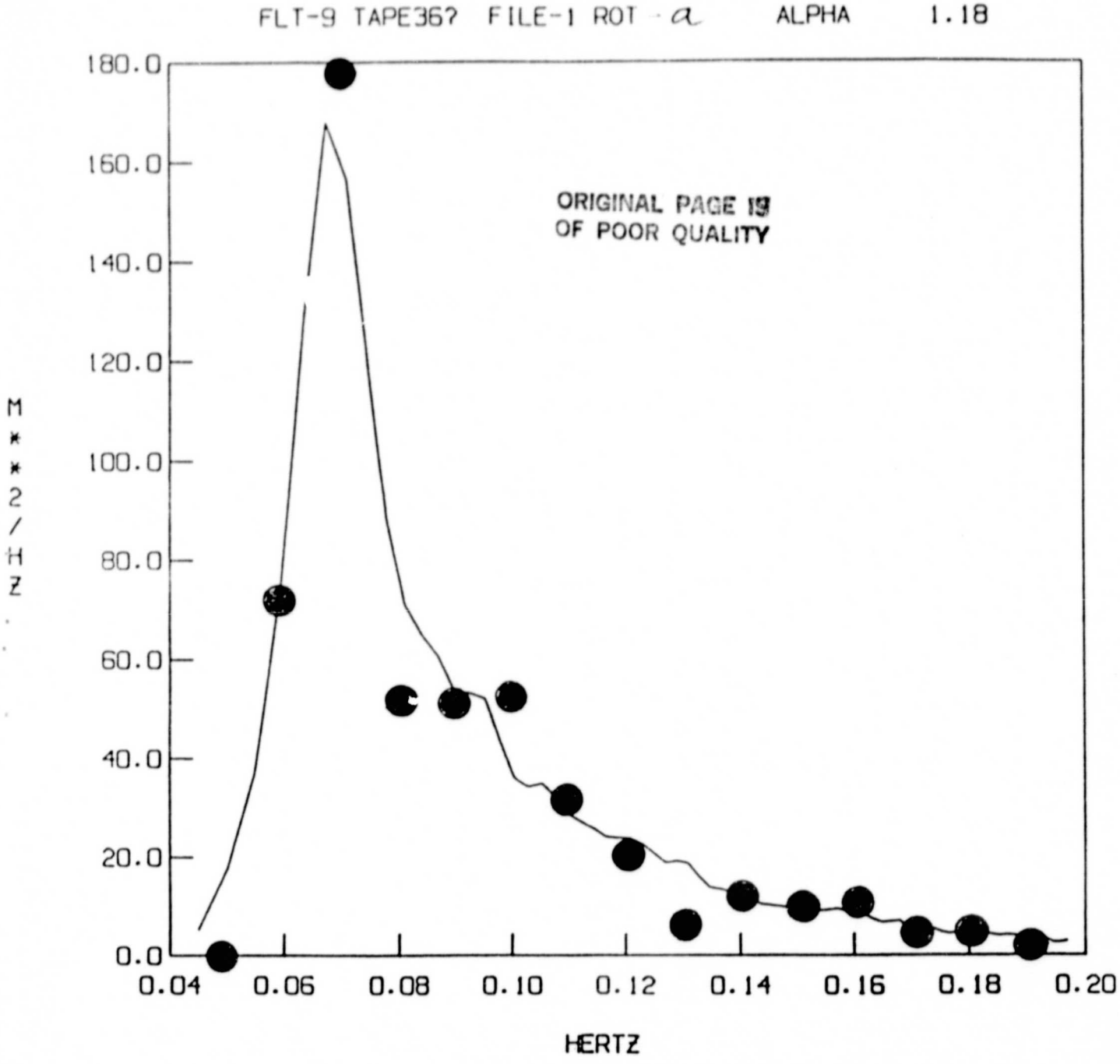

Figure 3.20 Comparison of ROWS frequency spectrum and estimated spectrum from Tromsoflakket, for radar file A Flight 9. (from Jackson, 1983).

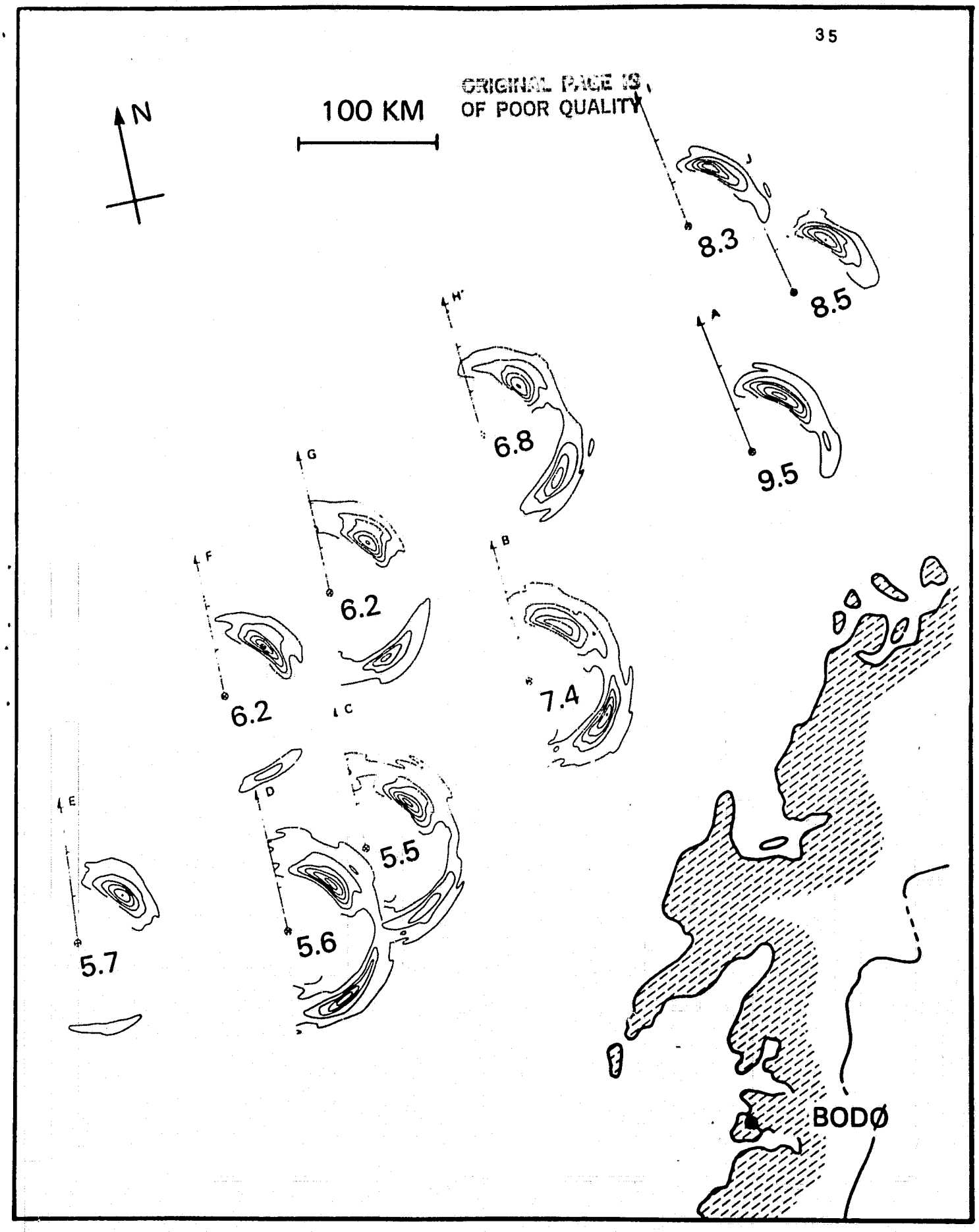

Figure 3.21 Contour plots of directional spectra, shown in the plane of the maps, as estimated by ROWS in files A through J in Flight 9, with the significant wave height (m) also indicated for each measurement.

The northeasterly wave energy is evident also at all other ROWS files in the flight box, where it is best described as "swell" or "dead sea" left behind by the fast moving wind field. It should be recalled that the translation velocity of the wind field varied between 50 and 25 knots between 1-3 November, while the group velocity of spectral components at the spectral peak (~ .068 hz) is only 22 knots.

The southeasterly directed wave energy seen at files B, C, D, F, G, H apparently is a transient pulse of swell propagated into the box from a generating area in the left rear quadrant of the storm as suggested in the isobaric pattern of Figure 3.1. The most striking feature of Figure 3.21 is the absence of wave energy in the directions of the strong-to-gale-force west northwesterly winds which were blowing at the time of the flight in the northeastern half of the box.

To compare the hindcasts and ROWS directional wave spectra we have juxtaposed contoured variance arrays presented in the FNOC/SOWM/ODGP frequency-direction format. The comparisons for files A, B and C, shown in Figures 3.22, 3.23 and 3.24 respectively, represent the kinds of difference observed.

At file A, the ODGP model hindcast shows a relative maximum at a frequency of .0806 and direction of 60°, in good agreement with the ROWS, but the hindcast also produced a second maximum at the same frequency but travelling downwind 105°-120°, where the ROWS shows little energy. However for frequencies higher than about .10hz, the hindcast and the ROWS show maximum energy travelling downwind.

At file B, the ROWS spectrum is distinctly bimodel in direction with one relative maximum in variance at a frequency of .0917 and direction of 135°, and the other at a frequency of .0806 and direction of 45°-60°. The corresponding ODGP spectrum shows both wave trains. Indeed, the two spectra are in good agreement except again for more downwind energy in the hindcast than in the ROWS. Again the SAIL model spectrum is unimodal about the local wind direction. The comparisons at file C are very much like those of file B.

We conclude tentatively, that the directional characteristics of the ODGP model hindcast are remarkably good considering that model development and tuning was based exclusively on nondirectional wave data. There

HINDCAST I

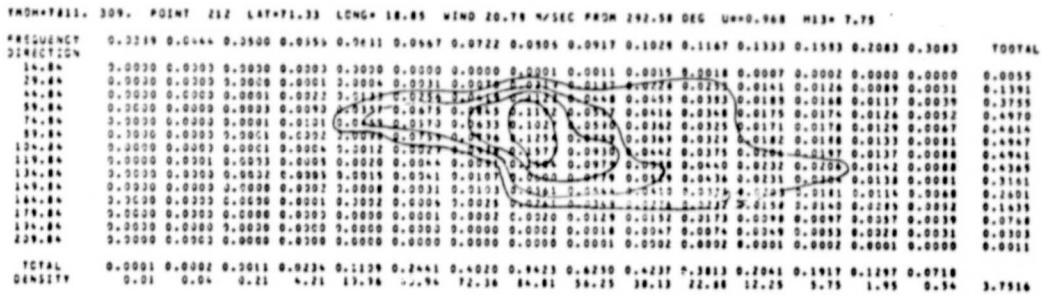

HINDCAST II

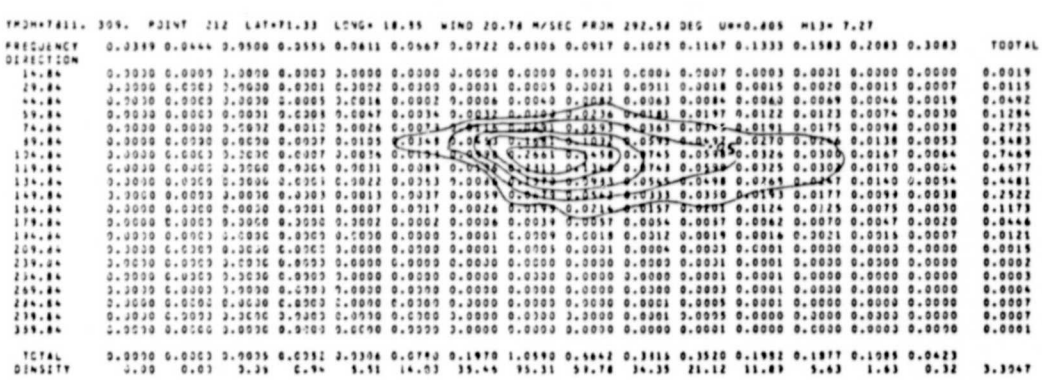

FIGURE 3.22 COMPARISON OF ROWS AND HINDCAST TWO DIMENSIONAL VARIANCE SPECTRA FOR FILE A, IN TERMS OF CONTOURS ON SPECTRAL MATRIX REPRESENTATION IN 15° DIRECTIONAL BANDS AND 15 FREQUENCY BANDS USED IN THE SOWM/ODGP$_2$ MODELS. CONTOUR LEVELS ARE .02, .05, .08, .11, .14 FT^2.

ROWS

HINDCAST I

HINDCAST II

FIGURE 3.23 SAME AS FIGURE 3.22, EXCEPT FOR FILE B.

ROWS

HINDCAST I

HINDCAST II

FIGURE 3.24 SAME AS FIGURE 3.22, EXCEPT FOR FILE C.

is evidence, however that in nature, the growth of downwind wave energy is suppressed relative to the growth rate modelled in the presence of a significant background sea travelling off the local wind direction. There is also a suggestion that the directional relaxation rate of wave energy in a turning wind in the rear face of the spectrum is too fast in the model. These deficiencies of the ODGP algorithm appear to be exaggerated in the SAIL model. That is, the adjustment of the spectrum on both the forward and rear face to the local wind direction is so fast in the SAIL model that the spectrum was almost always specified to have a unimodel directional distribution in the flight box. However, in the SAIL model, the treatment of growth on the forward face and the directional relaxation rate on the rear are readily tunable. ROWS type data provide a hitherto unavailable and powerful basis for such model refinement.

4. QE2 Storm Study of Impact of SASS Winds on Sea State Specification

4.1 Storm Description

The storm which battered the QE2 in September, 1978 has been the subject of several intensive investigations. Gyakum (1980) first collected ship logs and satellite images that allowed a far better definition of the evolution of the storm from conventional data than was possible in real time. In that study, he also began to investigate the physical mechanisms responsible for the development of the storm. Gyakum (1983 a, b) has recently completed a more comprehensive study of the dynamic and thermodynamic structure of the storm.

Cane and Cardone (1981) used the QE2 storm as the basis of a discussion of the potential value of SASS data in improving the detection and forecasting of severe extratropical storms. As part of the evaluation of SASS wind retrieval algorithms, Cardone provided an analysis of surface winds from conventional data alone in two orbit segments over the QE2 storm (see Jones et al., 1982). The storm also was used in the evaluation of SEASAT SMMR wind estimates (Cardone et al., 1983). Finally, the storm scenario has been used to test various numerical weather forecasting models. An extensive series of numerical experiments on the QE2 storm was reported by Anthes et al. (1983).

A general picture of the evolution of the QE2 storm is depicted in Figures 4.1 a-l, which are sections of the 6-hourly Northern Hemisphere Surface Analyses prepared in real time at the NOAA National Meteorological Center (NMC). The storm formed on a stationary front which extended from the Great Lakes into the Atlantic near Delaware at 0000GMT 9/9/78. A small low on the New Jersey coast is shown on the front at 0600 GMT 9/9/78 as the first sign of development. By 1200 GMT the center had moved eastward between two NOAA data buoys 44003 and 44004. At that time, buoy 44004 measured surface winds (at 5m) of 32 knots from the northwest, indicating that surface winds had already reached gale force. Winds also reached gale force on Georges Bank during the afternoon, where the fishing dragger Captain Cosmo was lost.

The storm moved eastward at first early on the 10th then northeastward very rapidly, crossing the N. Atlantic shipping lanes on the 10th

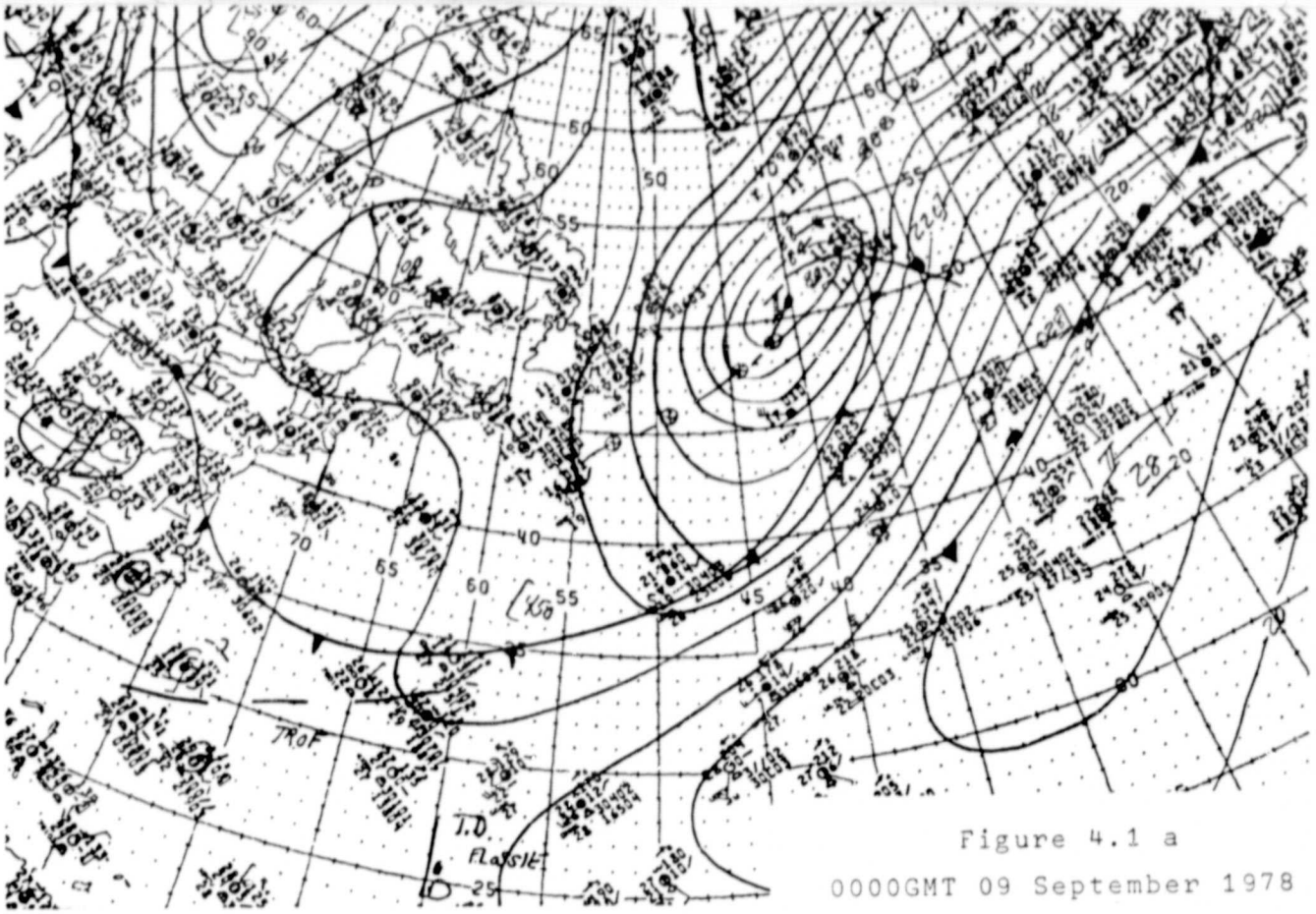

Figure 4.1 a

0000GMT 09 September 1978

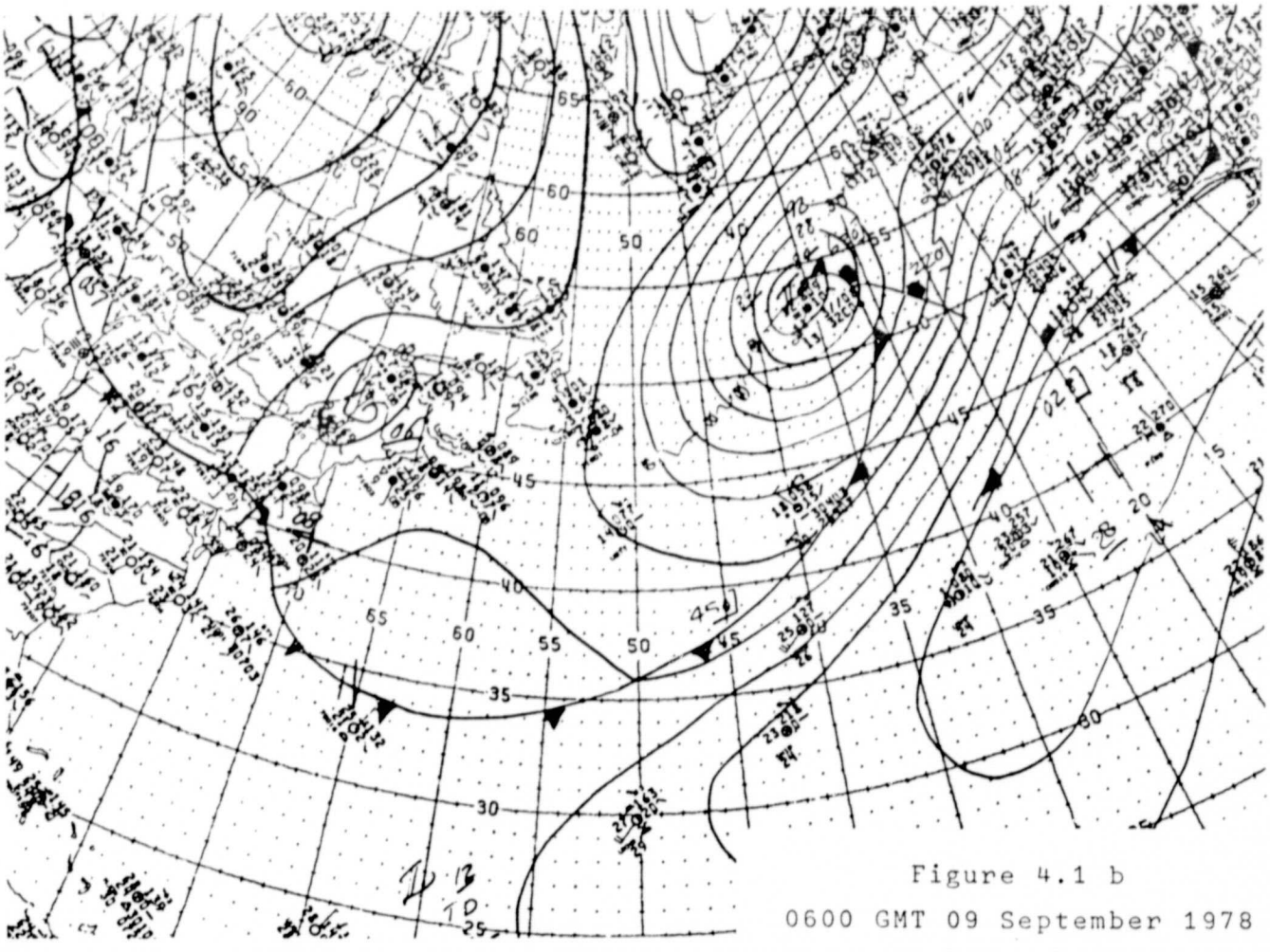

Figure 4.1 b

0600 GMT 09 September 1978

Figure 4.1 a-l. NMC final analysis surface weather maps at 6-hourly intervals. 0000 GMT 9 September 1978 - 1800 GMT 11 September 1978.

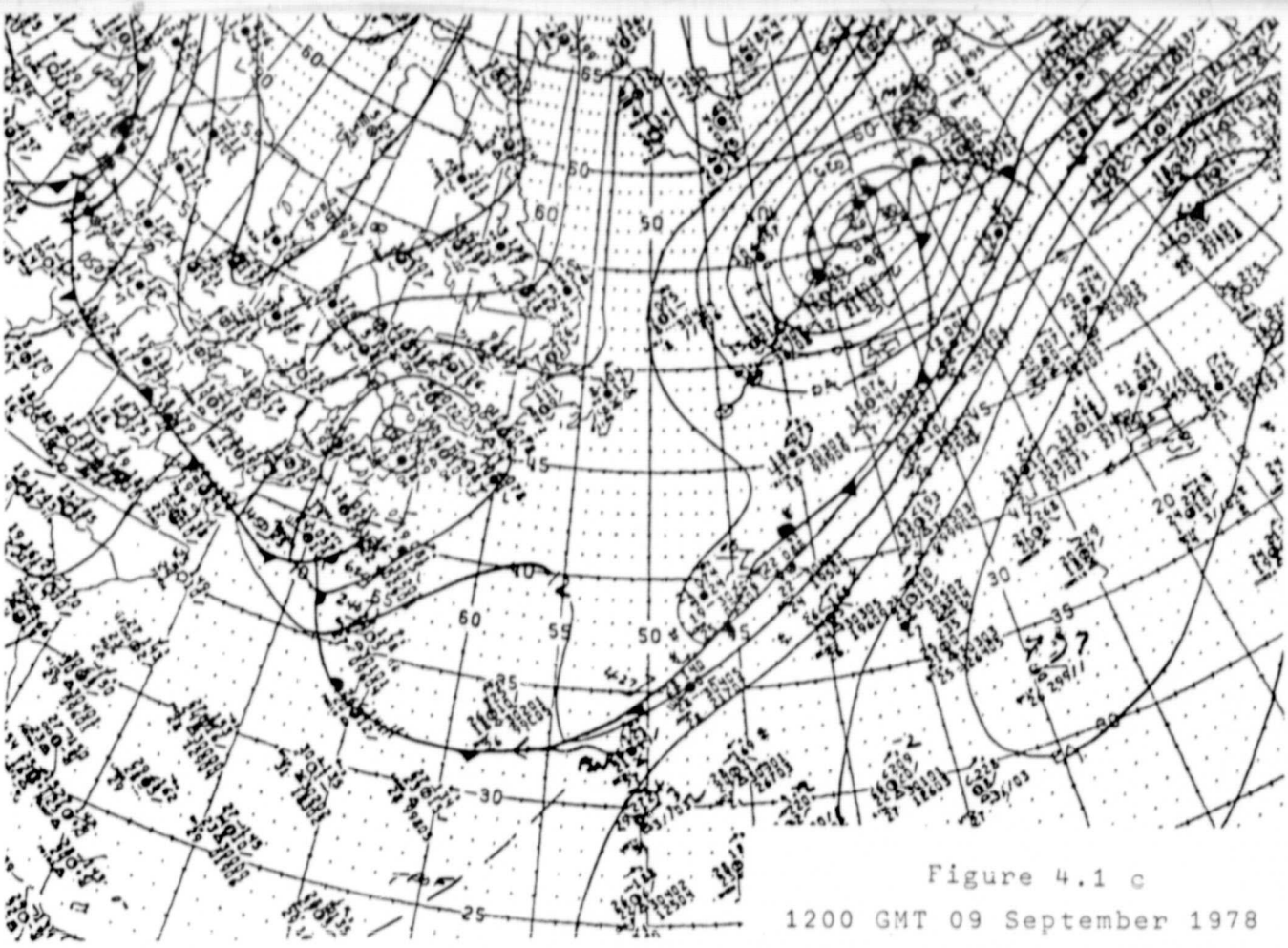

Figure 4.1 c
1200 GMT 09 September 1978

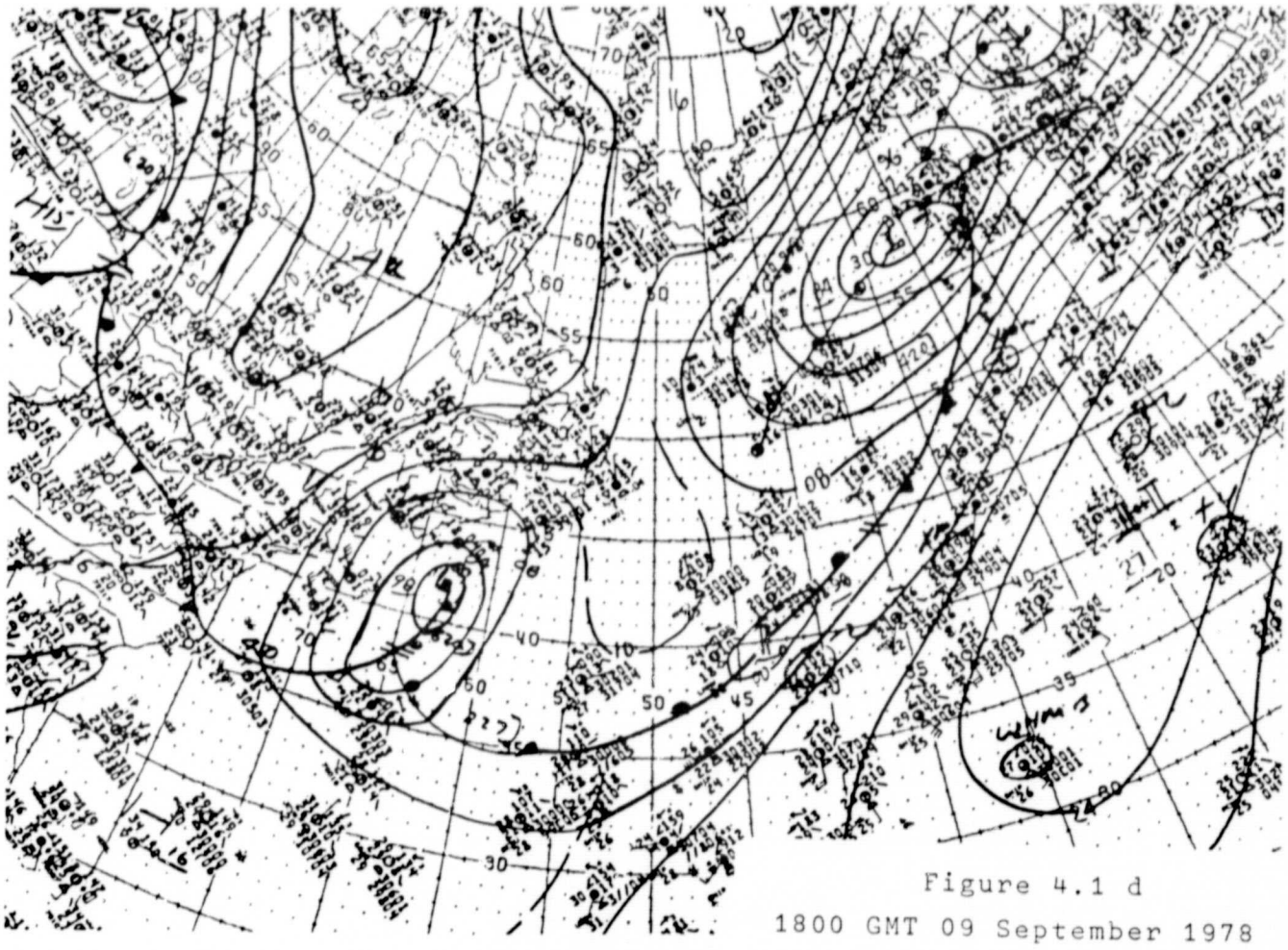

Figure 4.1 d
1800 GMT 09 September 1978

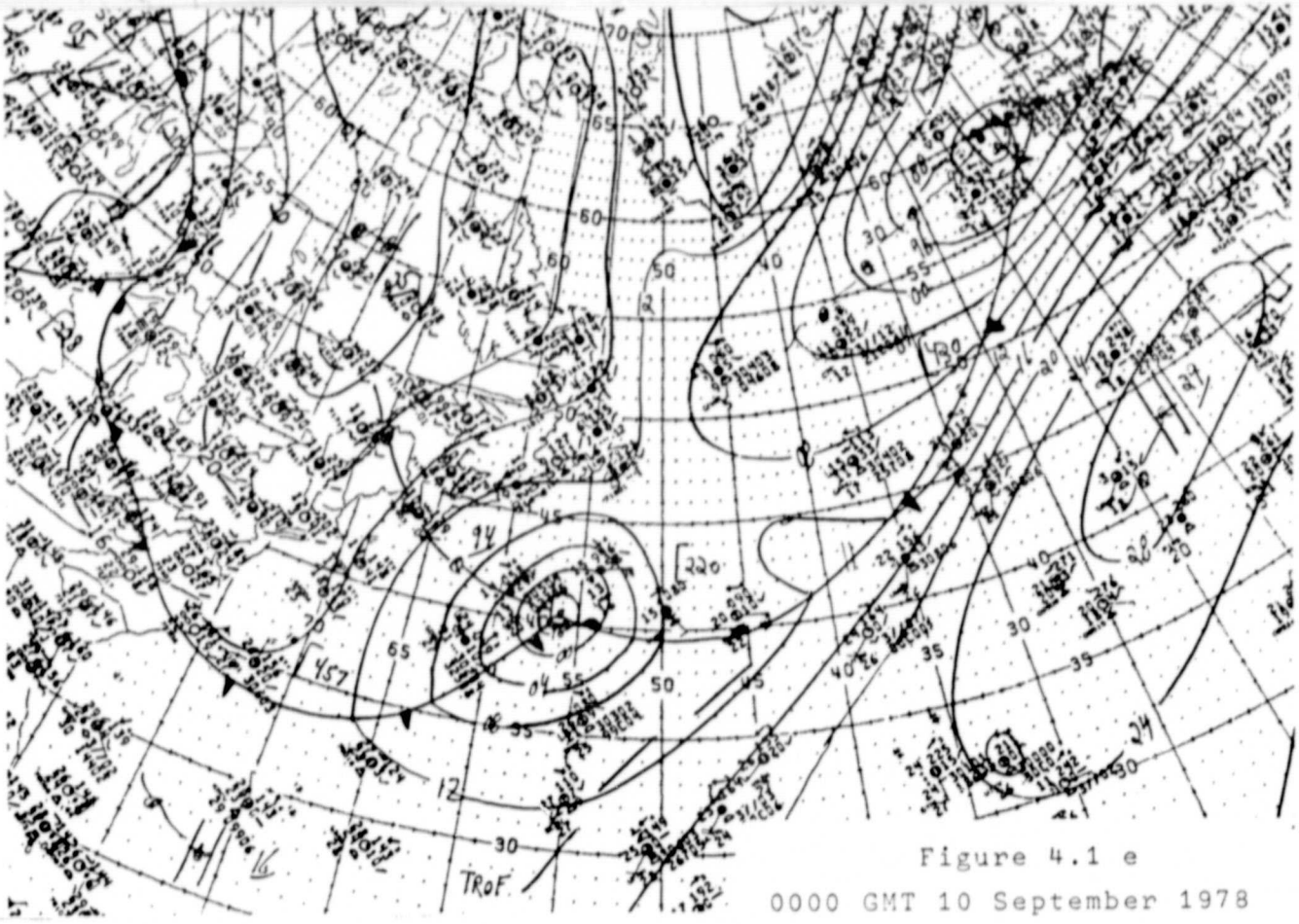

Figure 4.1 e
0000 GMT 10 September 1978

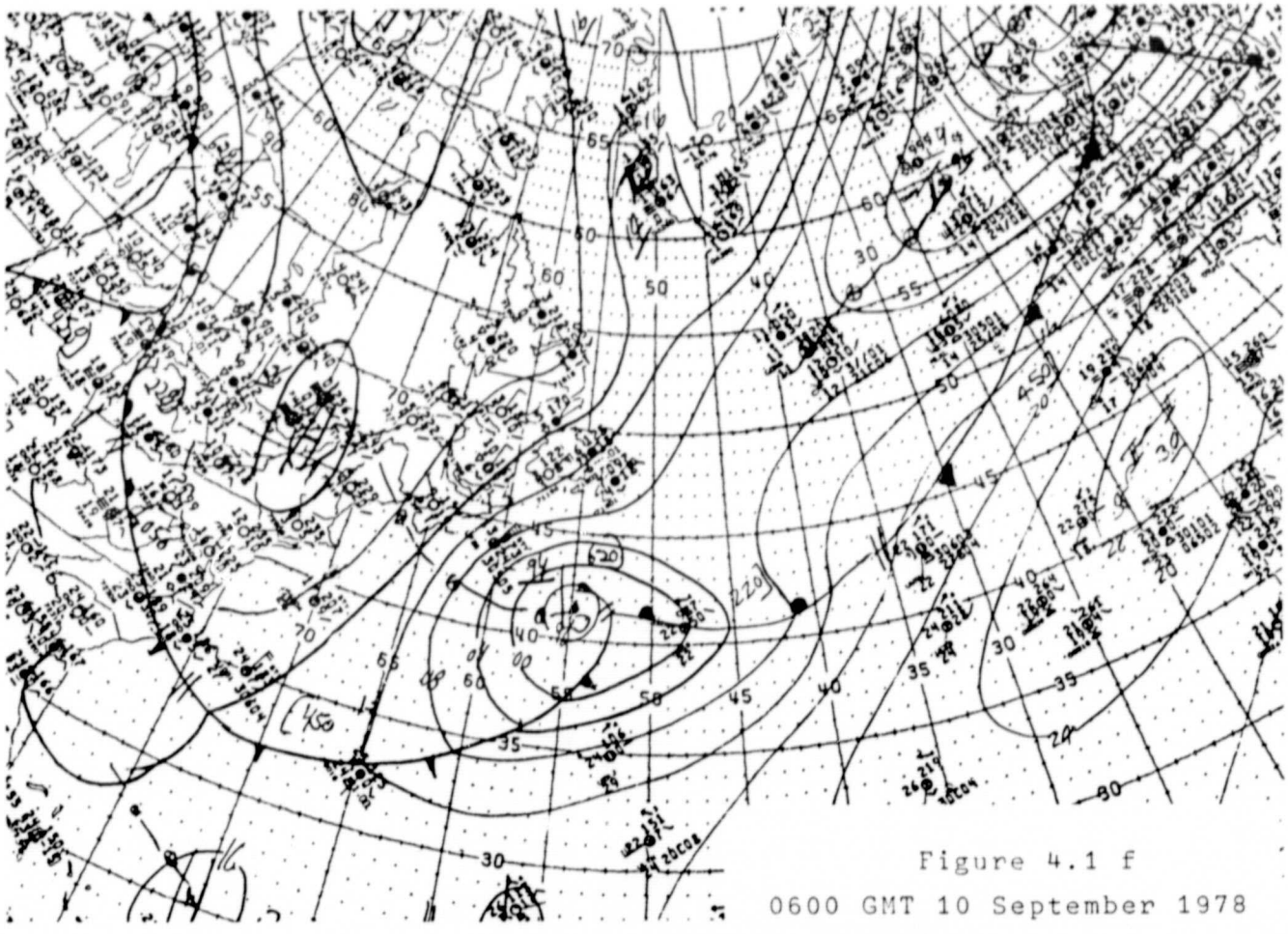

Figure 4.1 f
0600 GMT 10 September 1978

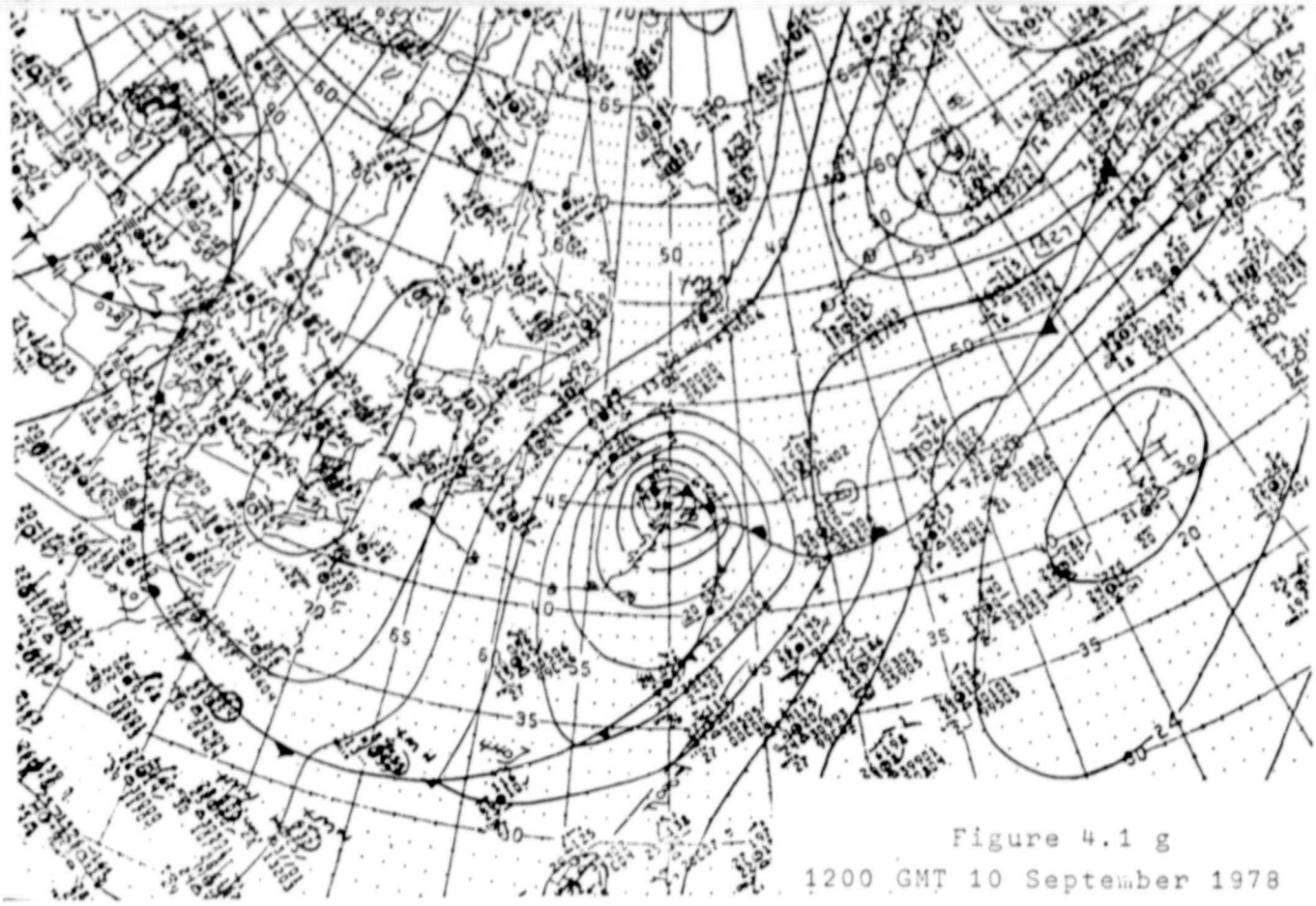

Figure 4.1 g
1200 GMT 10 September 1978

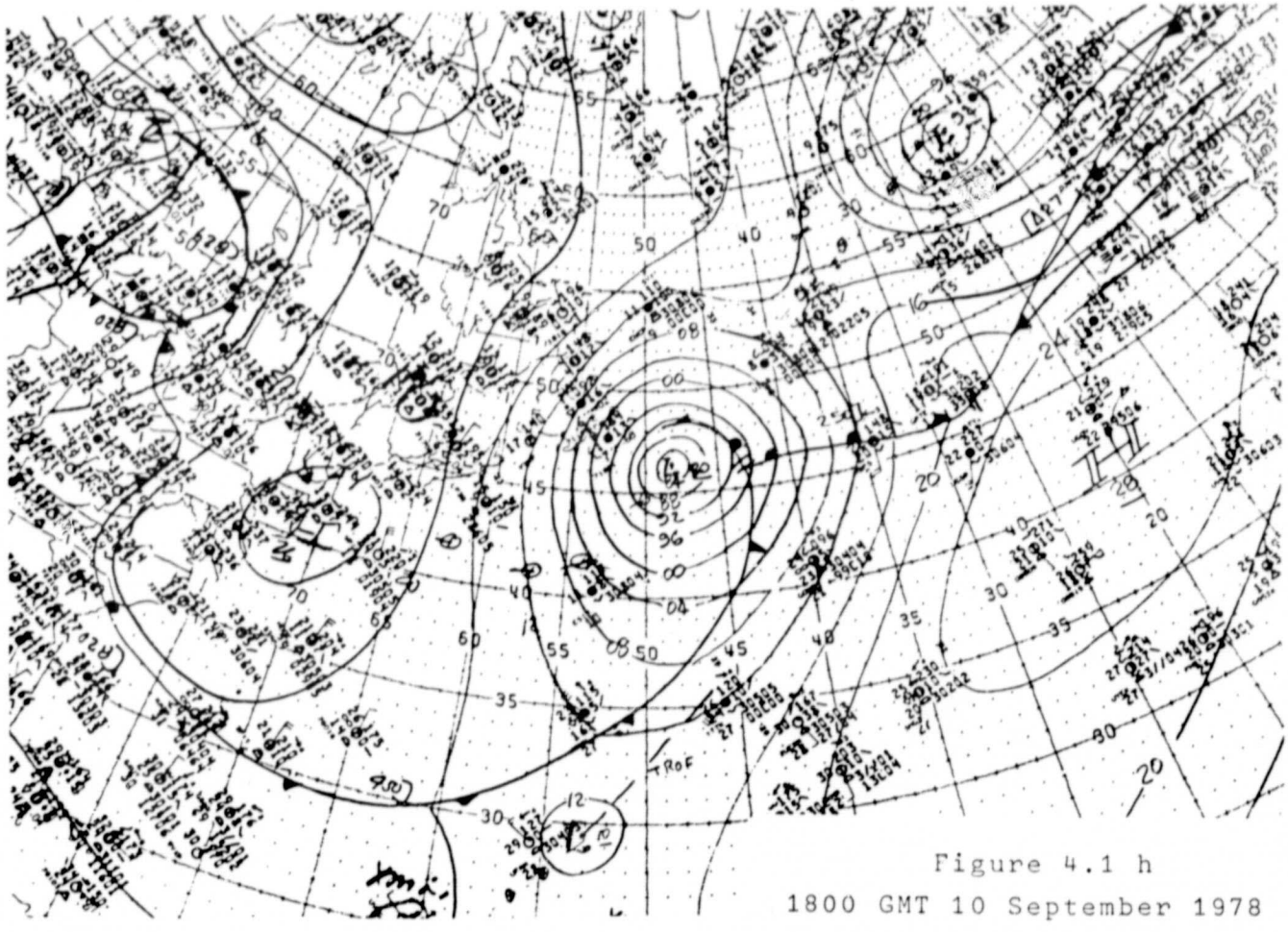

Figure 4.1 h
1800 GMT 10 September 1978

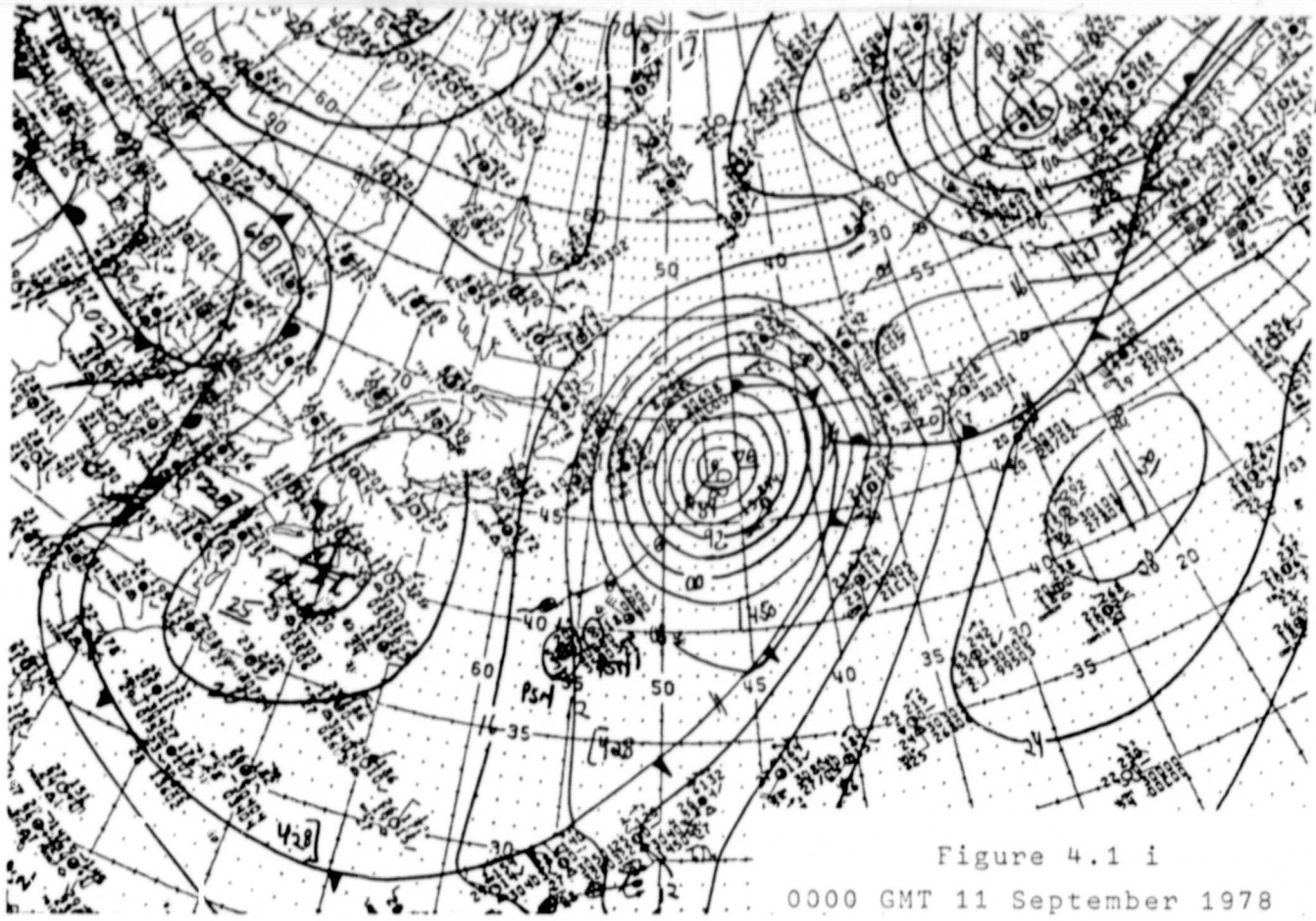

Figure 4.1 i
0000 GMT 11 September 1978

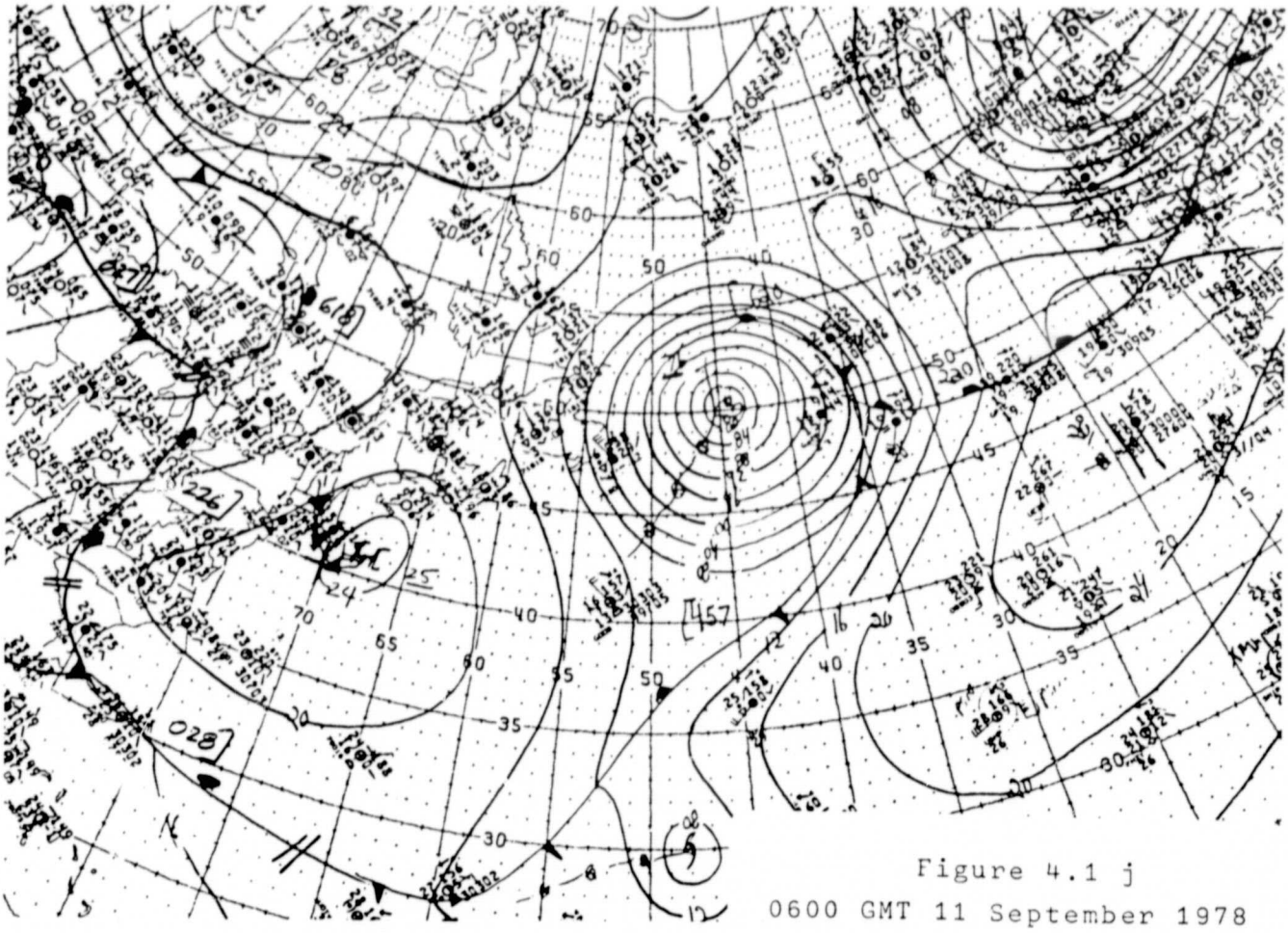

Figure 4.1 j
0600 GMT 11 September 1978

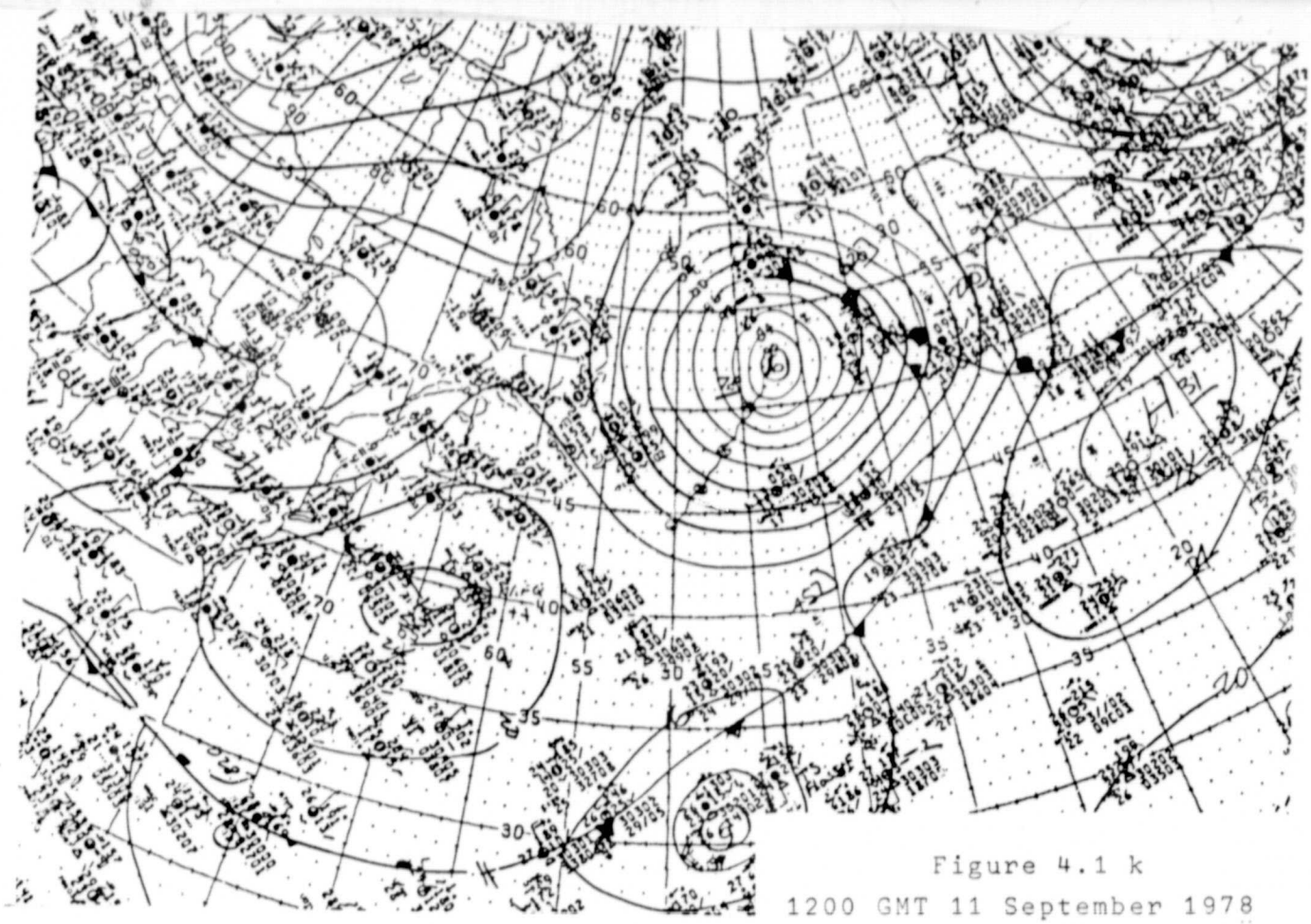

Figure 4.1 k
1200 GMT 11 September 1978

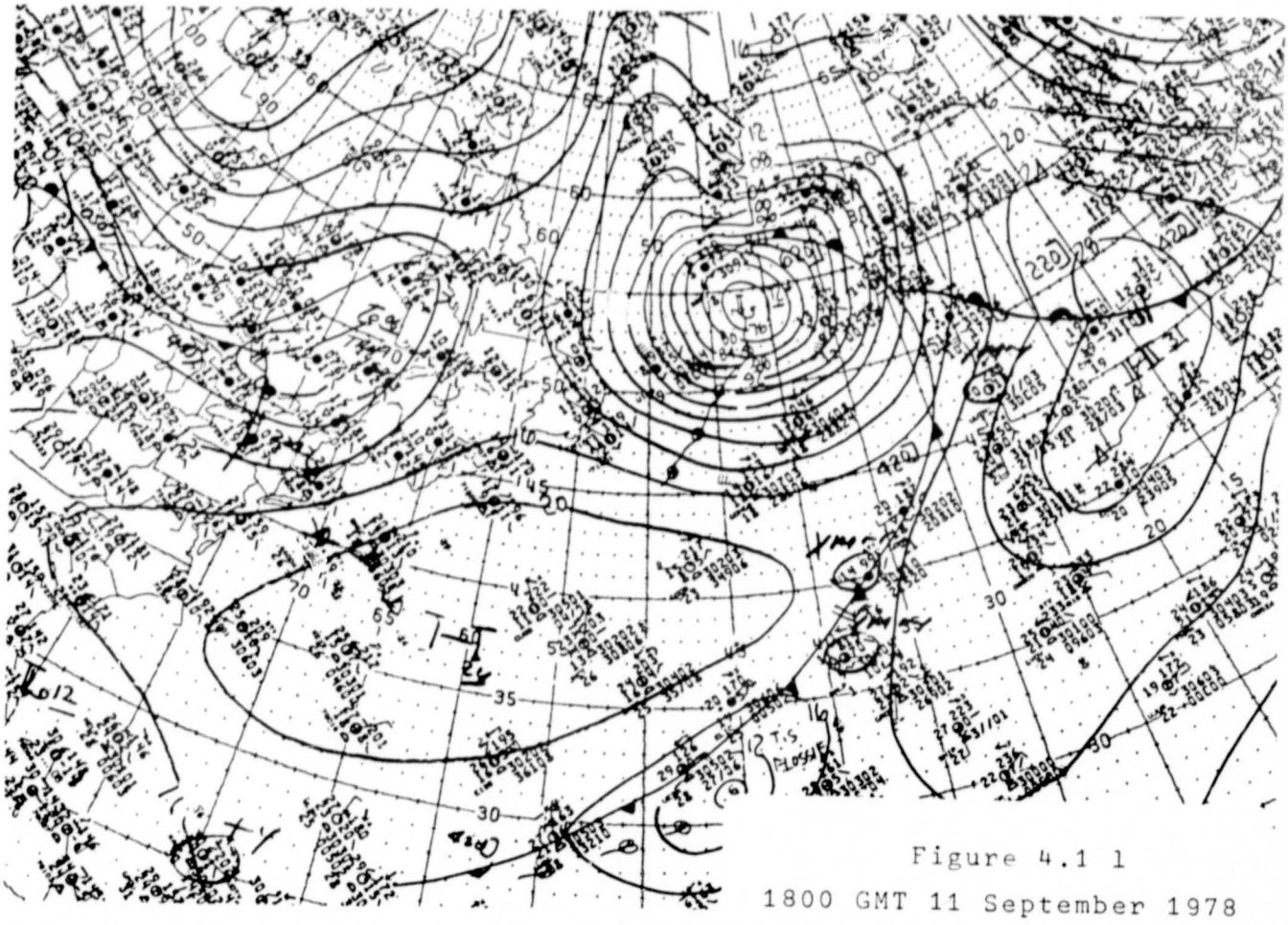

Figure 4.1 l
1800 GMT 11 September 1978

and 11th before slowing and turning north late on the 11th, at which time the size of the storm had grown to immense proportions, with its cyclonic circulation covering almost all of the N. Atlantic Ocean north of 45°N.

The NMC charts do not correctly depict the track and rate of intensification of the storm. Conventional data not available to the analyst in real time however provide a reasonable estimate of the position and rate of intensification as described by Gyakum (1980). Particularly useful were DMSP satellite imagery and the synoptic reports and barograph received from the ship Euroliner. At 1200 GMT September 10, the Euroliner observed a central pressure of 960.3 mb, winds of 58 knots and average seas of 9 meters. The ship was located near 43°N,50°W (see 4.1g), probably within 60 miles of the storm center,which was estimated to have a central pressure of about 950 mb from an analysis of the barograph trace. The corresponding NMC analyses shows a 980 mb low centered about 120 n.mi. north of the ship.

Figure 4.2 shows the distribution of ship reports in the western N. Atlantic available for 1200 GMT September 10 in the data base assembled for this study. There are about a factor of two more reports in this data base than available in real time. Figure 4.3 is an isobaric analysis constructed manually from the ship data. Such analyses constructed at 6-hourly intervals through the storm evolution provided an excellent initial estimate of storm wind field structure within which to incorporate the SASS data. Figure 4.4 compares our final estimate of the time history of central pressure and maximum surface wind in the QE2 storm with those extracted from the NMC analyses. The maximum surface winds are derived mainly from SASS data taken in orbits 1066, 1074, 1080, 1088, 1093/1094.

During the period of explosive development between 1200 GMT September 9 and 1200 GMT September 10, central pressure fell about 55 mb making the QE2 storm a "superbomb". Only modest deepening of the vortex was indicated on the NMC charts. It is this period of explosive development that was investigated intensively by Gyakum (1983) and Anthes et al, (1983). On September 11, the day the QE2 actually encountered the storm, the central pressure and maximum winds in the storm had stabilized at near 976 mb and 26 m/sec respectively. For the evaluation of the SASS wind retrieval

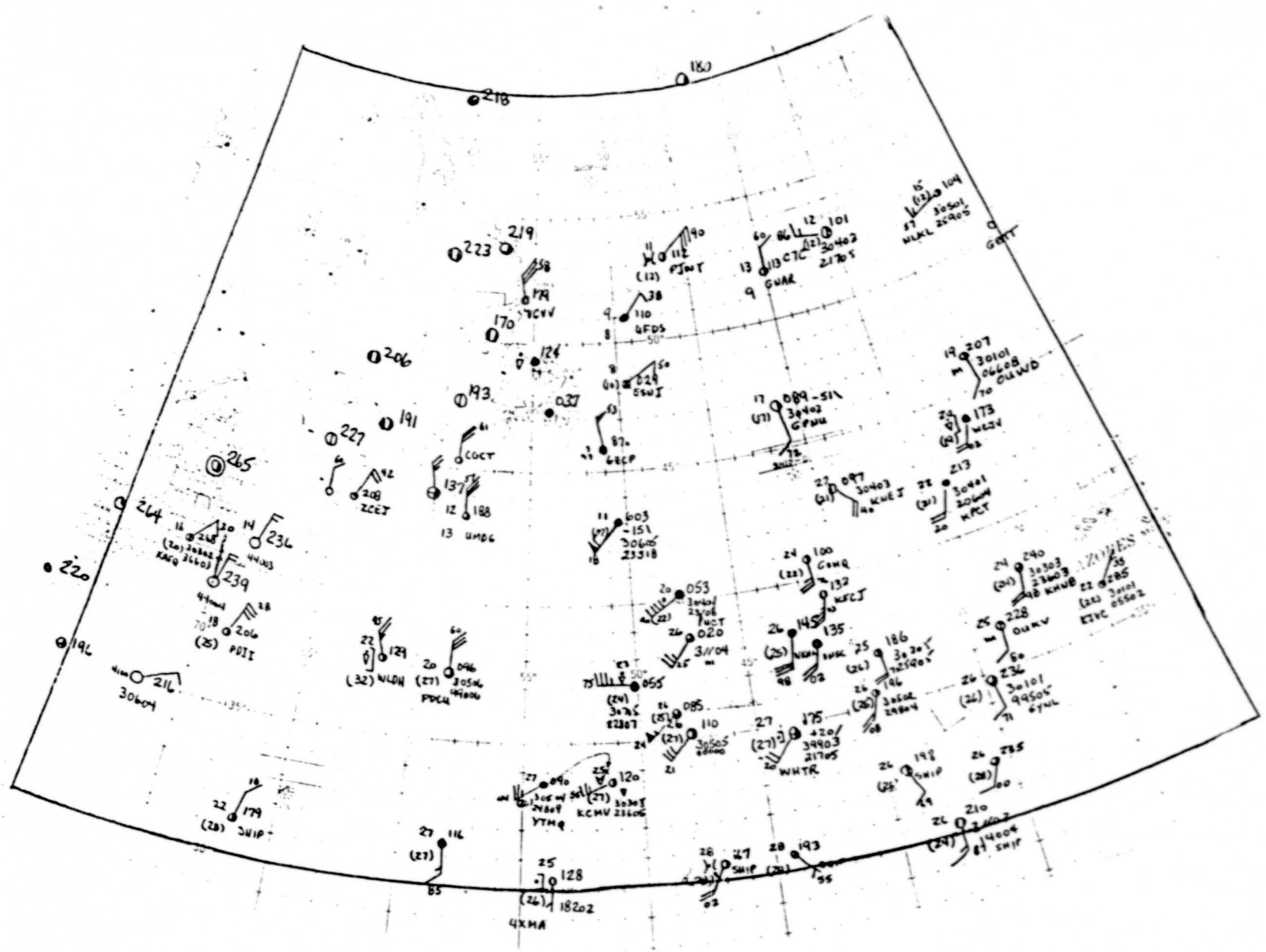

Figure 4.2 Distribution of surface ship reports (combined radiotelegraphed reports and ship log data) in N. Atlantic at 1200 GMT September 10, 1983. Ship Euroliner is near 43°N, 50°W. QE2 (call sign GBTT) is near 50°N, 25°W.

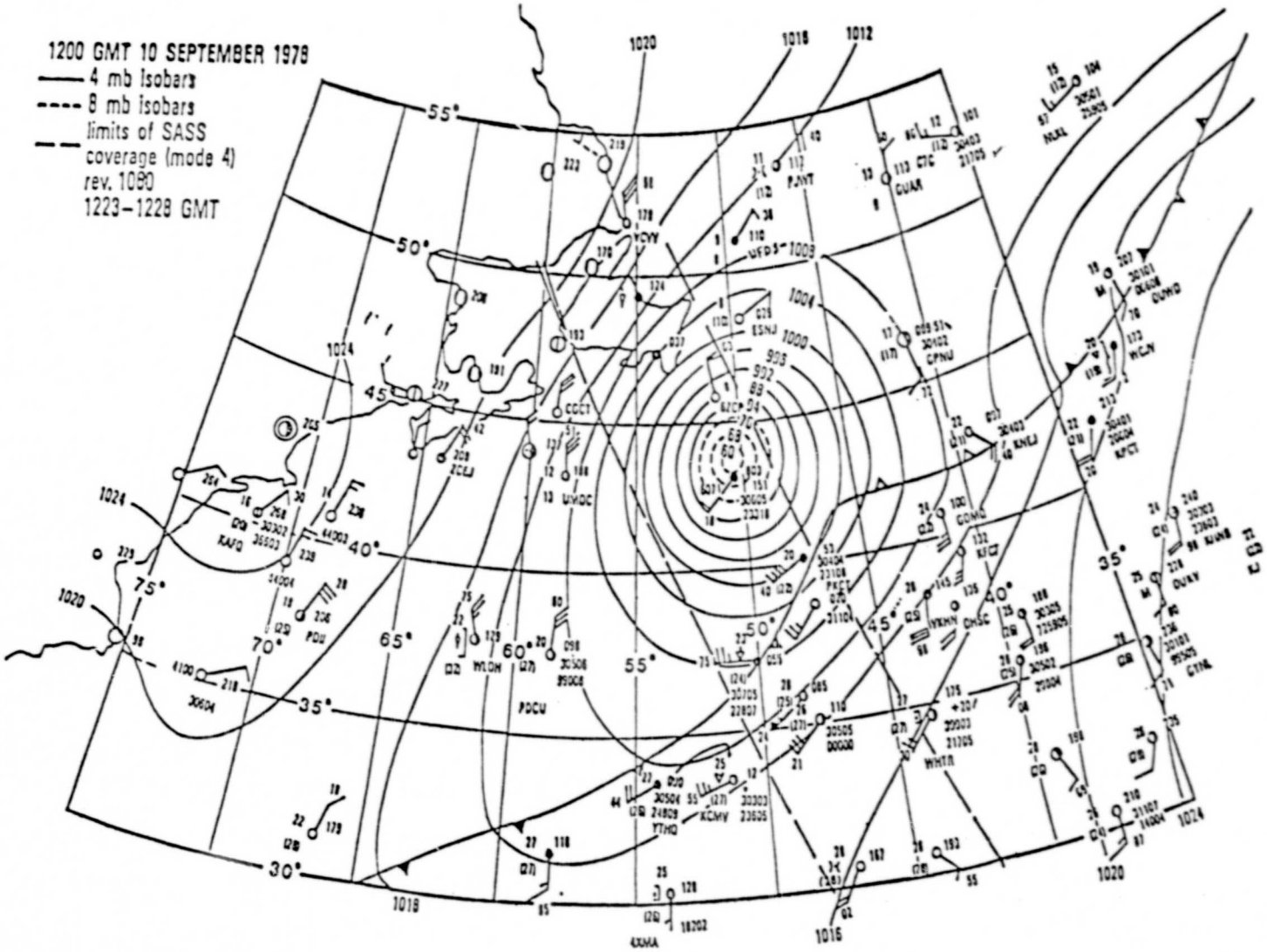

Figure 4.3 Reanalysis of surface pressure for 1200 GMT September 10, 1978 based upon all ship data. Limits of swath of SASS data in rev 1080 also shown.

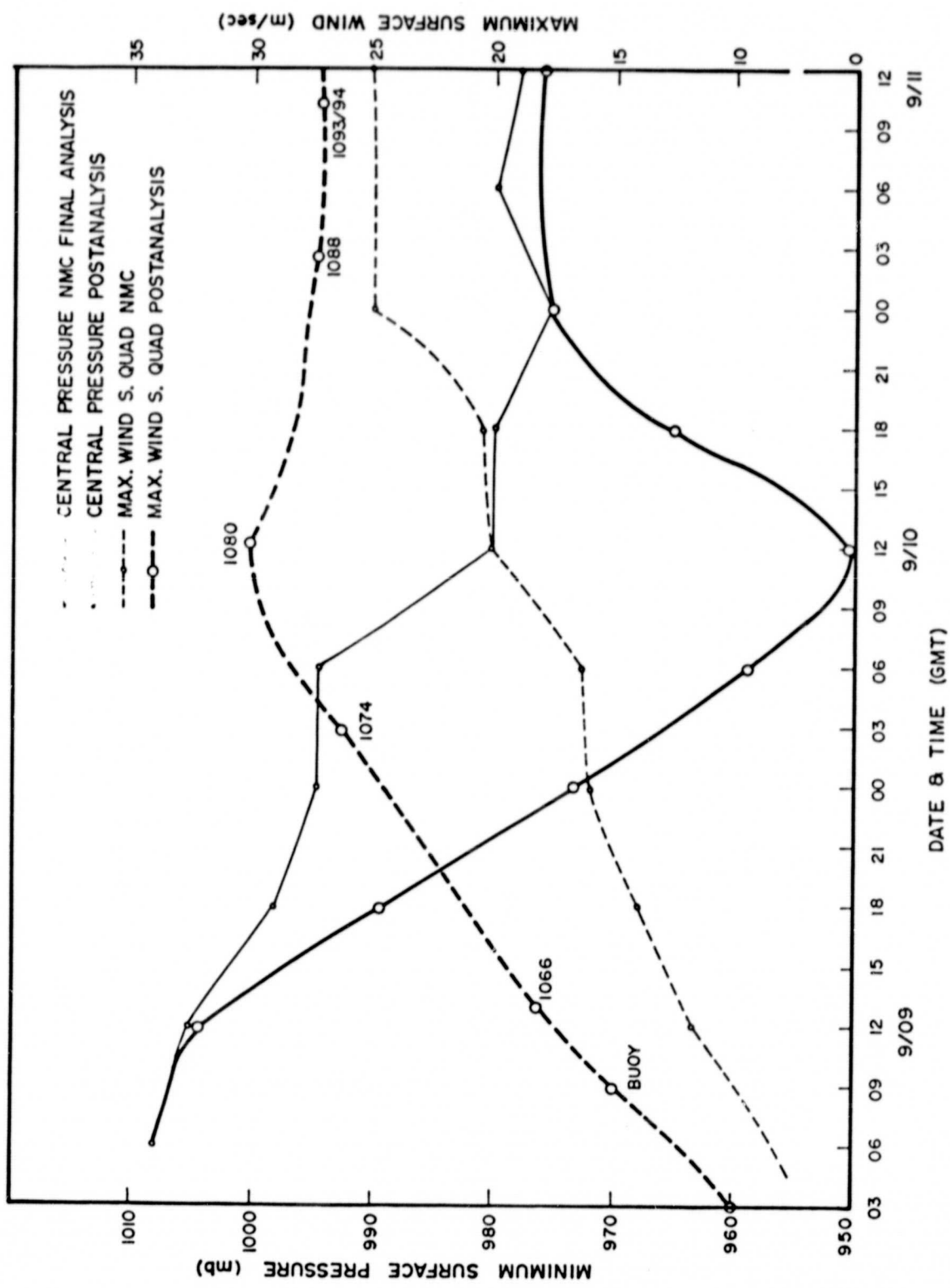

Figure 4.4 Comparison of time history of central pressure and maximum surface wind derived from NMC final analysis and post-analysis based upon combined conventional and SASS data.

algorithm, Cardone composited all ship data within 12 hours of 1200 GMT September 11 with respect to the moving center and performed a detailed kinematic analysis of the surface wind field for comparison with the SASS data obtained in revs 1093 and 1094. Figure 4.5 shows a simplified streamline/isotach pattern, the location of the ship, the storm center and the boundaries of the SASS data. The QE2,travelling west-southwestward, is shown entering the area of strongest winds, southeast of the storm center. James (1979) has described the encounter of the vessel with the storm. Figure 4.6, from James, gives a subjective analysis of the wave height field in the storm and the tracks of the storm and the ship. The avoidance maneuver taken by the Captain of the QE2 probably averted a much greater threat to the ship.

4.2 SASS Data

Table 4.1 lists the revs used in this study. Coincidentally, each rev segment occurred within 3 hours of the 0000 GMT and 1200 GMT standard weather observation times. Only off-nadir SASS data were considered.

Schroeder et al. (1982) trace the development of various models that relate surface winds from measurements of ocean normalized radar cross section (NRCS),measurements from initial versions based upon aircraft data through to the final form used for the processing of the entire SASS data set. That model was integrated into the SASS-1 algorithm.

SASS-1 provides estimates of the neutral stability wind vector at the 19.5 m reference height. The concept of the neutral wind was introduced by Cardone (1969); it is the wind speed that would result from a given wind stress in a neutrally stratified atmosphere. The algorithm provided estimates from so called cell pairs, each formed from a matching of measurements of NRCS from the forward and aft SASS antennas.

Each SASS footprint represents an area 70 km by 17 km. The centers of matched cells could be up to 35 km away. The NRCS pairs therefore may represent approximately a 50 km circle, if the pairs are indeed colocated, or about 70 km, if they are separated by the maximum allowable distance. For each cell pairing, the algorithm provides estimates of the true wind sampled and up to three additional "aliases". Selection of the "true" wind estimate therefore requires an initial estimate of the wind direction,

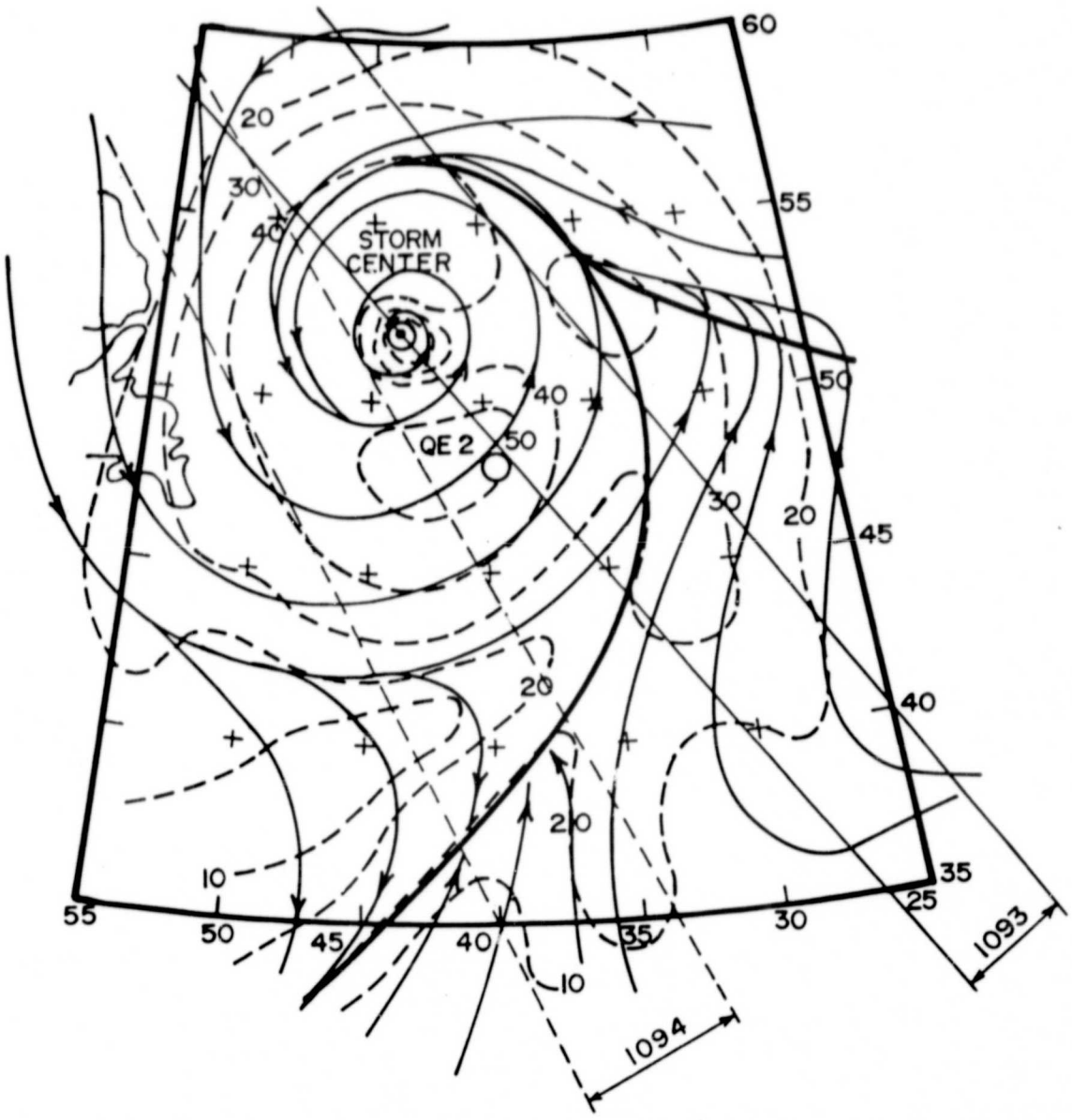

Figure 4.5 Kinematic analysis of surface wind field in QE2 storm from conventional data alone for 1200 GMT September 11, 1978. Position of QE2 and limits of SASS data in revs 1093/1094 also shown.

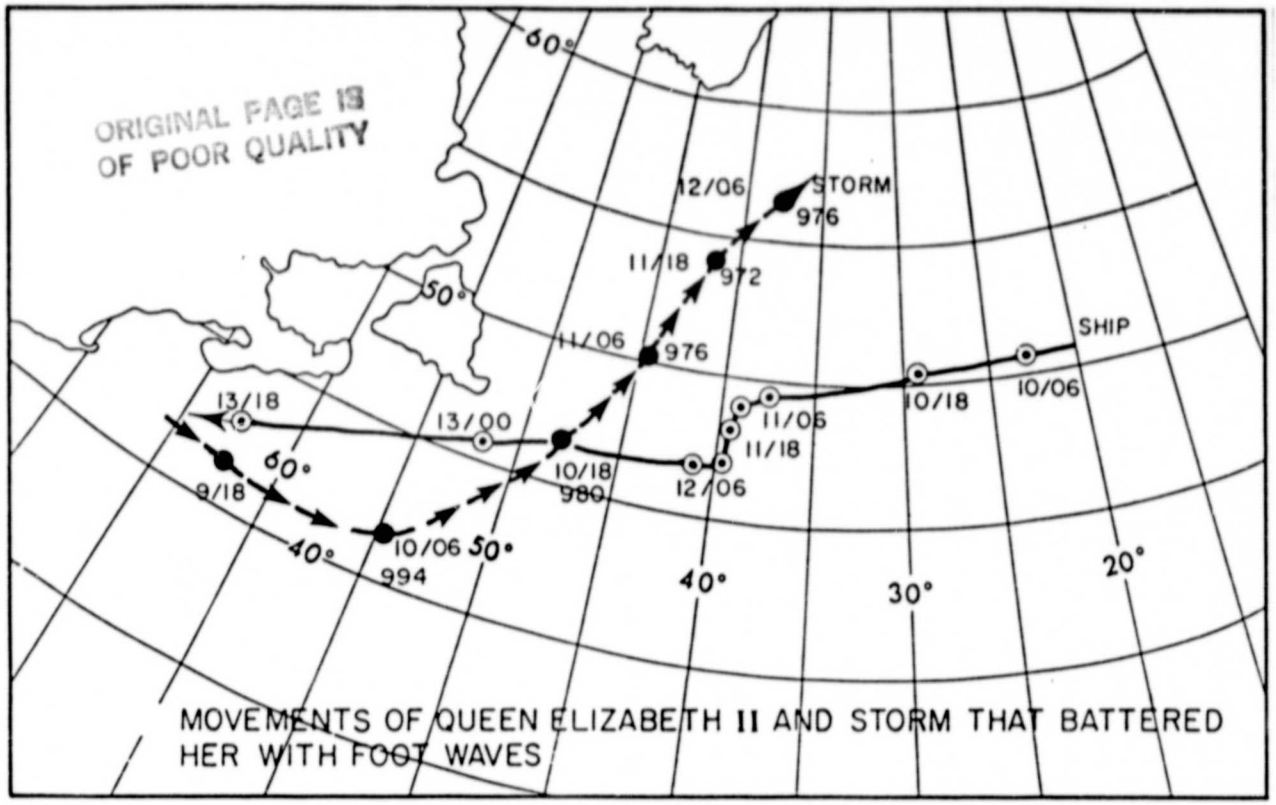

Track of the severe September storm in relation to the QUEEN ELIZABETH II. Note the diversion to the south that avoided the extreme waves.

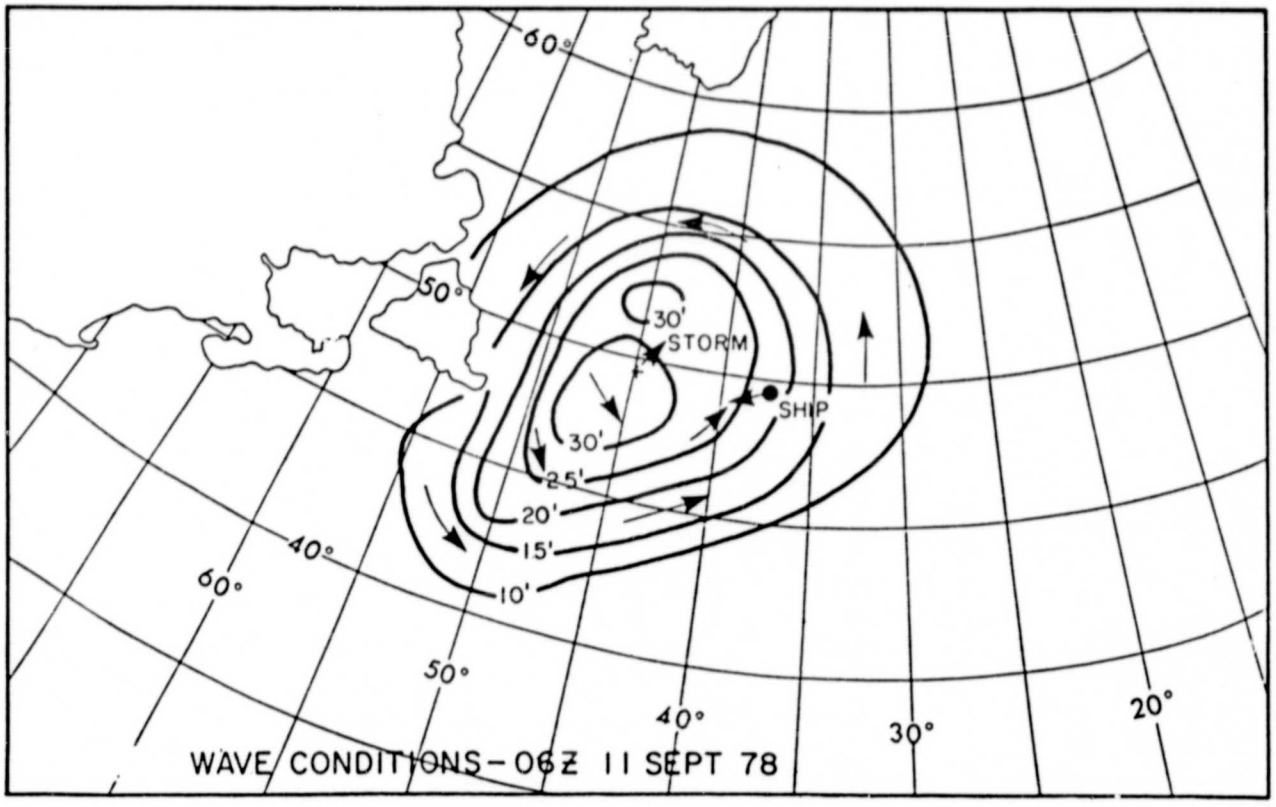

Significant wave height analysis for 0600 September 11, 1978.

Figure 4.6 Relative tracks of QE2 storm center and QE2 (above) and subjective analyses of significant wave height at 0600 GMT September 11, 1978 (below) (from James, 1979).

TABLE 4.1 SEASAT Orbits in QE2 Storm

REV #	MODE	DATE	TIME (GMT)
1066	Ascending	September 09	1252-1257
1074	Descending	September 10	0245-0250
1080	Ascending	September 10	1223-1228
1088	Descending	September 11	0209-0219
1093	Ascending	September 11	1013-1023
1094	Ascending	September 11	1154-1202

though Wurtele et al. (1982) describe procedures based upon pattern recognition, for the selection of the true solution even in the absence of in-situ data.

Figure 4.7 is an example of de-aliased SASS winds for rev 1093, which viewed the eastern part of the QE2 storm. Figures 4.8 and 4.9 compare the wind speeds and direction from SASS for the selected solution and the winds provided by the kinematic analyses (Figure 4.5). The data agree to within ± 2 m/sec in wind speed and 16° in wind direction. Figure 4.10 compares the SASS wind speeds and winds observed by ships within the area viewed by revs 1093/1094. Agreement is as good as could be expected considering the errors at ships' wind observations.

The SASS data used in this study were provided by the Atmospheric Environment Service, Canada. The data differ from the initial production processing of Seasat version data only in the use of cell grouping instead of cell pairing. That is, the NRCS data are converted to winds after all individual cells are binned over 100 km boxes. The binned data are believed to provide somewhat more accurate winds, and to be more representative of the synoptic scale than winds derived from cell pairs, though no evaluations of the reprocessed data have been reported to date.

4.3 Wave Hindcast Experiments

Two numerical wave hindcasts of the QE2 storm were made. The first, or base case hindcast was intended to provide the most accurate specification of sea states possible. That hindcast used wind fields derived from a combination of conventional and SASS wind data using the most accurate wind field analysis techniques available. The second hindcast used wind fields derived from the NMC surface analyses. This hindcast was intended to represent the best sea state specifications which could reasonably be derived from operational data available in real time.

All QE2 hindcasts were made using the ODGP hindcast model adapted on the two dimensional grid shown in Figure 4.11. The grid spacing is 1.25° in latitude and 2.5° in longitude, and extends basically from 20°W to 80°W and 25°N to 67.5°N. The hindcasts simulated the 72 hour period beginning at 0000 GMT September 9, which is 12 hours before the storm developed a closed circulation south of Georges Bank.

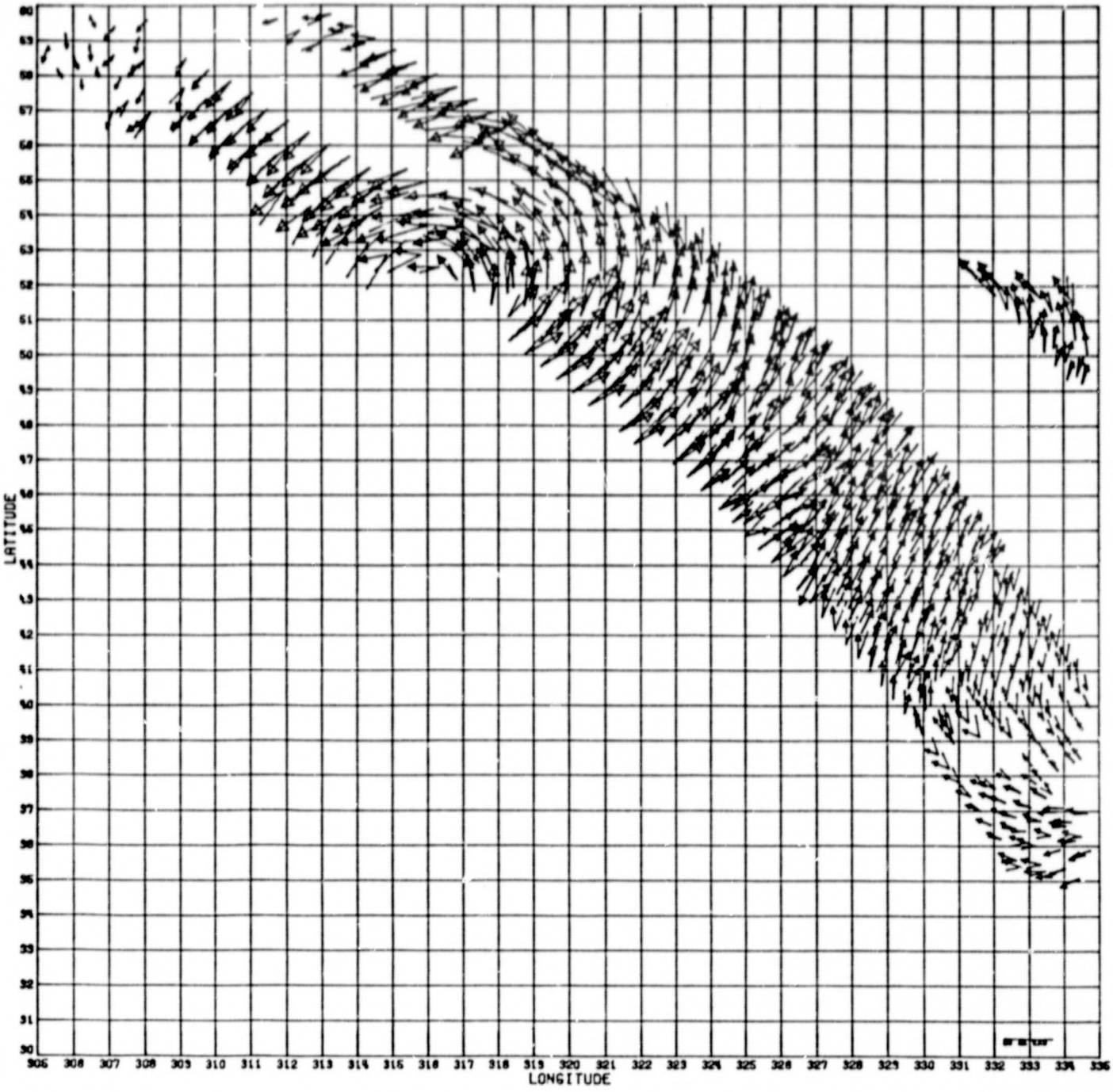

Figure 4.7 Dealiased wind vectors in rev 1093 from SASS-1 algorithm applied to SASS cell pairs.

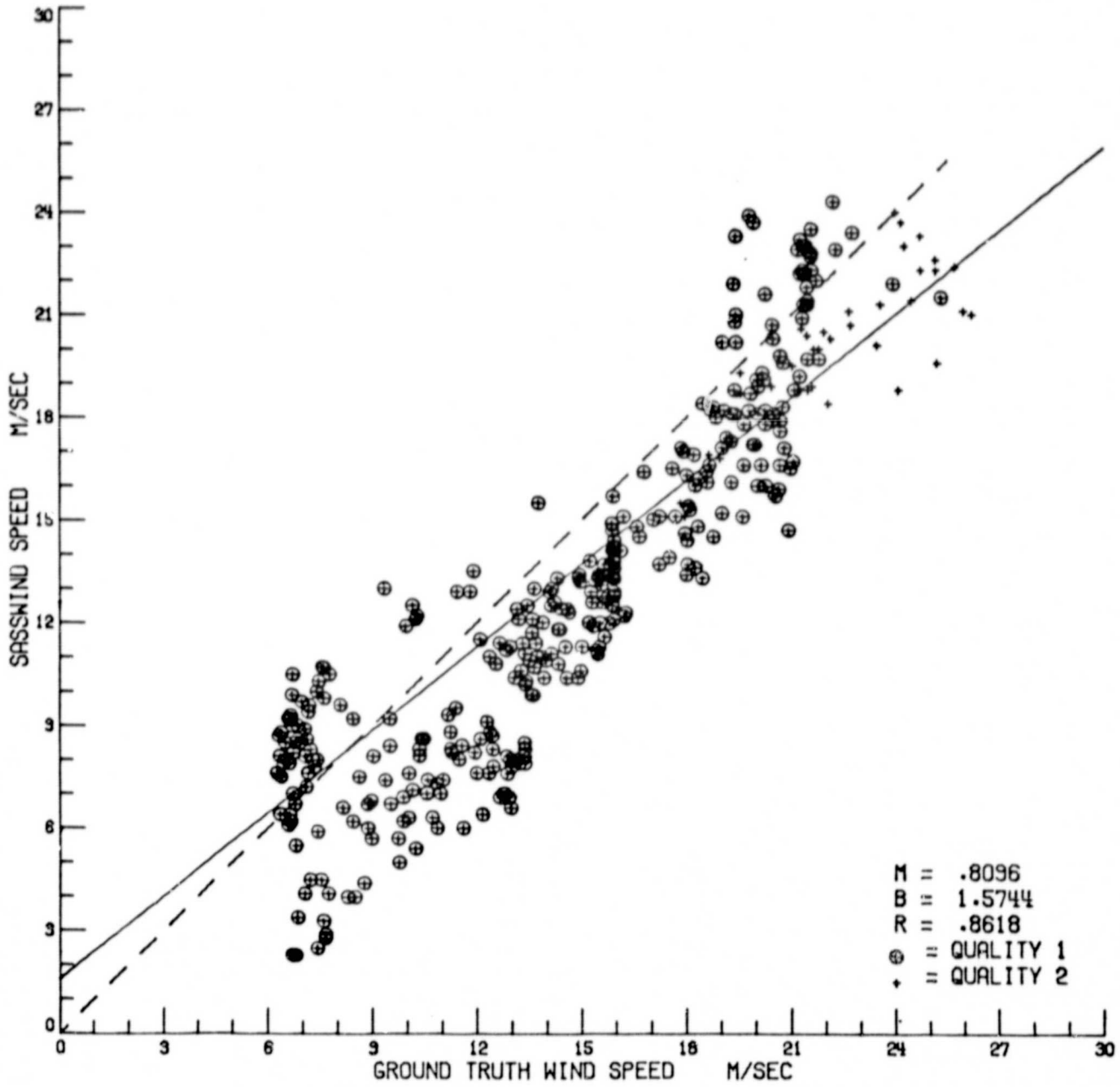

Figure 4.8 Comparison of SASS wind speed and kinematic analysis (from Figure 4.5) wind speed in rev 1093.

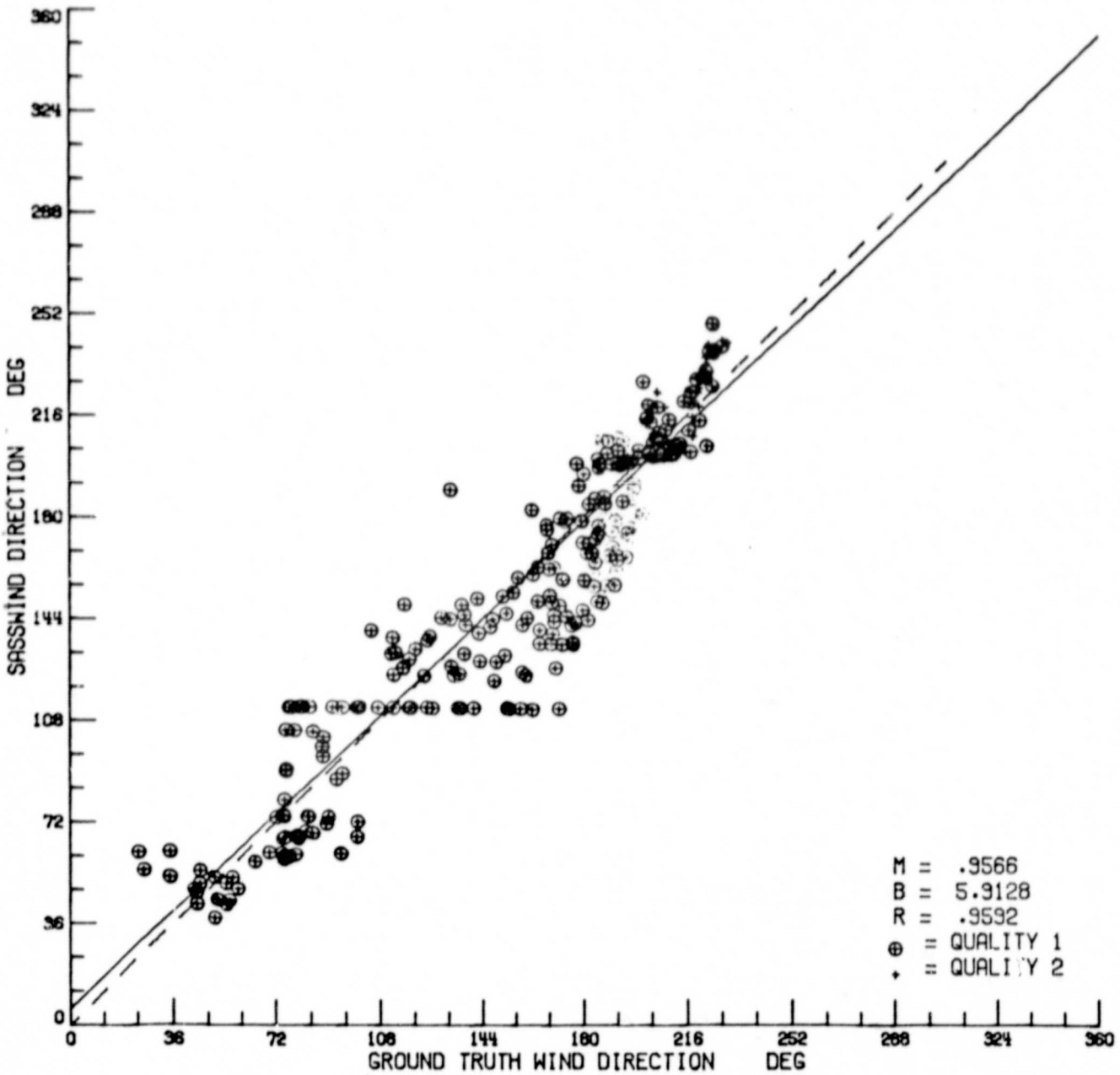

Figure 4.9 Comparison of SASS wind direction and kinematic analysis wind direction in rev 1093.

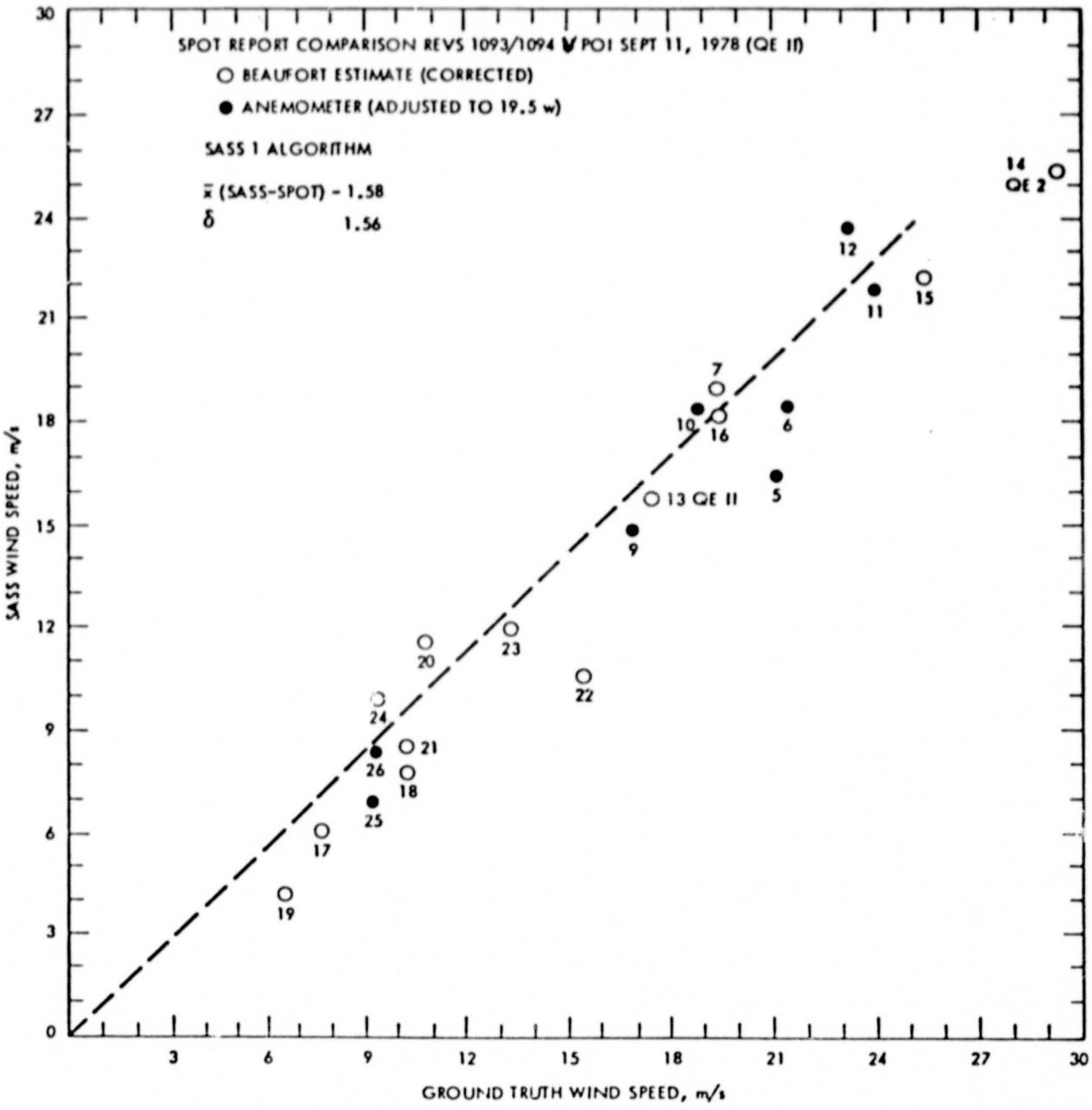

Figure 4.10 Comparison of SASS-1 wind speed and surface wind speed reported by ships within SASS swath of revs 1093/1094.

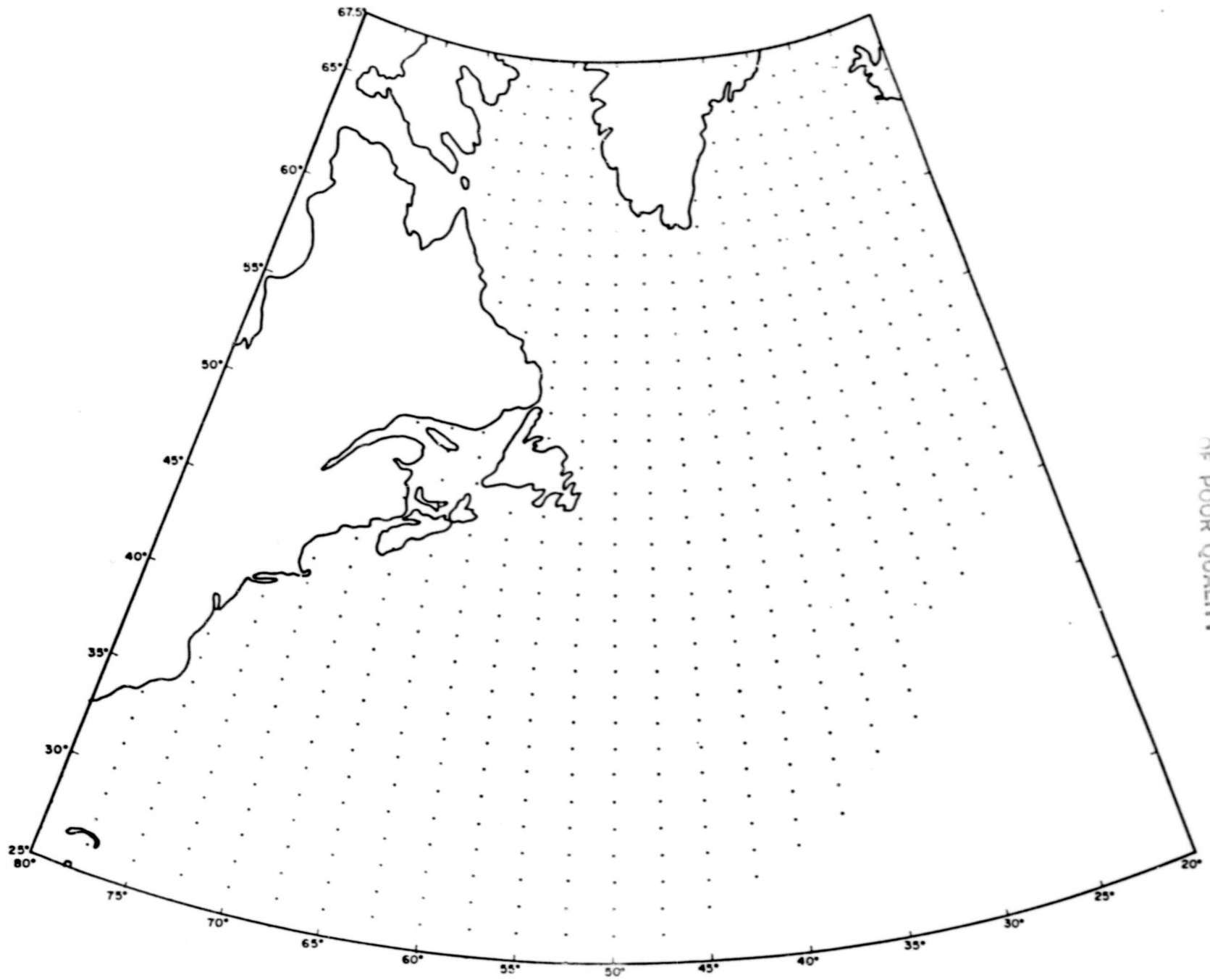

Figure 4.11 Grid system of ODGP and SAIL wave models used for QE2 storm simulations.

4.3.1 Operational Wind fields

Wind fields for the simulated operational sea state specification were derived exclusively from the sea level pressure analyses shown on the 6-hourly NMC Final Analyses Series (Figure 4.1). The procedure is objective and is based upon the use of a model of the wind profile in the planetary boundary layer (PBL) that relates the surface marine wind velocity to the local pressure gradient, the air-sea temperature difference, and the atmosphere thermal advection.

The PBL model of Cardone (1969) was used. That model has been tested in a number of studies, as reviewed by Cardone et al. (1980). The model appears to be capable of providing unbiased estimates of the wind fields from accurate pressure fields, to within ±2 m/sec and 20° (rms) in speed and direction, respectively. In practice however, errors in the pressure fields cause significantly larger wind field errors. For example, Overland and Gemmill (1977) found the model to provide the most accurate wind fields in the New York Bight of four methods tested. The specified winds were compared with winds measured at a NOAA data buoy over a period of five months: for measured winds in excess of 12.5 m/s the PBL model winds had rms errors of 2.9 m/s and negligible bias. Cardone et al. (1976b) used the model to specify winds from N. Atlantic pressure analyses produced at FNOC and found wind errors of 4.5 m/s. The increase in the errors from the New York Bight and the open N. Atlantic reflects the greater errors in the pressure fields for the open ocean area.

To provide pressure gradients for the PBL model for the QE2 storm, the NMC isobaric analysis were digitized using a curve following digitizer. Pressures were interpolated to each wave model grid point from the digitized pressures by fitting a polynomial surface locally at each point to the nearest 8 points. Meridional and zonal pressure gradient components were computed by centered differencing. The air-sea temperature difference was specified at each point as a function of the local geostrophic wind direction; the function provided maximum unstable stratification ($T_{air-sea}$ = -8°C) for northerly winds and neutral stratification for southerly winds. The thermal advection parameter was specified by assuming a mean air-temperature gradient.

4.3.2 Base Case Wind fields

The assimilation of SASS wind data in computer-based objective analysis schemes remains a difficult problem because of the existence of multiple wind solutions for each radar measurement. However, SASS data may be readily assimilated using subjective kinematic analyses techniques provided there is sufficient conventional data to define a reasonably accurate initial guess of the wind direction. The data base assembled from both real time and non real time ship reports, as shown in Figure 4.2, provides an excellent initial estimate of the streamline pattern about the QE2 storm. The assimilation of SASS wind data was therefore straightforward. First, maps such as Figure 4.2 were prepared at 12-hourly intervals, at the standard Greenwich observing times nearest the time of the Seasat revs (Table 4.2). Then the SASS multiple wind solutions were plotted at the centers of the 100 km bins used for the cell grouping. The SASS wind solution whose direction most nearly matched the direction of the initial guess wind field was taken to be the "true" wind. Finally, a detailed kinematic analysis was performed to the five maps containing the SASS winds. The analyses procedure considered the slight time shift between the SASS winds and ship data. The streamline/isotach analyses effectively translated the SASS data into data void parts of the analyses by imposing space/time continuity principles (see Cardone et al., 1980 for a more complete discussion of kinematic analyses of surface marine wind fields).

Figures 4.12 and 4.13 are examples of the final kinematic analyses. Figure 4.12 provides a view of the wind field about the QE2 storm at the beginning of the 24 hour period of explosive deepening. SASS data from both left and right side antennas were available. The data show the wind field to be very asymmetric with respect to the center, with winds of 30-35 knots covering a large area west and south of the center. The center of the storm is defined well by conventional ship and buoy data. The area of very light winds extending northeastward from the center is confirmed by both SASS and conventional data.

The kinematic analysis shown in Figure 4.13, defines the surface wind field at the end of the period of explosive development. Only the left side SASS scan was available for this rev but the wind field east of the center was viewed about 12 hours earlier and later in revs 1074 and 1088

TABLE 4.2 QE2 Storm Hindcast Wind Fields

Hour GMT	Date	BASE CASE	OPERATIONAL
0000	Sept 09	PBL NMC	PBL/NMC Analyses
0600	Sept 09	Interpolated	PBL/NMC Analyses
1200	Sept 09	Kinematic-rev 1066	PBL/NMC Analyses
1800	Sept 09	Interpolated	PBL/NMC Analyses
0000	Sept 10	Kinematic-rev 1074	PBL/NMC Analyses
0600	Sept 10	Interpolated	PBL/NMC Analyses
1200	Sept 10	Kinematic-rev 1080	PBL/NMC Analyses
1800	Sept 10	Interpolated	PBL/NMC Analyses
0000	Sept 11	Kinematic-rev 1088	PBL/NMC Analyses
0600	Sept 11	Interpolated	PBL/NMC Analyses
1200	Sept 11	Kinematic-rev 1093/94	PBL/NMC Analyses
1800	Sept 11	Interpolated	PBL/NMC Analyses
0000	Sept 12	PBL/NMC	PBL/NMC Analyses

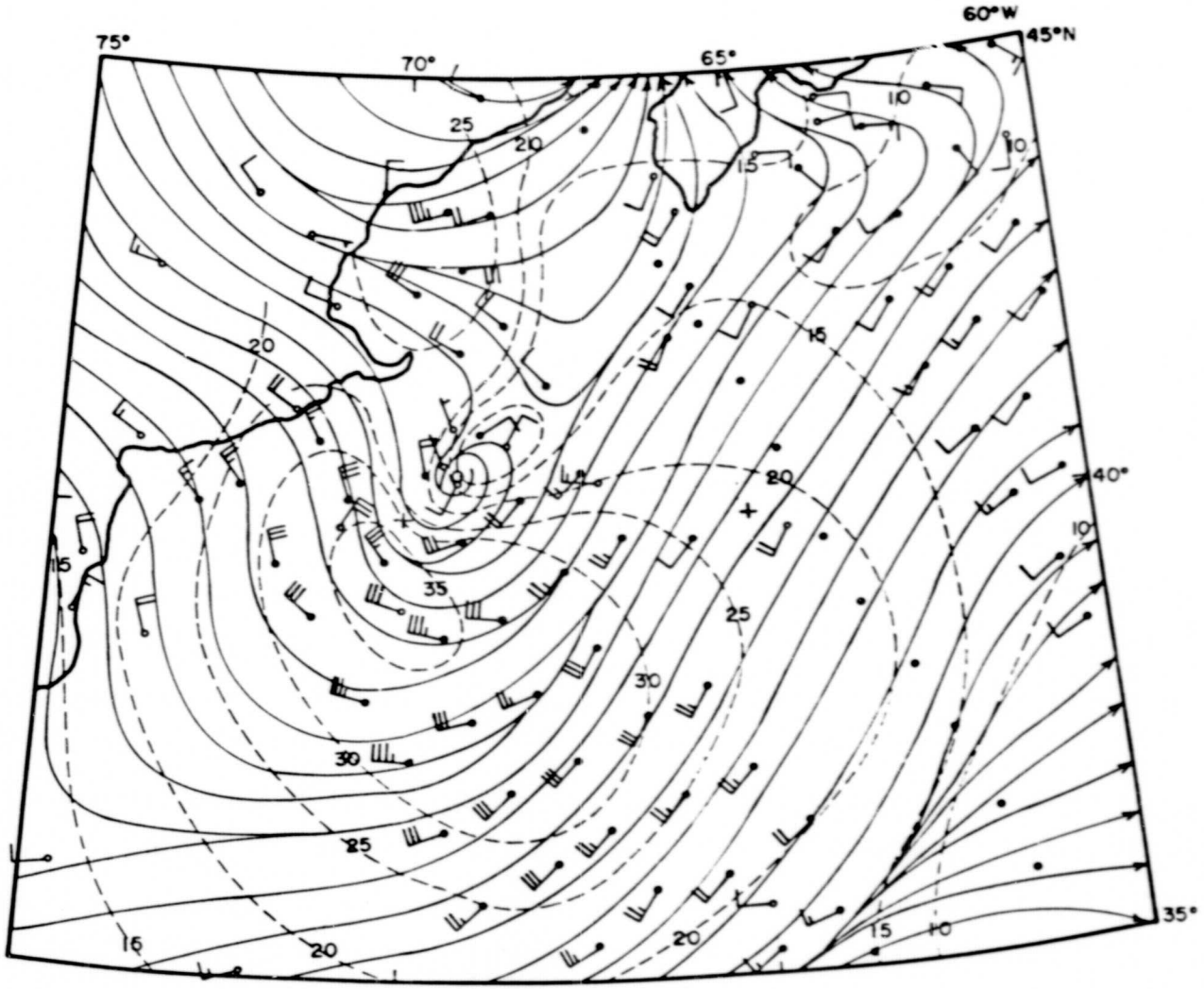

Figure 4.12 Kinematic analyses of surface wind field at 1200 GMT September 10, 1978. Dashed lines are streamlines, solid lines are isotachs (labelled in knots). Ship and buoy reports represented as wind barbs and vectors from open circles; dealiased SASS wind in 100 km bins represented as wind barbs and vectors from filled circles. SASS data from rev 1066.

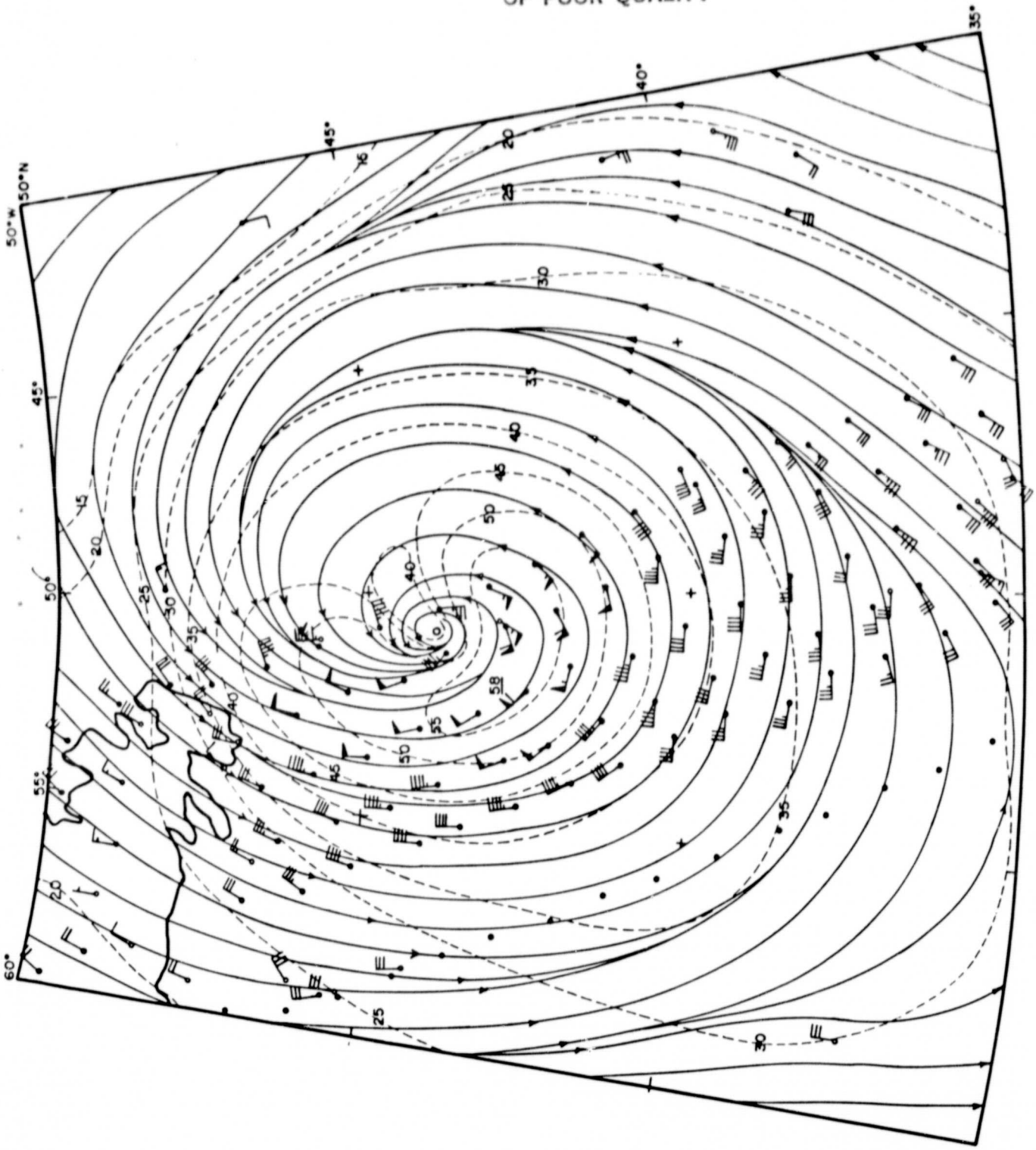

Figure 4.13 Same as Figure 4.12, except analysis for 1200 GMT September 10, 1978. SASS data from rev 1080.

respectively. The streamline/isotach pattern shown in Figure 4.13 defines the wind pattern after the storm has attained its minimum central pressure. The asymmetric velocity pattern is basically maintained but maximum surface winds are about 58 knots west and south of the center. At this time, however, winds of 50 knots or more also have extended into the NW quadrant of the circulation.

In the following 24 hours, the kinematic analyses showed the storm circulation expanding, with maximum winds slightly lower. At 1200 GMT September 11, the SASS data from revs 1093/1094 allowed a further improvement of the fairly accurate initial guess wind field derived from post-analyses of conventional ship data (figure 4.5). Maximum surface winds of 50-55 knots were observed by SASS mainly in the southern quadrant of the storm, as depicted in the initial guess field, with the maximum wind specified to be 54 knots.

The wave hindcast model is driven by 6-hourly wind fields. To provide winds at the intermediate 6-hourly times (0600, 1800 GMT) from the base case kinematic winds, a simple interpolation was performed which averages grid point values of meridional and zonal wind components outside the sphere of influence of the storm (defined by an effective radius of the circulation specified externally); for grid points which lay inside the radius of the circulation on the intermediate maps time, the winds were averaged with respect to the storm center. This interpolation procedure effectively propagates the SASS data, available basically at 12-hour intervals, to 6-hourly intervals as well.

4.3.3 Comparison of Base Case and Operational Hindcasts

The base case wind fields show that the surface wind field intensified without much change in shape, as the strongest winds were located consistently to the south of the center. Figure 4.4 compares the time history of the maximum surface wind in the south quadrant of the circulation in the alternate wind fields. The operational wind speeds are much lower south of the center than the base case wind speeds until late in the history of the storm on September 11 when the storm intensity is reasonably well specified by conventional data.

Figure 4.14 compares the alternate surface wind fields in the storm

region at the time of maximum storm intensity (in terms of central pressure). The conventional wind field has the storm center misplaced about 120 n.mi. north of the true position, and the strongest winds northwest of the center, while the SASS winds place the strongest winds south of the center. The differences between the two wind fields are large and spatially coherent and therefore can be expected to induce larger differences in the alternate wave hindcasts made from the two wind field series.

Such differences were indeed found. Table 4.3 gives mean and rms differences in wind speed, wind direction and significant wave height between the operational and base case hindcasts. The statistics were completed only from data at grid points within the storm domain. The domain specified expanded from approximately a 10° latitude by 15° longitude box centered on the storm early in the hindcast to a 20° latitude by 30° longitude box at the end of the hindcast.

The wind speeds specified from conventional data were generally negatively biased with respect to the base case wind fields derived from SASS data, with the largest errors found during the period of most rapid development. Mean differences in wind direction were small and rms differences were acceptably low, the latter a reflection of the ability to specify the simple streamline pattern about a large cyclone from even sparse conventional ship reports.

The errors in significant wave height given in Table 4.3 do not at first glance appear excessive with mean errors generally under 1m. Of more operational significance however are differences between the hindcasts in the specification of the location and severity of the maximum storm generated sea states. Figure 4.15 compares the alternate significant wave height fields at 1200 GMT September 10. The wave height differences are very large south of the center in the area of highest sea states, where the operational hindcast is more than a factor of 2 low. Twenty-four hours later (Figure 4.16) the wave height pattern in the conventional hindcast is in better agreement with the base case hindcast but peak significant wave heights are still much lower than the base case. Figure 4.16b shows the 12-hour track of the QE2 during which the storm encountered damaging sea states and veered to the south. The QE2 visual

TABLE 4.3

Errors relative to base case hindcast in hindcast (operational) of surface wind and significant wave height derived from conventional data alone. Base case hindcast made from wind fields derived from combined conventional and SASS data. Mean errors are computed as operational minus base case hindcast.

Day/Hour (GMT)	Wind Speed		Wind Direction		Significant Wave Height	
	Mean (m/s)	RMS	Mean (deg)	RMS	Mean (m)	RMS
Sept 09 1200	-1.30	3.07	10.66	35.86	- .43	.54
Sept 10 0000	-3.85	5.34	8.09	27.33	-1.09	1.19
Sept 10 1200	-1.32	5.05	3.59	23.31	- .78	1.51
Sept 11 0000	- .95	3.65	7.00	35.63	- .31	.93
Sept 11 1200	-1.43	4.01	8.19	36.58	- .30	.92

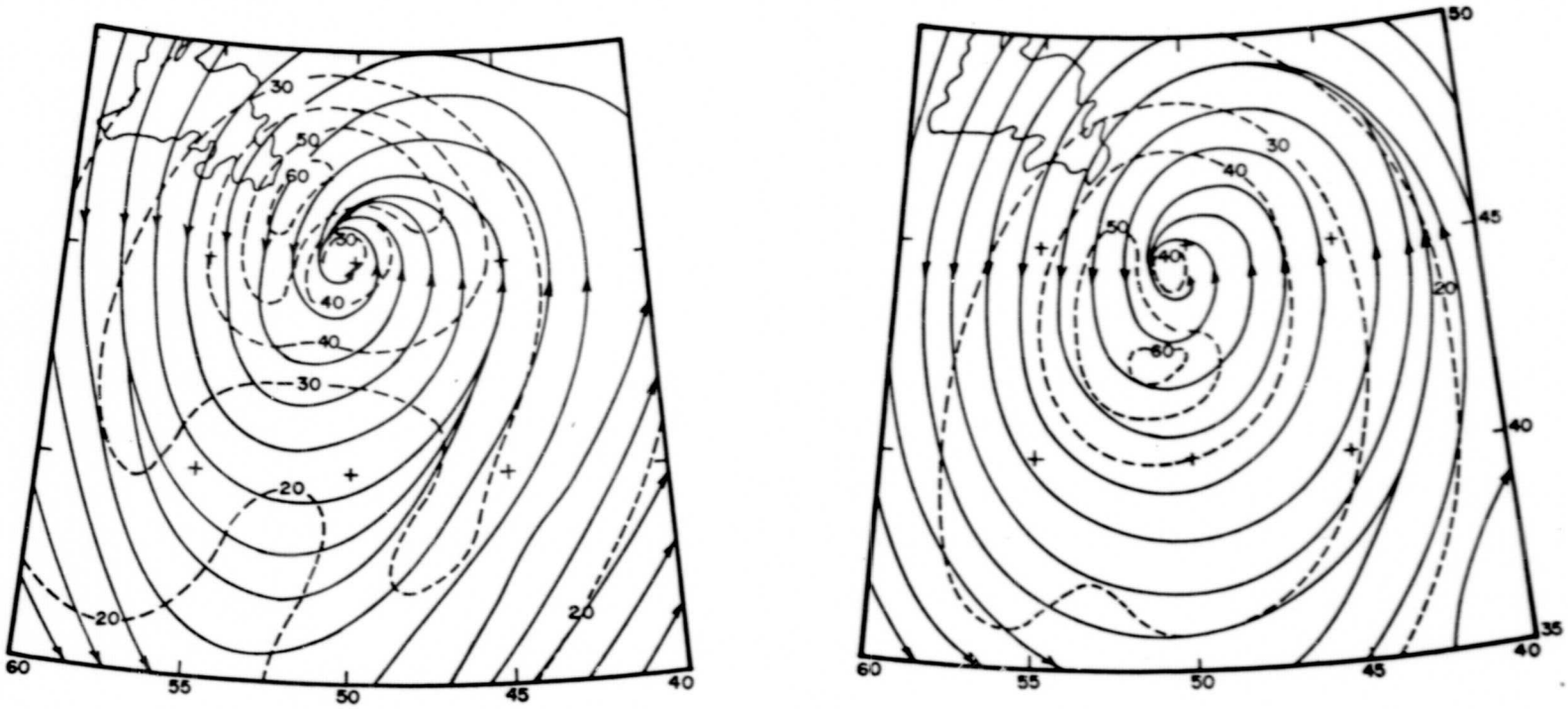

Figure 4.14 Comparison of (operational) surface wind field derived from NMC final analysis pressure field (left) and (base case) wind field from combined SASS and conventional data (right) for 1200 GMT September 10, 1978.

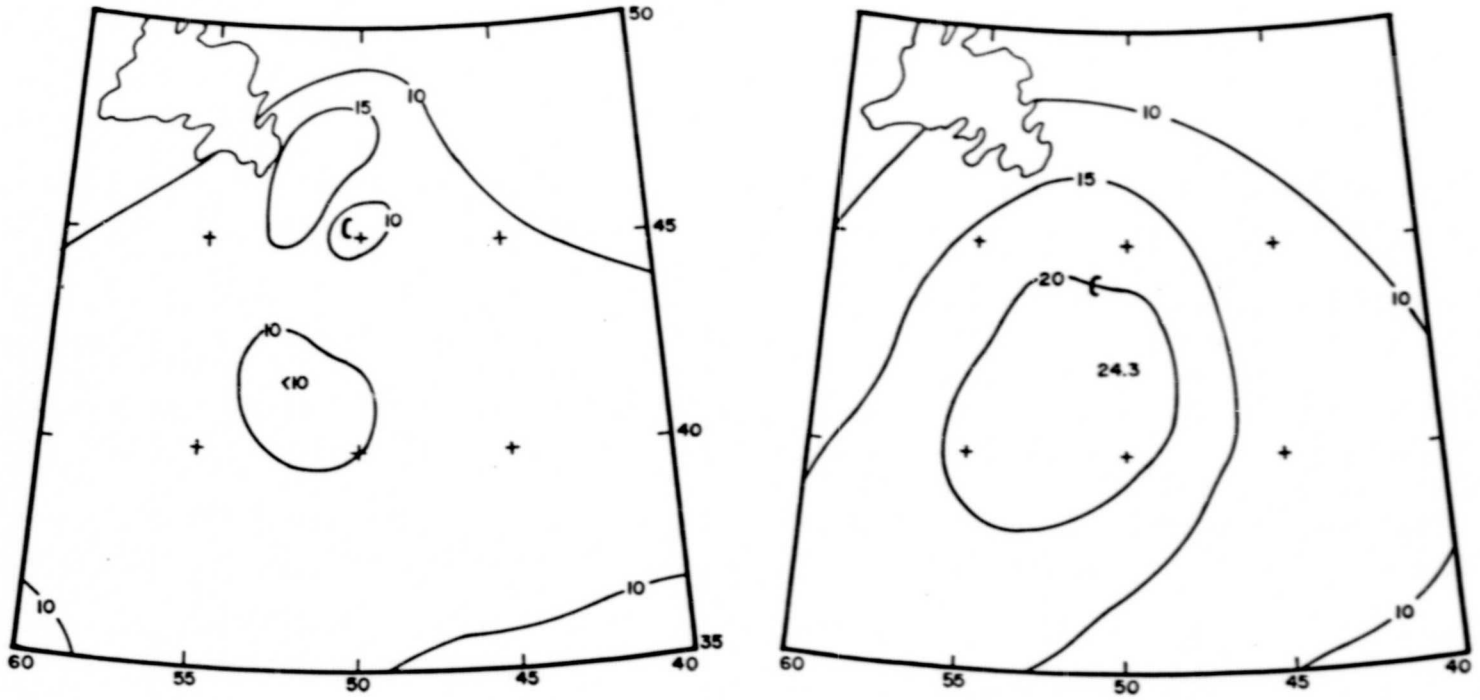

Figure 4.15 Comparison of hindcast significant wave height (contour interval is 5 feet) from simulated operational wind field (left) and wind field derived from SASS data (right) at 1200 GMT September 10, 1978. Location of storm center indicated as C. Maximum hindcast significant wave height also indicated.

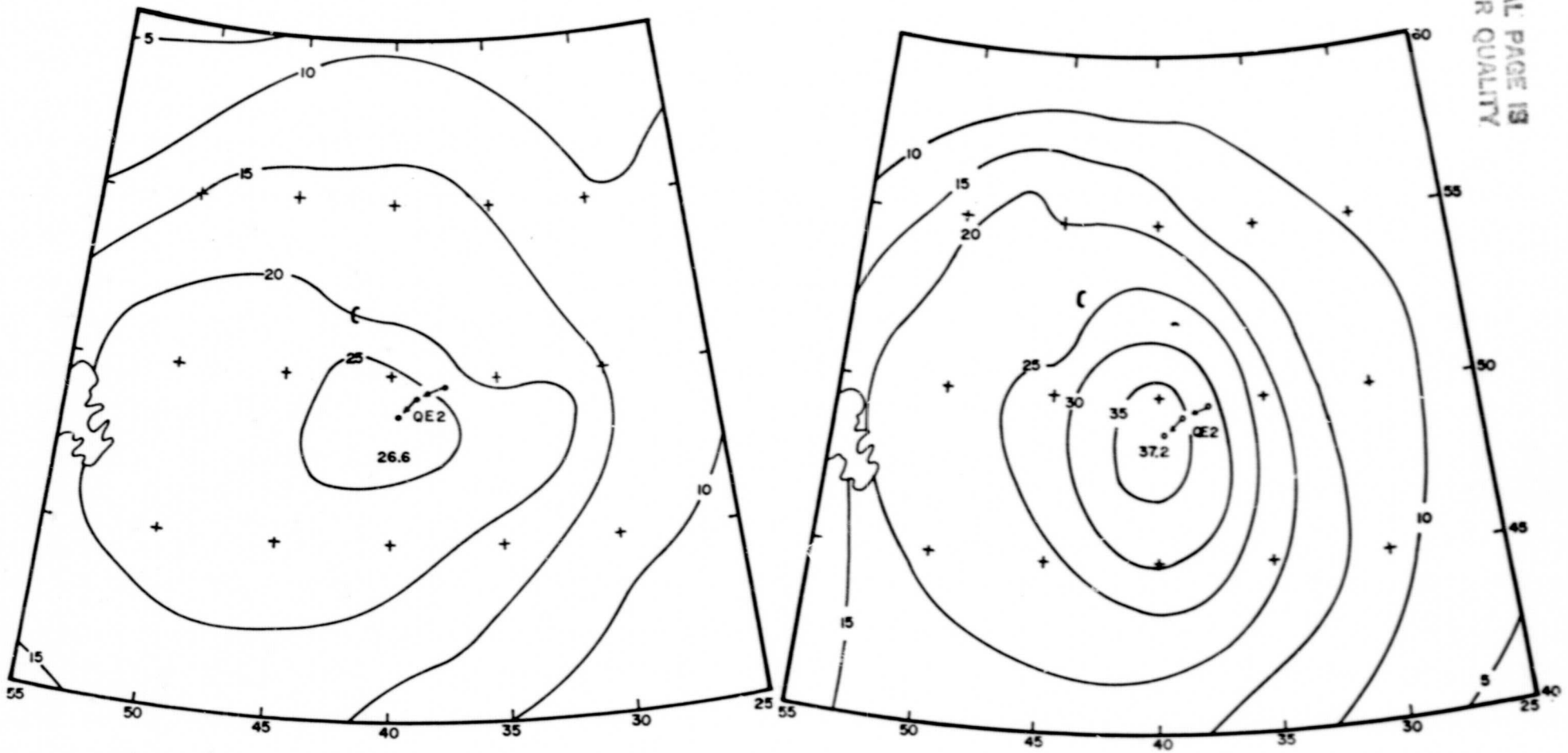

Figure 4.16 Same as Figure 4.15, except for 1200 GMT September 11, 1978. Route of QE2 storm during encounter with storm seas indicated.

wave height report of 39 feet average seas and individual wave heights in excess of 50 feet, is entirely consistent with the location and level of the maximum sea states of the base case hindcast.

The wave analyses available in real time considerably underestimated the peak sea states in the QE2 storm even on September 11. Figure 4.17, for example, is the NMC N. Atlantic wave height analyses for 1200 GMT September 11. Peak sea states are a factor of four too low relative to the base case hindcast.

4.4 Wave Forecast Experiments

A series of experiments were performed with the ODGP wave model to assess the impact of SASS data on sea state forecasts. Each experiment consisted of the simulation of a 24-hour wave forecast starting from an initial wave state specified from either the base case or operational hindcast. In all experiments, the simulated wave forecasts were verified against the base case hindcast at 6-hourly intervals using the same regions for the calculation of mean and rms errors in wind speed and significant wave height specified for the comparison of the alternate hindcasts.

Five separate forecast runs were made. Three of the runs addressed the 24-hour period of explosive development ending 1200 GMT September 10 from initial conditions specified for 1200 GMT September 9. Two of these runs simulated wave forecasts made from operational pressure analyses and forecasts, with the FNOC PE-model used to to provide winds. The third run used the base case hindcast initial state and pressure field forecasts reported by Anthes et al, (1983), who used SASS enhanced initial fields and a high resolution numerical weather prediction model to simulate the period of explosive development of the QE2 storm. The last two forecast runs covered the 24-hour period prior to 1200 GMT September 11, at which time peak storm sea states were indicated in the base case hindcast. These two runs differed only in the initial state specification as described below, with forecast winds provided from NMC PE-model surface pressure field forecasts.

4.4.1 24-hour Forecasts from 1200 GMT September 9

Figure 4.18, (after Gyakum, 1983) shows the initial analysis and 12 and 24-hour forecast sea level pressure fields provided by the FNOC (formerly

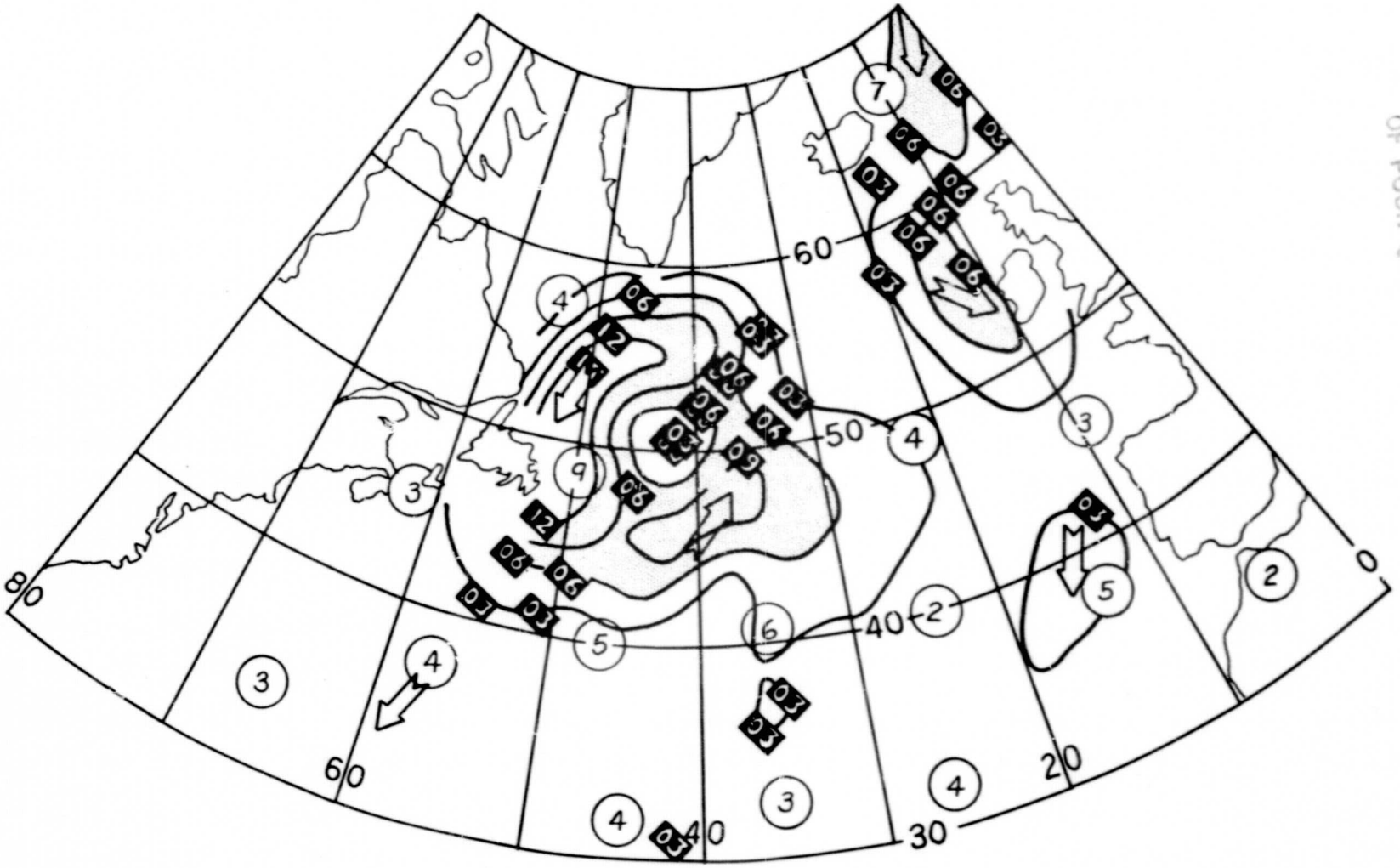

Figure 4.17 NOAA NMC wave height analysis for 1200 GMT September 11, 1978. Wave height contours in feet.

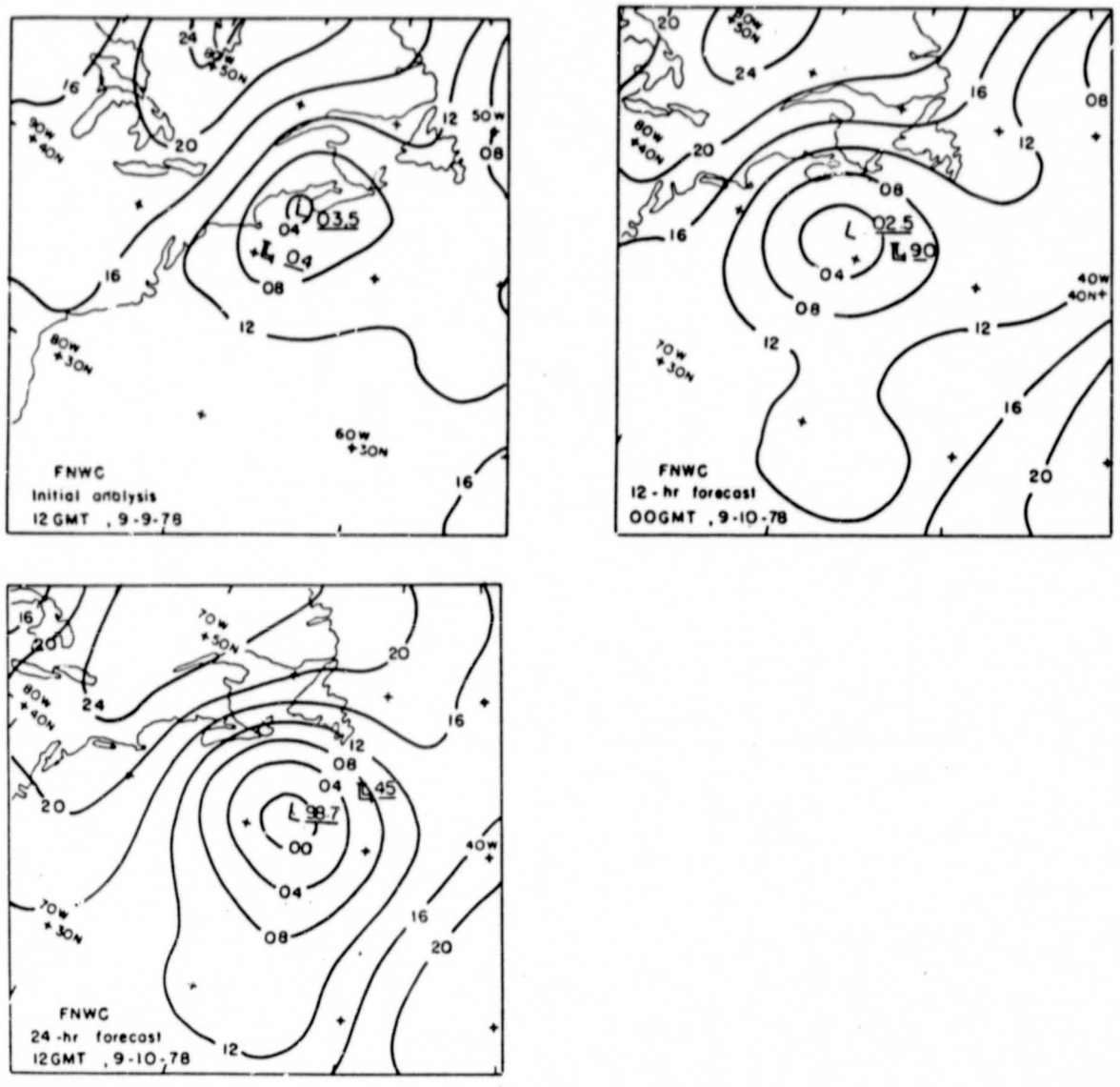

Figure 4.18 FNWC (presently FNOC) model analyses at 1200 GMT September 9, 1978 and 12-hour and 24-hour forecast of sea level pressure fields (solid lines are isobars at 4 mb intervals). Minimum central pressures are also shown. (from Gyakum, 1983a).

FNWC) PE-model in real time, for the period of explosive deepening. The model captured less than 15% of the observed deepening, and moved the vortex too slowly. The center was forecast to 42°N, 61°W at 12 hours and 42°N, 57°W at 24 hours. Actual positions were 41°N, 57°W and 44°N, 51°W, respectively.

One simulated forecast started from the initial wave state for 1200 GMT September 9 calculated in the operational hindcast, with forecast winds derived from the FNOC pressure fields using the same digitization scheme and PBL model used for the operational hindcast. That forecast is compared statistically to the base case hindcast in Table 4.4. As expected large negative biases characterize both the forecast wind speeds and wave heights with rapid growth of wind speed errors in the first 12 hours and growth of wave height errors to 24 hours.

A second run from the FNOC forecast pressure field was made but with the forecast storm track adjusted to agree with the observed track. This procedure removed contributions to forecast errors from simple phase shifts in the forecast winds and wave height pattern. Table 4.5 gives the errors found for this run. Much of the negative bias in the forecast fields remains.

Forecast winds for the third forecast covering this period were provided from experiment #4 of the series of QE2 storm numerical weather forecasts reported by Anthes et al, (1983). Figure 4.19 shows the properties of that forecast at 24 hours. Experiment #4 was the control experiment in Anthes et al. (1983) series. It used a numerical weather prediction model with 90 km grid spacing, ten vertical layers, simulation of the fluxes of momentum, heat and water in the boundary layer, and a parameterization for convective heating in the entire troposphere. Great care was taken in their study to provide as accurate an initial state as possible at 1200 GMT September 9. Initial fields were provided by Gyakum (1983) from a combination of all conventional surface and upper air data and SASS winds over the ocean from rev 1066.

The NWP model forecast provided a vortex with central pressure of 984mb at 24 hours at a position only 100 km from that observed, and maximum boundary layer winds of 32 m/s (estimated surface winds of 21 m/sec). We

TABLE 4.4

Errors relative to base case hindcast in 24-hour forecast from 1200 GMT September 9 of surface winds and significant wave heights based upon operational FNOC surface pressure field forecasts. Initial state for forecast specified from operational hindcast.

Day/Hour (GMT)	Forecast τ	Wind Speed		Wind Direction		Significant Wave Height	
		Mean	RMS	Mean	RMS	Mean	RMS
	(hours)	(m/s)		(deg)		(m)	
Sept 09 1200	0	-1.29	3.07	10.6	35.7	- .43	.54
Sept 09 1800	6	-5.02	5.79	9.8	38.5	- .55	.66
Sept 10 0000	12	-7.02	8.08	3.0	50.2	-1.33	1.47
Sept 10 0600	18	-6.29	7.71	- 6.9	47.2	-1.74	2.09
Sept 10 1200	24	-6.67	8.36	- 9.4	65.3	-1.86	2.44

TABLE 4.5

Errors relative to base case hindcast, in 24 hour forecast from 1200 GMT September 9, based upon operational FNOC surface pressure field forecasts, except forecast storm track adjusted to observed track. Initial state for forecast specified from operational hindcast.

Day/Hour (GMT)	Forecast τ	Wind Speed		Wind Direction		Significant Wave Height	
	(hours	Mean (m/s)	RMS	Mean (deg)	RMS	Mean (m)	RMS
Sept 09 1200	0	-1.29	3.07	10.6	35.7	- .43	.54
Sept 09 1800	6	-4.46	5.67	12.7	33.6	- .57	.71
Sept 10 0000	12	-5.52	6.95	- 1.1	30.0	-1.18	1.34
Sept 10 0600	18	-5.24	6.81	- 5.3	20.8	-1.50	1.89
Sept 10 1200	24	-4.80	6.81	- 7.7	37.1	-1.57	2.15

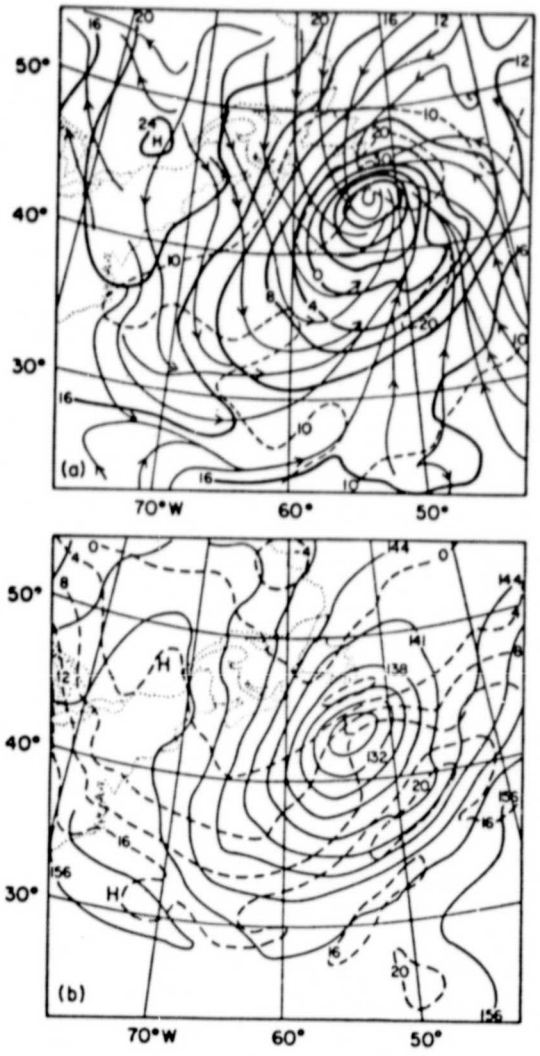

Figure 4.19 24-hour forecast boundary layer winds (streamlines and isotachs, m/s) and sea level pressure (isobar contour intervals 4 mb) in control experiment #4 of Anthes et al. (1983). Forecast verification time is 1200 GMT September 10, 1978.

note that Anthes et al, (1983) were able to simulate almost all of the observed deepening in some sensitivity experiments through modification of the numerics and physics of the models though usually at the expense of accuracy of forecast track. For the purposes of our study, however, we take their control experiment as representative of the impact of improved initial state specification over the ocean (as may be provided by SASS) on numerical forecasts of cyclogenesis with currect operational numerical weather prediction models.

Table 4.6 gives the errors in sea state forecasts driven by the control experiment sea level pressure field forecasts. To be consistent with the improved initial atmospheric states provided to the atmospheric model, the initial wave state for the wave forecast was provided by the base case hindcast. The errors are greatly reduced relative to the wave forecasts made from operational atmospheric forecasts. Indeed at 24 hours, the mean and rms wave height errors are comparable to errors achieved in hindcasts made from accurate wind fields. Maximum sea states are also reasonably well resolved, as shown in Figure 4.20, which compares the significant wave height fields at 24 hours derived from the FNOC and Anthes et al, atmospheric forecasts. Peak sea states however, in the latter forecast were still about 20% lower than those of the base case hindcast peak.

4.4.2 24-hour Forecast from 1200 GMT September 10

Two forecast runs were made for the 24-hour period following the period of explosive development, during which the storm pressure actually filled (see Figure 4.4). For this period, sea level pressure forecasts were taken from the operational NMC-PE atmospheric forecasts. Figure 4.21 shows the 24-hour sea level pressure forecast from the NMC-PE model. The central pressure is forecast to be about 20 mb higher than observed.

The two forecast runs both used wind fields derived from the NMC sea level pressure field forecasts. One run, however, began with initial states taken from the operational hindcast; for the second run the initial state specification from the base case hindcast was used. Tables 4.7 and 4.8 give the errors for each run. The effect of the "perfect" initial state is to provide a greatly improved forecast at 6-hours and 12 hours, but the advantage in the initial state is largely lost by 24 hours. This is

TABLE 4.6

Errors relative to base case hindcast in 24 hour forecast from 1200 GMT September 9, based upon sea level pressure forecasts in QE2 storm from experiment #4 of Anthes et al. (1983). Initial state for forecast specified from base case hindcast.

Day/Hour (GMT)	Forecast τ	Wind Speed		Wind Direction		Significant Wave Height	
	(hours)	Mean (m/s)	RMS (m/s)	Mean (deg)	RMS (deg)	Mean (m)	RMS (m)
Sept 09 1200	0	0	0	0	0	0	0
Sept 09 1800	6	-1.15	2.90	7.64	23.7	-.07	.26
Sept 10 0000	12	-2.06	5.03	7.58	29.4	-.26	.81
Sept 10 0600	18	-1.72	4.34	-1.54	13.9	-.19	1.04
Sept 10 1200	24	-2.30	5.46	-7.19	28.2	-.39	1.13

TABLE 4.7

Errors relative to base case hindcast in 24 hour forecast from 1200 GMT September 10, based upon NMC model sea level pressure forecast. Initial state specified from operational hindcast.

Day/Hour (GMT)	Forecast τ	Wind Speed		Wind Direction		Significant Wave Height	
	(hours)	Mean (m/s)	RMS (m/s)	Mean (deg)	RMS (deg)	Mean (m)	RMS (m)
Sept 10 1200	0	-1.37	5.12	3.4	22.7	- .79	1.52
Sept 10 1800	6	-3.06	4.28	5.1	16.9	- .76	1.49
Sept 11 0000	12	-4.65	6.57	11.6	31.8	- .97	1.47
Sept 11 0600	18	-4.55	6.15	6.6	22.7	-1.40	2.02
Sept 11 1200	24	-3.95	6.03	2.6	44.8	-1.51	2.25

TABLE 4.8

Errors relative to base case hindcast in 24 hour forecast from 1200 GMT September 10, based upon NMC model sea level pressure forecast. Initial state specified from base case hindcast.

Day/Hour (GMT)	Forecast τ	Wind Speed		Wind Direction		Significant Wave Height	
		Mean	RMS	Mean	RMS	Mean	RMS
	(hours)	(m/s)		(deg)		(m)	
Sept 10 1200	0	0	0	0	0	0	0
Sept 10 1800	6	-1.83	2.30	7.4	13.2	- .21	.29
Sept 11 0000	12	-4.65	6.57	11.6	31.8	- .71	.98
Sept 11 0600	18	-4.55	6.15	6.6	22.7	-1.16	1.64
Sept 11 1200	24	-3.95	6.03	2.6	44.8	-1.32	1.98

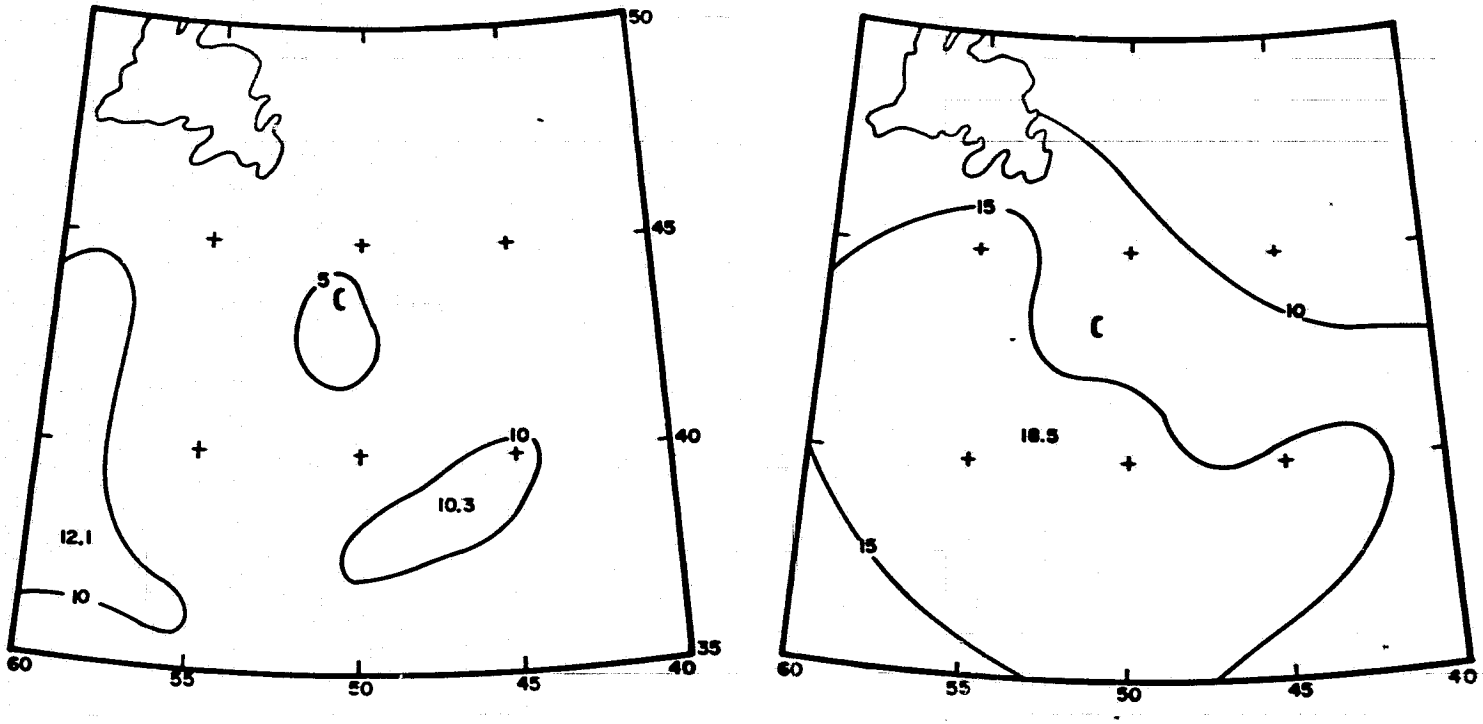

Figure 4.20 24-hour forecast valid 1200 GMT September 10, 1978 of significant wave height (contour interval is 5 feet) from FNWC sea level pressure forecast (left) and experiment #4 of Anthes et al., (1983) (right).

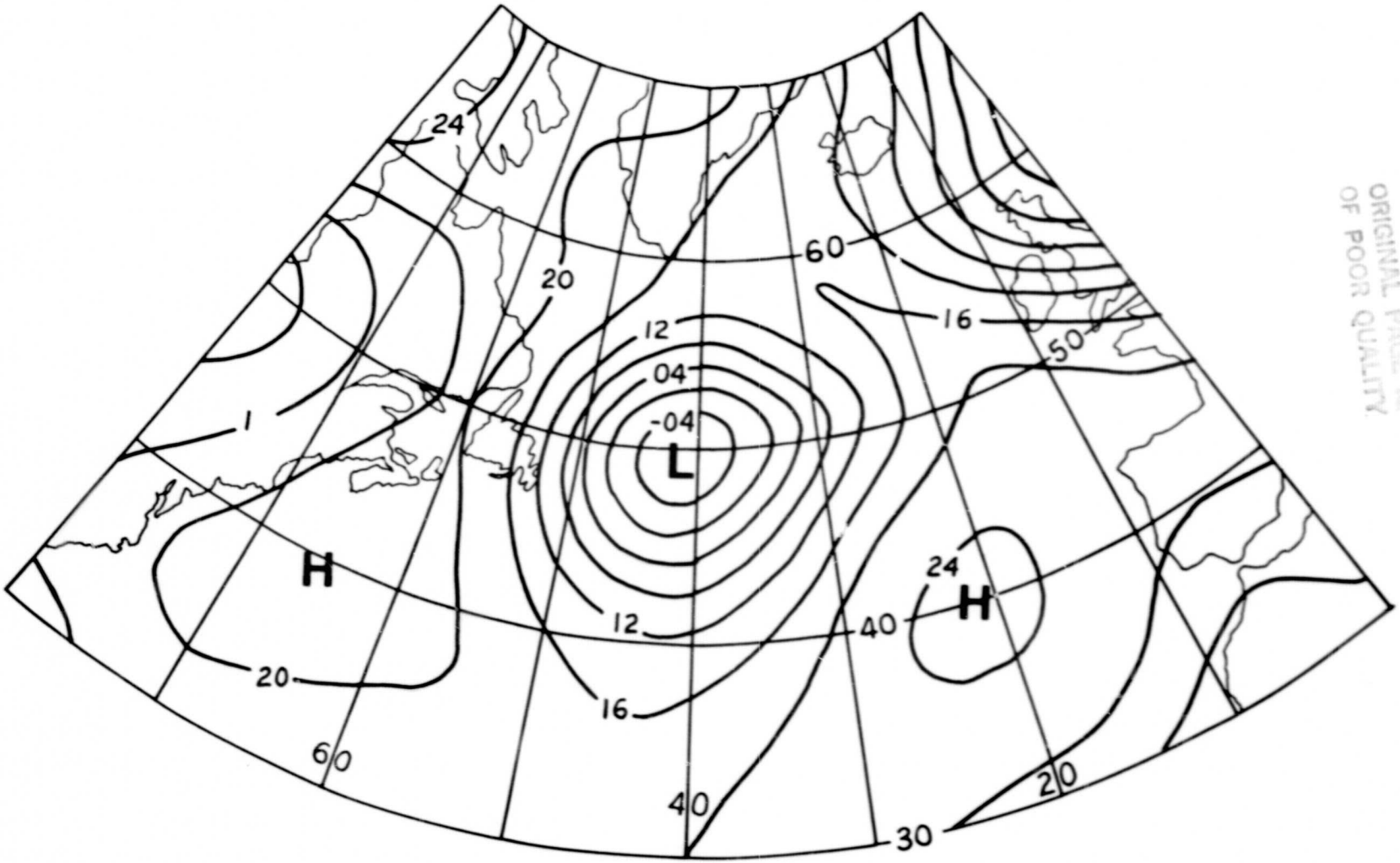

Figure 4.21 24-hour NMC PE-model sea level pressure forecast (contour interval is 4 mb) valid 1200 GMT September 11, 1978.

seen also in the significant wave height comparison for 24-hours shown in Figures 4.22. Both forecasts show the maximum wave height to be about half that specified in the base case hindcast. Thus, the effect of the improved initial wave state is largely masked by large errors in forecast winds after about 12 hours of forecast range.

The magnitude and location of the peak sea states specified in the simulated forecasts shown in Figure 4.22 is remarkably close to the corresponding features of the 24-hour wave forecast used in real time by the NMC and FNOC, as seen in their forecast wave contour analyses (Figures 4.23 and 4.24). In view of those wave forecasts, which serve as guidance to most operational marine warning and ship routing services, it is not surprising that several merchant ships and the QE2 did not evade the dangerous sea states generated by this storm.

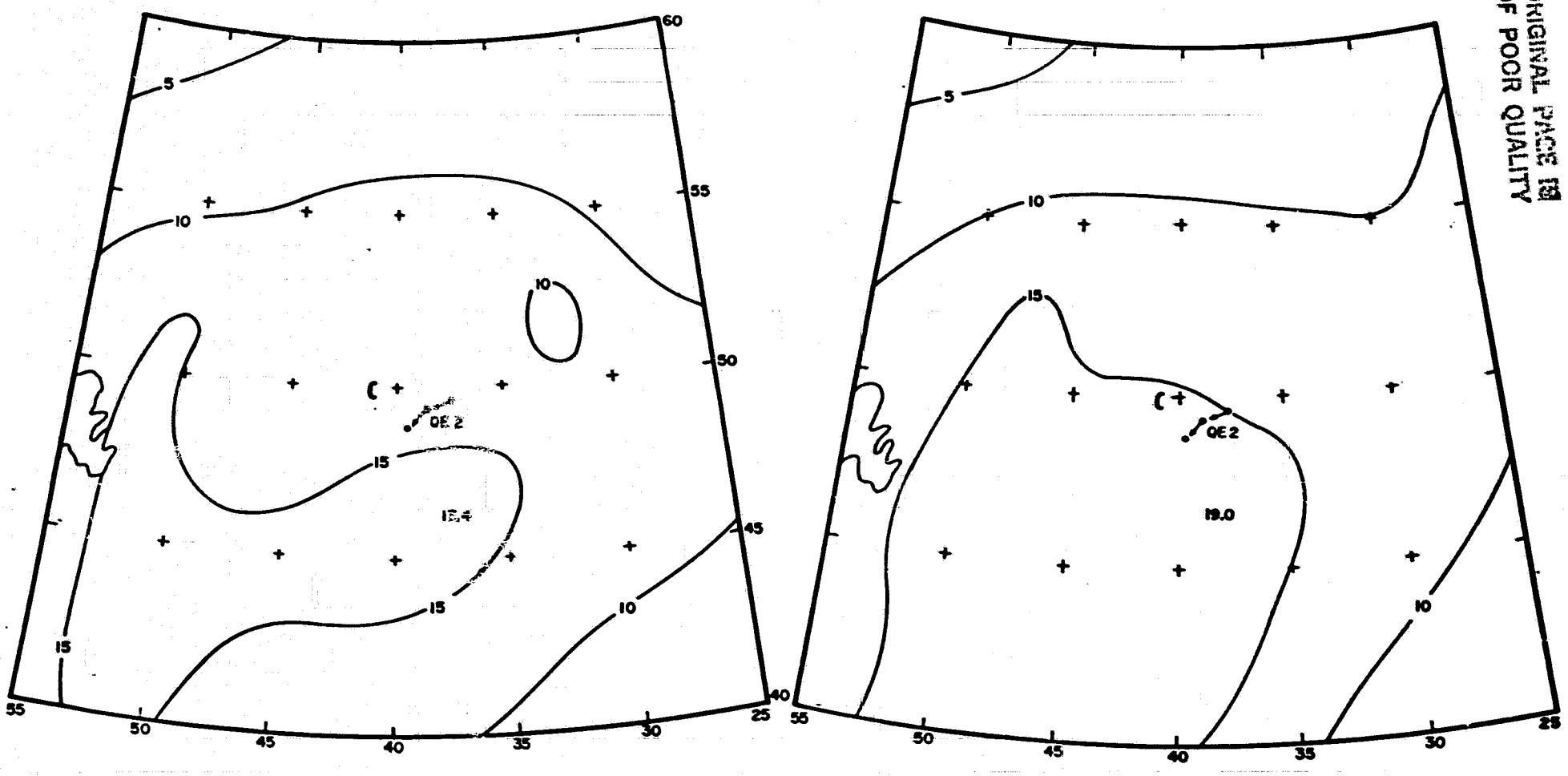

Figure 4.22 24-hour wave forecasts valid 1200 GMT September 11, 1978 of significant wave height (contour interval is 5 feet). Forecast winds from NMC PE-model sea level pressure forecast. Initial state (left) taken from operational wave hindcast. Initial state (right) taken from base case hindcast.

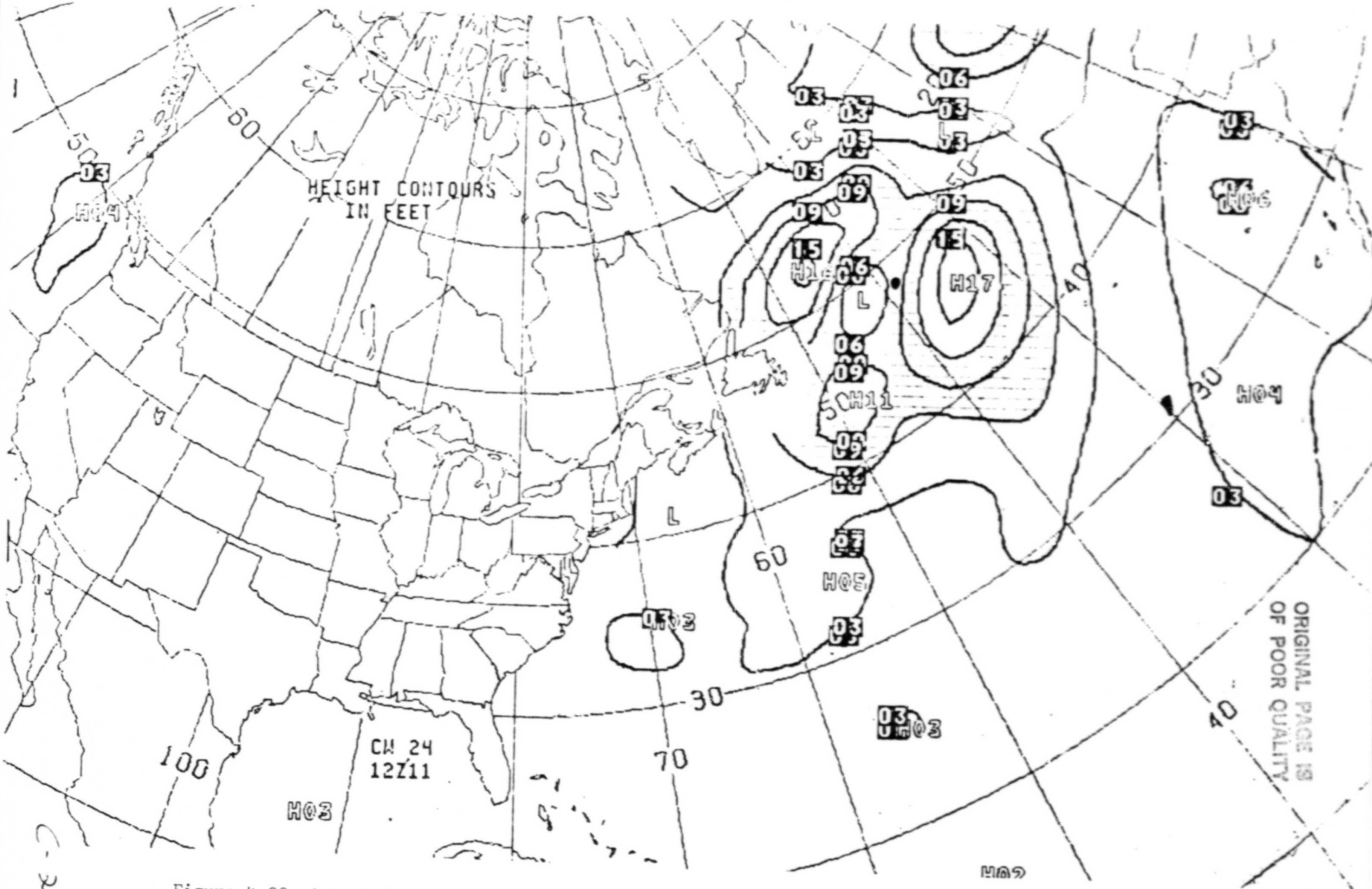

Figure 4.23 Actual 24-hour N. Atlantic wave height forecast map issued by NOAA NMC, valid 1200 GMT September 11, 1978 (contour interval is 3 feet).

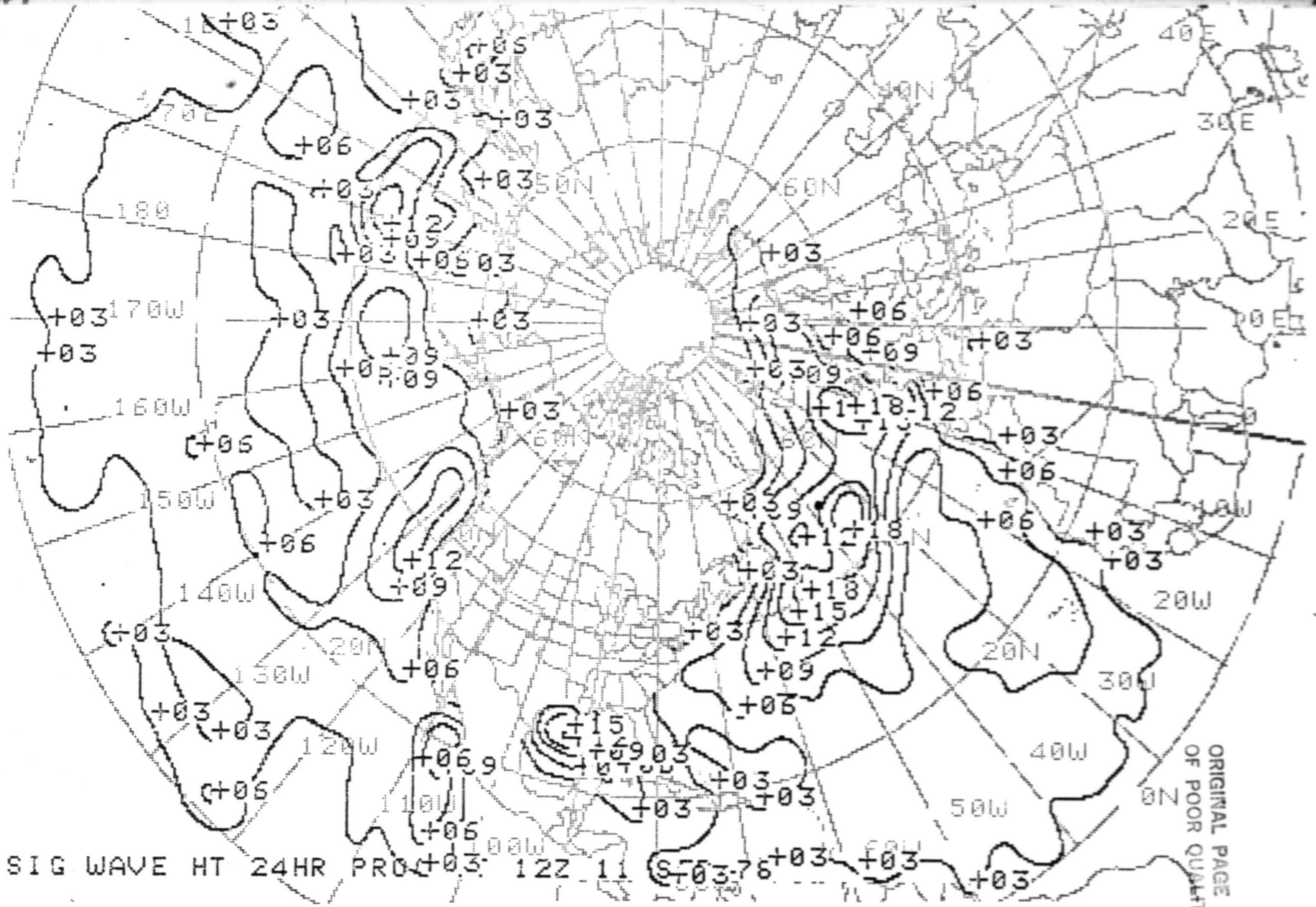

Figure 4.24 Actual 24-hour N. Atlantic wave height forecast map issued by FNOC, valid 1200 GMT September 11, 1978 (contour interval is 3 feet).

5. Conclusions

1. The SEASAT-A SASS provided wind data with sufficient coverage in space and time to allow the specification of the evolution of the surface wind field in the QE2 storm from an incipient vortex through the stage of explosive deepening to the fully mature stage as a large N. Atlantic extratropical cyclone. The SASS data allowed identification of large errors in wind fields derived from operational sea level pressure analyses and therefore in the pressure fields themselves. There were large errors found in the location of the center, in the location of the area of strongest winds and in the magnitude of peak surface winds. Conventional ship data aided greatly in the specification of the initial guess wind field used for the selection of the correct SASS wind, but the conventional data base assembled for this study consists of about twice the number of reports available in real time. Future operational versions of SASS should provide far greater spatial and temporal coverage than SEASAT and should therefore allow the detection of "bombs" in very early stages of development over the global oceans.

2. Application of a calibrated, validated spectral wave prediction model to the QE2 storm together with alternate wind field histories showed that extremely large errors can occur in wave analyses specified from conventional data alone. Given the probable errors in the surface wind history derived from the SASS data (± 2 m/sec rms, negligible bias), the errors in significant wave height in the base case hindcast are probably unbiased with rms errors near .75m. The hindcasts made from conventional data, however, were biased low by 1 m overall, but more significantly, that hindcast underspecified the average wave heights in the area of highest waves by a factor of 2 during the period of maximum deepening, and by about 30% in the mature storm stage. An independent verification of the base case hindcast from remote sensing data is not possible in the QE2 storm because the Seasat-A altimeter was not operational during this period. However, the wave hindcast model used for all the QE2 simulations has been extensively validated against in-situ wave measurements in many severe historical storms, including the storm in which ROWS directional spectra were acquired as

described in this report. The peak sea states specified in the base case hindcast also agree well with visual wave height estimates made from the QE2 during its encounter with the storm.

3. Simulated wave forecasts made from operational numerical weather prediction products agree closely with operational wave forecasts issued in real time from NMC and FNOC. Those forecasts seriously underpredicted the wave heights in the area of maximum seas. Since three very different wave forecast models produced very similar wave forecasts, it can be safely concluded that errors in forecast wind fields are the dominant source of errors in operational wave forecasts for storms of the type studied.

4. The degree to which SASS marine wind data can improve numerical weather forecasts remains a somewhat controversial issue. Most likely, the SASS data will show beneficial impact if combined with conventional data such that the sea level pressure field and the geopotential distribution in the entire troposphere may be updated. Such a procedure was followed for the numerical weather prediction experiments reported by Anthes et al. (1983). They found significant improvements in atmospheric forecasts of the explosive development, which were translated in this study to significantly improved sea state predictions.

5. Remote sensing wind data, augmented possibly by remote sensing wave data, applied operationally with a calibrated numerical spectral ocean wave model will allow accurate monitoring of the state of the sea globally. The resulting improved initial state specification for wave forecast systems should alone cause greatly improved short range (12-24 hour) wave forecasts in severe storms, and improved swell forecasts at larger range. However, improved sea state forecasts in storms beyond 24 hours will require improved operational numerical prediction of cyclogenesis and cyclone intensification.

6. Finally, all of our conclusions must be qualified as tentative, because they are based upon study of just one case. The QE2 storm, however, was special only in the sense that it was viewed by SASS during the short

Seasat experiment, and caused damage to a luxury oceanliner. Otherwise, the QE2 storm was a typical strong bomb, and the errors observed in conventional analyses and forecasts were quite typical of those observed in most such storms (see e.g. Sanders and Gyakum, 1980). We can be therefore more confident that the improvements in sea state analyses and forecasts to be derived from remote sensing data suggested by this study, would be realized routinely from data provided by an operational oceanographic remote sensing satellite system.

REFERENCES

R.A. Anthes, Y.H. Kuo and J.R. Gyakum. Numerical Simulations of a Case of Explosive Marine Cyclogenesis. Monthly Weather Review, 111, 1983. pp. 1174-1188.

M. Cane, V.J. Cardone, I. Halberstam, M. Halem. On the Sensitivity of Numerical Weather Prediction to Remotely Sensed Surface Wind and Temperature Data. A Simulation Study. Journal of Geophysical Research, 86, 1981. pp. 8093-8106.

M.A. Cane, V.J. Cardone. The Potential Impact of Scatterometry on Oceanography: A Wave Forecasting Case. Oceanography from Space, Edited by J.F.R. Gower, Plenum Publishing Corp., 1981. pp. 587-595.

V.J. Cardone. Specification of the Wind Field Distribution in the Marine Boundary Layer for Wave Forecasting. Report TR-69-1, Geophys. Sci. Lab, New York University. Available from NTIS AD#702-490, 1969.

V.J. Cardone, W.J. Pierson and E.G. Ward. Hindcasting the Directional Spectrum of Hurricane Generated Waves. J. of Petrol. Tech., 28, 1976. pp. 385-394.

V.J. Cardone, J.D. Young, W.J. Pierson, R.K. Moore, J.A. Greenwood, C.V. Greenwood, A.K. Fung, R. Salfi, H.L. Chan, M. Afarani, M. Komen. The Measurement of the Winds near the Ocean Surface with a Radiometer-Scatterometer on SKYLAB. 1976b. NASA Johnson Space Center, Houston, TX, Final Report on EPN 550, Contract # NAS-9-13642.

V.J. Cardone, and D.B. Ross. State-of-the-art Wave Prediction Methods and Data Requirements. Ocean Wave Climate, Edited by M.D. Earle and A. Malahoff, Plenum Publishing Corporation, 1979. pp. 61-91.

V.J. Cardone, A.J. Broccoli, C.V. Greenwood and J.A. Greenwood. Error Characteristics of Extratropical Storm Wind Fields Specified from Historical Data. J. of Petrol Tech. 32, 1980. pp. 873-880.

V.J. Cardone, T. Chester and R. Lipes. Evaluation of SEASAT SMMR Wind Speed Measurements. J. of Geophy. Res., 88, 1983. pp. 1709-1726.

G.Z. Forristall, E.G. Ward, V.J. Cardone and L.E. Borgman. The Directional Spectra and Kinematics of Surface Waves in Tropical Storm Delia. J. of Phys. Oceanogr., 8, 1978. pp. 888-909.

G.Z. Forristall, E.G. Ward and V.J. Cardone. Directional Wave Spectra and Wave Kinematics in Hurricanes Carmen and Eloise. Seventeenth International Conference on Coastal Engineering. 1980. Sydney, Australia.

J.A. Greenwood and V.J. Cardone. Development of a Global Ocean Wave Propagation Algorithm. Final Report to U.S. Navy Fleet Numerical Weather Central, Monterey, Calif., Contract N-00226-76-C-3081, 1977.

J.A. Greenwood, V.J. Cardone, L.M. Lawson. Intercomparison Test Version of the SAIL Wave Model. 1983. To appear in proceedings of IUCRM Symposium on Wave Dynamics and Radio Probing of the Ocean Surface, May 13-20, 1981, Miami Beach, Florida.

J.R. Gyakum. On the Evolution of the QE II Storm. Preprints, Eighth Weather Forecasting and Analysis Conference. AMS, Boston, 1980. pp. 23-28.

J.R. Gyakum. On the Evolution of the QE II Storm. I: Synoptic Aspects. Mon. Wea. Rev., 111, 1983. pp. 1137-1155.

J.R. Gyakum. On the Evolution of the QE II Storm. II: Dynamic and Thermodynamic Structure. Mon. Wea Rev.,111, 1983. pp. 1156-1173.

F.C. Jackson. An Analysis of Short Pulse and Dual Frequency Radar Techniques for Measuring Ocean Wave Spectra from Satellites. Radio Sci., 16, 1981. pp. 1485-1500.

F.C. Jackson, W.T. Walton and P.L. Baker. Aircraft and Satellite Measurement of Ocean Wave Directional Spectra using Scanning-Beam Microwave Radars. NASA Technical Memorandum 84008, Goddard Space Flight Center, Greenbelt, Maryland 20771, 1982.

F.C. Jackson. Microwave Radar Oceanographic Investigations. Proposal to continue RTOP 161-80-22-20 submitted by NASA Goddard Space Flight Center to Oceanic Processes Branch, NASA Headquarters, Washington D.C., July 18, 1983.

F.C. Jackson, W.T. Walton and P.L. Baker. Aircraft and Satellite Measurement of Ocean Wave Directional Spectra using Scanning Beam Microwave Radars. In. Proc. Symp. Wave Dynamics and Radio Probing of the Ocean Surface, edited by O.M. Phillips, Plenum Press, 1983. (in press).

R.W. James. Anatomy of a Storm. Mar. Wea.Log, 23, 1979. pp. 71-75.

W.L. Jones, L.C. Schroeder, D.H. Boggs, E.M. Bracalente, R.A. Brown, G.J. Dame, W.J. Pierson, and F.J. Wentz. The SEASAT-A Satellite Scatterometer: The Geophysical Evaluation of Remotely Sensed Wind Vectors over the Ocean. J. Geophys. Res, 87, 1982. pp 3297-3317.

C. Leary. Systematic Errors in Operational National Meteorological Center Primitive Equation Surface Prognoses. Mon. Wea. Rev., 99, pp. 409-413.

Oceanweather. Development and Evaluation of a Coupled Discrete Wave Prediction Model. Final report submitted to NOAA AOML SAIL 1983. Contract # NA80RAC00038.

J.E. Overland and W.H. Gemmill. Marine Winds in the New York Bight. Mon. Wea. Rev., 105, 1977. pp. 1003-1008.

W.J. Pierson, L.J. Tick and L. Baer. Computer based Procedures for Preparing Global Wave Forecasts and Wind Field Analyses Capable of Using Wave Data Obtained by a Spacecraft. In: Sixth Naval Hydrodynamics Symposium, ACR-136, Office of Naval Research, Dept. of the Navy, Washington D.C., 1966. pp. 499-532.

W.J. Pierson. Highlights of the SEASAT-SASS Program: A review. Satellite Microwave Remote Sensing, edited by T.D. Allan, Publishers Ellis Horwood Limited. 1983.

A.J. Reece and V.J. Cardone. Test of Wave Hindcast Model Results Against Measurements during Four Different Meteorological Systems. OTC #4323. 14th Annual OTC in Houston, TX, May 3-6, 1982

F. Sanders and J.R. Gyakum. Synoptic-Dynamic Climatology of the "Bomb". Mon. Wea. Rev., 108, 1980. pp. 1589-1606.

SWAMP (Sea Wave Modelling Project). An Intercomparison Study of Wind Wave Prediction Models. The SWMAP Group, 24 authors. To appear in Proceedings of IUCRM Symposium on Wave Dynamics and Radio Probing of the Ocean Surface, May 13-20, 1981, Miami Beach, Florida. 1983.

L.C. Schroeder, D.H. Boggs, G. Dome, I.M. Halberstam, W.L. Jones, W.J. Pierson, and F.J. Wentz. The Relationship between Wind Vector and Normalized Radar Cross Sections used to derive SEASAT-A Satellite Scatterometer Winds. Journal Geophys. Res., 87, 1982. pp. 3318-3336.

M.G. Wurtele, P.M. Woiceshyn, S. Peterherych, M. Borowski and W.S. Appleby. Wind Direction Alias Removal Studies of SEASAT Scatterometer-derived Wind Fields. Journal of Geophys. Res., 87, 1982. pp. 3365-3377.